Wisconsin Highway Research Program

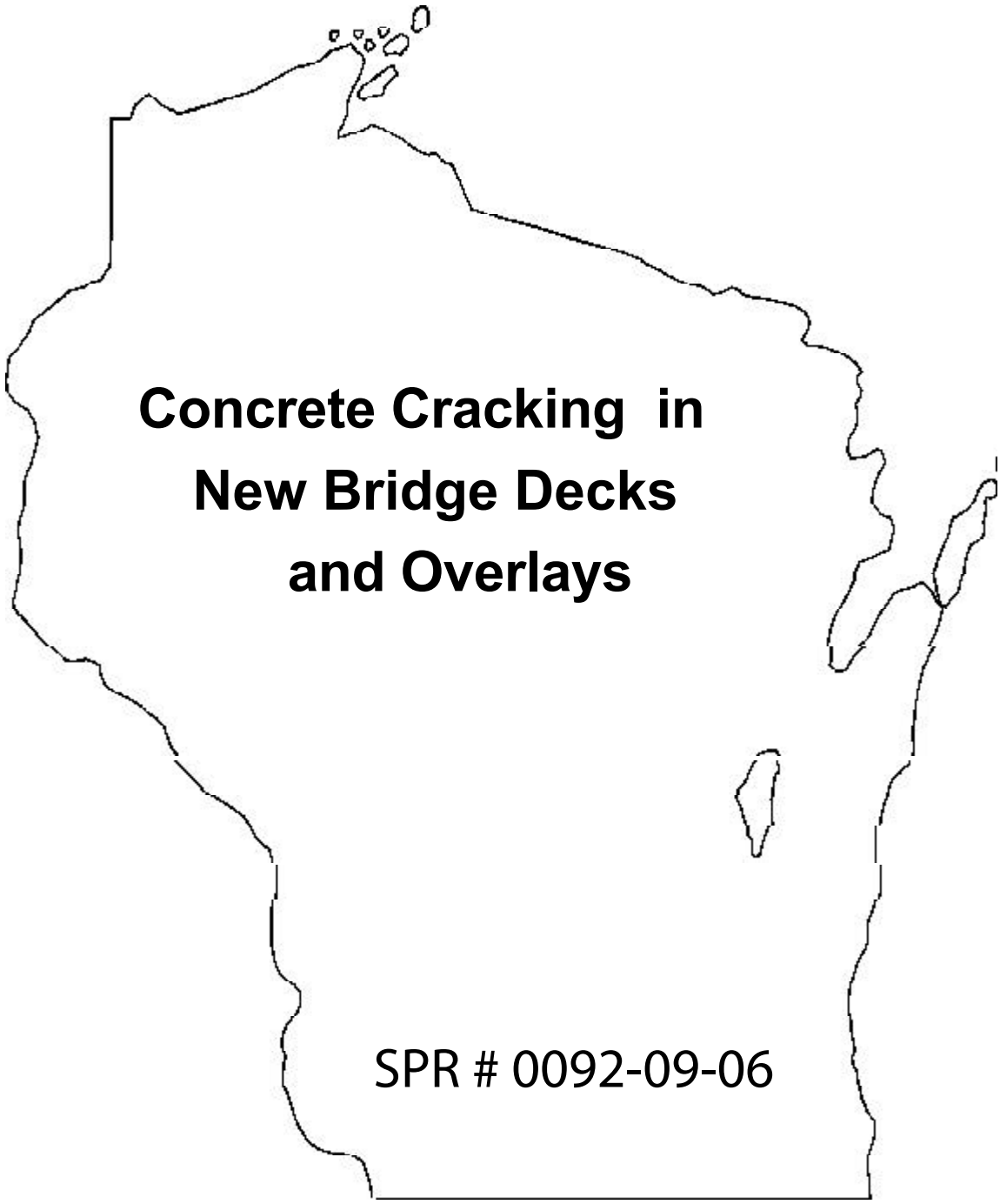

Concrete Cracking in New Bridge Decks and Overlays

SPR # 0092-09-06

Baolin Wan, Ph.D, Christopher Foley, Ph.D, P.E., and Jordan Komp
Transportation Research Center
Department of Civil and Environmental Engineering
Marquette University
March 2010

WHRP 10-05

Technical Report Documentation Page

1. Report No. WHRP 10-05	2. Government Accession No	3. Recipient's Catalog No
4. Title and Subtitle Concrete Cracking in New Bridge Decks and Overlays		5. Report Date February 2010 6. Performing Organization Code Wisconsin Highway Research Program
7. Authors Baolin Wan, PhD; Christopher M. Foley, PhD, PE; and Jordan Komp		8. Performing Organization Report No.
9. Performing Organization Name and Address Department of Civil & Environmental Engineering Marquette University, Milwaukee, WI		10. Work Unit No. (TRAIS) 11. Contract or Grant No. WisDOT SPR# 0092-09-06
12. Sponsoring Agency Name and Address Wisconsin Department of Transportation Division of Business Services Research Coordination Section 4802 Sheboygan Ave. Rm 104 Madison, WI 53707		13. Type of Report and Period Covered Final Report, 2008-2010 14. Sponsoring Agency Code
15. Supplementary Notes		

16. Abstract

There appears to be a trend for new bridge decks in the state of Wisconsin to develop early-age transverse cracks and map cracks on concrete overlays. A comprehensive literature review of the potential causes of concrete bridge deck cracking is provided. Fifteen bridge structures found in the recently completed Marquette Interchange were analyzed using 21 variables thought to cause early-age bridge deck cracking. Visual inspection of sixteen bridges in Milwaukee is described. The inspections show that the continuous superstructures have more cracks than the simply-supported bridges. A finite element model was created for a typical two-span continuous superstructure with HL-93 truck loads and concrete shrinkage-induced strains. The FE simulations indicate that the normal traffic load by itself will not cause concrete deck cracking. However, tensile stress introduced by concrete shrinkage may cause transverse cracks as early as 4 to 8 days after pouring concrete. Concrete samples were taken from two continuous superstructure bridge decks and unconfined compression testing was conducted. The experimental results indicate that the decks' 28-day unconfined compression strength of the concrete was much higher than the design target. Furthermore, the unconfined compression strength at 3-5 days is very near the target 28-day unconfined compression strength. The rapid development of compression strength and elastic modulus may result in significant shrinkage and tensile stresses in the deck, and therefore early age cracking in bridge decks. Recommendations for reducing deck cracking and future research are provided.

17. Key Words	18. Distribution Statement
Concrete Bridge Deck, Crack, Concrete Shrinkage, Finite Element Analysis	No restriction. This document is available to the public through the National Technical Information Service 5285 Port Royal Road Springfield VA 22161

19. Security Classif.(of this report) Unclassified	19. Security Classif. (of this page) Unclassified	20. No. of Pages	21. Price

Form DOT F 1700.7 (8-72) Reproduction of completed page authorized

DISCLAIMER

This research was funded through the Wisconsin Highway Research Program by the Wisconsin Department of Transportation and the Federal Highway Administration under Project 0092-09-06. The contents of this report reflect the views of the authors who are responsible for the facts and accuracy of the data presented herein. The contents do not necessarily reflect the official views of the Wisconsin Department of Transportation or the Federal Highway Administration at the time of publication.

This document is disseminated under the sponsorship of the Department of Transportation in the interest of information exchange. The United States Government assumes no liability for its contents or use thereof. This report does not constitute a standard, specification or regulation.

The United States Government does not endorse products or manufacturers. Trade and manufacturers' names appear in this report only because they are considered essential to the object of the document.

TABLE OF CONTENTS

ACKNOWLEDGEMENTS v
EXECUTIVE SUMMARY vi
Chapter 1 Introduction 1
Introduction 1
Objectives 1
Report Outline 2
Referennces 3
Chapter 2 Literature Review 5
Introduction 5
Background Information 5
Loading 6
Crack Classification 11
Variables Contributing to Bridge Deck Cracking 12
Summary 24
References 25
Chapter 3 Marquette Interchange Data Synthesis 35
Introduction 35
Background 35
Variables Affecting Deck Cracking in Marquette Interchange 36
Summar and Conclusions 41
References 42
Chapter 4 Field Investigation of Deck Cracking in Milwaukee Area 52
Introduction 55
Bridges with Severe Cracks 56
Bridges with Medium Amount of Cracks 57
Bridges with Minor Cracks 58
Summary and Conclusions 59
Chapter 5 Finite Element Analysis 85
Introduciton 85
Bridge Prototype 85

Finite Eliment Model of Bridge B-20-133/134 86
Finite Element Model Calibration 87
HL-93 Interior Moment Loading 90
Simulation of Concrete Deck Shrinkage 92
Cracking Analysis 96
References 97
Chapter 6 Concrete Properties of Bridge Deck 121
Introduction 121
Racine Avenue Bridge Concrete Testing 121
Humboldt Avenue Bridge Concrete Testing 126
Summary 127
References 127
Chapter 7 Summary, Conclusions, Recommendations and Future Research 137
Summary 137
Conclusions 138
Recommendations 140
Future Research 141
References 142

ACKNOWLEDGEMENTS

The authors would like to acknowledge the support and help from the following individuals at the Wisconsin Department of Transportation: Travis McDaniel, Joan Bonack, and John Bolka.

EXECUTIVE SUMMARY

There appears to be a trend for new bridge decks in the state of Wisconsin to develop transverse cracks and map cracks in concrete overlays. There are many reasons for concrete bridge deck cracking including constituent components of the concrete, construction method, and superstructure configuration. Cracking in bridge decks can accelerate the penetration of water, sulfates, chloride and other harmful agents, and therefore accelerate the corrosion of steel reinforcement, facilitate early spalling behavior, and as a result, deterioration. This degradation often requires costly maintenance or repair, and can shorten the service life of the bridge deck. Key factors that lead to early-age cracking have been very difficult to identify. Furthermore, the role of mix design and subsequent specification in leading to early-age cracking in bridge decks has yet to be quantified. Finally, the role of construction practice and superstructure configuration in leading to early-age cracking has yet to be quantified.

The objectives of this research effort are to gain better and more up-to-date understanding of early concrete cracking of bridge decks and overlays; identify the key factors which cause early concrete cracking in the bridge decks in Wisconsin; and provide recommendations for concrete mixture design, construction practice and superstructure configuration and design for future bridge construction to eliminate or reduce early-age concrete cracking. The research also intends to provide recommendations with regard to laboratory and/or field studies, finite element analysis to simulate early-age behavioral characteristics, and analytical studies to estimate the stresses in concrete decks at early ages.

The research team conducted an extensive review of available U.S. and international research findings, performance data, and other information related to concrete bridge deck cracking. While the exact causes are unknown, the variables potentially affecting cracking were categorized as material properties, site conditions, construction procedures, design specifications, and traffic/age. Fifteen bridge structures in the recently completed Marquette Interchange were analyzed using 21 variables thought to contribute to deck cracking. It appeared as though none of the variables evaluated had a significant effect on bridge deck cracking. However, it should be noted that specific constituent proportions of components in the concrete mixes, hardened concrete properties, and traffic data were not obtained for any of the structures.

Sixteen bridges in the Milwaukee area were investigated through visual inspection. Because most factors likely to affect deck cracking were not available for further investigation in these bridges only the superstructure configuration can be considered. Furthermore, several important parameters (e.g. concrete properties, traffic, etc.) were not available and the number of bridges investigated is relatively small. As a

result, no definitive conclusion can be drawn with regard to bridge superstructure type. However, this part of investigation indicates that the bridge structure type is definitely a factor that may affect early-age deck cracking and it appears that continuous superstructures are more susceptible to deck cracking than simply-supported spans.

In order to quantify the tendency for shrinkage and traffic-induced strains to cause cracking in bridge decks of continuous superstructures, a finite element simulation focusing on a typical precast girder two-span continuous superstructure bridge was conducted. The finite element model was calibrated using the in-situ field load testing data. Two HL-93 truck loading models were simultaneously applied to the model to study the traffic load-introduced strains. Temperature load was used to represent strains induced by drying shrinkage in order to evaluate tendency for shrinkage introduced tensile strains in the concrete bridge deck to cause premature (early-age) cracking. Finite element analysis shows that traffic loading by itself will likely not cause concrete deck cracking. However, the tensile stress introduced by concrete shrinkage may cause transverse cracks as early as 4 to 8 days after placing the concrete deck. Even if the deck is not cracked due to concrete shrinkage, the combination of traffic load and concrete shrinkage appears capable of causing transverse cracking in the bridge deck over interior supports.

The literature review and finite element analysis conducted indicates that concrete shrinkage is a major factor affecting the likelihood and severity of deck cracking. Concrete shrinkage can be related to concrete compressive strength at specific ages. The finite element simulation conducted shows that the tensile stress in concrete deck is affected by the material's modulus of elasticity. When the tensile stress is larger than the tensile strength of concrete, the deck will crack. Therefore, the concrete properties at early ages are very import for studying the deck cracking. Cylinders were collected from two newly constructed bridges in the Milwaukee area (Racine Ave. Bridge and Humboldt Ave. Bridge). The cylinders were tested at different ages. The data from cylinder testing conducted at several time intervals up to 28 days indicates that the unconfined compression strength accrues very quickly. In fact, the target 28-day unconfined compression strength is reached in less than 4-5 days after placement. Elastic modulus and tensile strength also increases with the unconfined compression strength. Such quick development of strength and modulus may cause significant shrinkage and tensile stress in the deck, and therefore may cause cracking in the deck.

The previous research review and the results of this study show that simply supported structures have less cracks than continuous structures. This is because simply supported structures have less constraint on the bridge deck. Therefore, when concrete shrinks, less tensile stress will be introduced.

Therefore, when it is possible, it is recommended to use simply supported bridge superstructure configurations to reduce the tendency for early-age deck cracking.

The FE simulations conducted in this study show that concrete shrinkage can introduce significant tensile stresses in bridge decks within continuous superstructure configurations of sufficient magnitude to cause early-age cracking in the concrete the deck. Therefore, any method that can reduce concrete shrinkage will be helpful to reduce early-age deck cracking. During construction, the concrete should be covered to prevent evaporation, wind-induced evaporation, and sunshine-induced heat gain to reduce shrinkage. Also, mix designs known to have lower tendency for shrinkage should be used. Typically, such concrete has low amounts of cement and relatively low water/cement ratio. Thus, the research results seem to indicate that lower-strength concretes (e.g. 4,000 psi) should have lower tendency for early age deck cracking. As a result, the 28-day strength should be as close to the target level of 4,000 psi. Typical modern bridge decks often have concretes that achieve this magnitude of unconfined compression strength at 3-5 days.

Bridges built before the 1980's appear to have less cracking problems than those built after the 1990's. High strength concrete has seen much wider spread use after the 1990's. Modern bridge construction also includes significant pressure to open bridges to traffic very quickly after deck casting. As a result, unconfined compression strength gain in modern concretes used for bridge decks is very rapid and the targeted 28-day strength is often reached at 3-4 days. Thus, modern bridge deck concrete is trending toward high-strength concrete behavior.

It is well known that high strength concrete has a higher tendency for increased shrinkage, rapid development of unconfined compression strength, and elastic modulus. This likely has a tendency for the formation of larger tensile stress in the bridge deck at early age and therefore, may cause early-age cracking. Therefore, lower strength concrete, especially lower strength development rate at early age should be used whenever the strength is enough for the traffic load requirement. It is also common that actual concrete strength achieved at 28 days is much larger than the design specified strength. Therefore, controlling the strength gain of the bridge deck concrete appears to be of benefit in reducing early-age deck cracking. It is recognized that opening bridges to traffic as early as possible is a necessity. However, a cost-benefit analysis of early opening and long-term degradation due to excessive cracking should be performed.

If it is possible, it is recommended that a longer curing period be provided and opening a bridge superstructure to traffic at later ages of the concrete appears to be beneficial. In such situations, concrete

will have larger tensile strength when the deck is subjected to traffic load. Therefore, it will reduce the possibility of cracking.

This page has intentionally been left blank.

Chapter 1
Introduction

INTRODUCTION

A relatively recent National Cooperative Highway Research Program (NCHRP) study reported that there were more than 100,000 bridges in the United States suffering from early transverse cracks (Krauss and Rogalla 1996). Bridges in Wisconsin also have experienced early-age cracking. There appears to be a trend for new bridge decks in the state of Wisconsin to develop transverse cracks and map cracks in concrete overlays. There are many reasons for concrete bridge deck cracking including constituent components of the concrete, construction method, and superstructure configuration. Cracking in bridge decks can accelerate the penetration of water, sulfates, chloride and other harmful agents, and therefore accelerate the corrosion of steel reinforcement, facilitate early spalling behavior, and as a result, deterioration of the bridge deck. This degradation often requires costly maintenance or repair, and can shorten the service life of the bridge deck. Key factors that lead to early-age cracking have been very difficult to identify. Furthermore, the role of mix design and subsequent specification in leading to early-age cracking in bridge decks has yet to be quantified. Finally, the role of construction practice and superstructure configuration in leading to early-age cracking has yet to be quantified.

OBJECTIVES

The objectives of this research effort are to gain better and more up-to-date understanding of early concrete cracking of bridge decks and overlays; identify the key factors which cause early concrete cracking in the bridge decks in Wisconsin; and provide recommendations for concrete mixture design, construction practice and superstructure configuration and design for future bridge construction to eliminate or reduce early-age concrete cracking. The research also intends to provide recommendations with regard to laboratory and/or field studies, finite element analysis to simulate early-age behavioral characteristics, and analytical studies to estimate the stresses in concrete decks at early ages.

Successful completion of the proposed effort will provide WisDOT with better understanding of the causes of concrete bridge deck early cracking and map cracking in concrete overlays. It will identify the key factors which affect these types of cracking in Wisconsin practice. Finally, the completed research will result in recommendations for concrete mixture design, construction practice and structural design to eliminate or reduce the early cracking in concrete bridge deck and concrete overlay in Wisconsin.

REPORT OUTLINE

The research report includes the results of a comprehensive review of literature addressing the causes of concrete bridge deck cracking. A synthesis of the literature then supports identification of the major variables that are thought to contribute to early-age bridge deck cracking.

Twenty-one bridge variables identified in the literature synthesis are evaluated with respect to the levels deck cracking seen in fifteen bridge superstructures included in the Marquette Interchange in Milwaukee, Wisconsin. The bridge data was collected from the Wisconsin Department of Transportation bridge plans, and the bridge deck conditions were determined from field reports. Crack data and extent was inferred through lineal footage of cracks that required sealing after initial construction. Once gathered, data was correlated to a specific bridge such that each variable could be independently analyzed with respect to the level of cracking. This procedure allowed the role the each variable in the cracking seen on the decks in the Marquette Interchange bridge super-structures to be identified.

The research team also visited thirteen bridges, which were built or re-decked in a period similar to the construction period of the Marquette Interchange. These site visits allowed the research team to investigate and evaluate the cracking levels in the decks in these bridges. The deck cracking in these bridges were grouped into three categories: serious, moderate, and minor to no deck cracking. Conclusions with regard to bridge deck cracking seen in bridges constructed during similar time frame as the Marquette Interchange superstructures are provided.

The tendency for shrinkage and traffic-induced strains to cause cracking in bridge decks of continuous superstructures is evaluated using finite element simulation. The model was calibrated using *in-situ* load test results. The strains and stresses induced in the bridge deck model by an HL-93 truck loading are quantified. Strains induced in the bridge deck resulting from simulation of concrete shrinkage strains are also evaluated.

The literature review and finite element simulation show that concrete shrinkage is a major factor affecting the early-age cracking in bridge decks. Therefore, it appears that concrete properties in early ages appear to be very import for understanding the causes of early-age deck cracking. The research team then collected cylinders from two newly constructed bridge decks in Milwaukee area. These cylinders were tested to identify the rate at which the unconfined compression strength of the concrete increases for the standard WisDOT mixes.

REFERENCES

Krauss, P.D. and Rogalla, E.A. (1996). *Transverse Cracking in Newly Constructed Bridge Decks, NCHRP Report 380*, Transportation Research Board, National Research Council, Washington, D.C.

This page has intentionally been left blank.

Chapter 2
Literature Review

INTRODUCTION

This chapter summarizes the results of a comprehensive literature review on the causes of concrete bridge deck cracking. The review summarizes why concrete cracking is significant and provides insights with regard to the implications of cracking on bridge decks. The formation of bridge deck cracking is then analyzed within the context of loading conditions and volumetric restraints present. Major types of cracks commonly seen on bridge decks are defined based on their orientation. The review concludes with identification of major parameters thought to contribute to early-age bridge deck cracking.

BACKGROUND INFORMATION

Early-age cracking in concrete bridge decks has undergone an increased frequency of occurrence since the late 1980's. The annual direct cost of corrosion in highway bridges in 2002 was $8.3 billion, and indirect costs to users due to traffic delays and lost productivity is theorized to reach up to 10 times that amount (Koch et al. 2002). Cracks often form relatively early in the life of a concrete component. Cracks may form well in advance of a bridge being open to traffic, and sometimes immediately following construction (Schmitt and Darwin 1995; Saadeghvaziri and Hadidi 2002). Department of Transportation (DOT) surveys report that, on average, 42% of bridge decks that show cracking crack within the first week after constrution (Krauss and Rogalla 1996).

A bridge deck's exposure to deicing chemicals often results in cracks growing wider than the 0.18 mm limit often recommended common building design specifications (ACI 1995). This ACI limit is based on the premise that the surface tension of water across a small opening (such as a crack) will provide an impenetrable barrier over the surface of that opening, thereby helping to prevent corrosion and further ingress of moisture into the component. That limit, however, must also take into consideration the possible effects of impact loading (traffic), which may force chloride solutions and other harmful chemicals into the cracks (Keller 2004).

If a crack becomes too large, water and harmful chemicals easily penetrate into the deck, resulting in deterioration of the steel reinforcement and increasing the potential for spalling through the expansive nature of corrosion of the rebar. Chloride-induced corrosion of reinforcing steel is widely accepted as the primary cause of premature deterioration in concrete bridge decks (Keller 2004). Such deterioration can reduce the shear and moment capacity of the reinforced bridge deck. Additionally, as

the iron oxides accumulate around the surface of the steel reinforcing, the corrosion fills the space surrounding the rebar and concrete. When the corrosion exceeds the void space, an expansive force is generated against the surrounding concrete, and therefore causes cracking as seen in Figure 2.1.

Deterioration of the bridge deck can drastically reduce the service life of a bridge, and as a result, increase maintenance and life-cycle cost. Although cracking in bridge decks has been a problem for quite some time, the factors that lead to early-age deck cracking are still not fully understood. The following is a summary of research and findings in the field of bridge deck cracking.

LOADING

Cracking in bridge decks occurs whenever the tensile stress in the concrete exceeds the tensile strength of the concrete. The strength of concrete changes with time, especially in the early stages after the concrete is placed. As such, the tensile stress required to crack the concrete also changes with time, taking more stress to crack the concrete as it matures. It is interesting to note, however, that studies have also shown that as concrete is drying, there is a tendency for the concrete to fail at a tensile stress of 80% of the assumed tensile strength of the concrete at any given time (Grasley 2003).

Direct Loading

Tensile stresses can be created through direct loading, which includes loading applied through traffic and self weight. Although it is generally believed that direct loading does not have a direct impact on cracking, some researchers have suggested that static and dynamic loading of trucks can cause cracking (Ramey et al. 1997). Finite element analysis research has shown an increased tendency for cracking when the stresses developed under dead load and live load exceed 250 psi (Cheng and Johnston 1985). It is also possible that large average annual daily traffic loading (AADT) applied early in the life of a bridge could increase cracking. The traffic loading interacting with the residual stresses built into the concrete during construction may result in additive tensile stress that can exceed the tensile strength of the concrete materials used in the bridge. This assumes that these additive stresses occur before creep would have a chance to “relax” some of the residual stresses (Schmitt and Darwin 1995).

Indirect Loading (Restraint)

Indirect loading results through prevention of free volumetric change within the concrete. This type of loading can be caused by restraint arising from several sources including: girders, shear studs, reinforcement, and abutments (Schmitt and Darwin 1995). Because girders restrain the bottom surface of the bridge deck, the deck is subjected to an eccentric restraint causing both bending stresses and in-plane stresses (Krauss and Rogalla 1996). The external restraint scenario in this situation results in the free volume change of concrete in the deck being prevented along a variety of locations within the

superstructure. The tensile stresses, therefore, cannot relax over time as they would for the case of free shrinkage (Grasley 2003).

Indirect loading can also be caused by internal restraint, including unequal shrinkage caused by differing rates of moisture loss through a bridge deck thickness and temperature gradients throughout the thickness of the concrete bridge deck. In cases of unequal restraint through the height of the concrete deck, it is common for tensile stresses to develop near the surfaces of the deck, while compressive stresses develop in the inner portions of the deck thickness (PCA 1970).

Volumetric Change

When concrete is cast, it can be subject to variations in size and shape, without the addition of physical loading. This variation in size is most commonly due to concrete shrinkage. Shrinkage is generally caused by moisture evaporation, and chemical reactions between varying components of the concrete. Volume changes within concrete are often characterized as occurring in two stages: when the concrete is in a plastic state, or when the concrete has hardened. The concrete migrates from a plastic state to the hardened state as part of the hydration (curing) process.

Plastic Shrinkage

The most common volume change when the concrete is in its plastic state is plastic shrinkage. This shrinkage is caused when free moisture on the surface of the concrete element evaporates more quickly than it can be replaced by bleeding water from within (Schmitt and Darwin 1995). Studies show that the loss of surface moisture is affected by the concrete mix proportions and thickness of concrete (PCA 1957). It has also been suggested that ambient temperature, temperature of the concrete during the curing period, relative humidity, and wind velocity play a large role in plastic shrinkage (PCA 1957). Increases in the rate of evaporation of surface moisture resulting from environment conditions are very important.

Plastic shrinkage is fairly well understood and if proper precautions are taken, its effects can be negated or at least minimized (Schmitt and Darwin 1995; PCA 1957; Saadeghvaziri and Hadidi 2002). The key to controlling of plastic shrinkage lies in controlling the moisture loss. The following construction practices have been recognized to significantly reduce the frequency of cracking arising from plastic shrinkage (PCA 1957):

1. Applying a membrane curing compound as early as possible.
2. Protecting the concrete with temporary coverings or applying a fog spray during any appreciable delay between placing and finishing.
3. Erecting windbreaks to reduce the wind velocity over the surface of the concrete.
4. Providing sunshades to control the temperature at the surface of the concrete.

Settlement Cracking

Settlement cracking is also common when concrete is in a plastic state. This cracking is caused by the tendency for the concrete to sag in between reinforcing bars, creating tensile stresses above each bar. Settlement cracking depends on the size of reinforcing bar, the slump of the concrete, the spacing of the reinforcement, and the cover thickness over the top of the reinforcement in the bridge deck. It has been suggested that paying more attention to the vibration of the concrete and the use of smaller reinforcement bar diameters may help reduce the tendency for settlement cracks to form in the bridge deck (Schmitt and Darwin 1995).

Autogenous Shrinkage

It is still possible for cracks to form in bridge decks when proper precautions are taken to prevent plastic shrinkage and settlement (Holt 2001). Such cracking is attributed to autogenous shrinkage, which is the change in concrete volume that occurs without a loss of moisture. That change in volume occurs as a result of internal chemical reactions within the individual components of the concrete (Schmitt and Darwin 1995; Holt 2001).

In the past, autogenous shrinkage was ignored, as its effects are less in magnitude than drying shrinkage. With increasingly low water/cement ratios being used, increased use of silica fume and other water-reducing admixtures, and the increasing popularity of high performance concretes, researchers have believed that the effects of autogenous shrinkage have increased (Saadeghvaziri and Hadidi 2002; Holt 2001). As autogenous shrinkage is still not fully understood, determining the effects of this shrinkage is still quite difficult. However, research has shown that varying w/c ratios (maintaining equal amounts of cement) and addition of silica fume can increase cracking (Paillere et al. 1989). Figure 2.2 illustrates the impact of varying w/c ratio on concrete cracking (Paillere et al. 1989).

To help further prevent autogenous shrinkage, researchers have suggested focusing more attention on the testing of the individual constituents of the concrete to ensure that there is a low chance of chemical reaction (Schmitt and Darwin 1995). The process of developing concrete however, involves several chemical reactions and without confirming which reactions cause the autogenous shrinkage, it is difficult to focus any type of research.

Drying Shrinkage

Once concrete has attained measurable compressive strength, it is very common for drying shrinkage to occur. This shrinkage is caused by a loss of water volume from the cement paste in the concrete matrix. The concrete matrix includes water stored in small voids (capillaries) within the cement paste and

hardened calcium silicate gel (Schmitt and Darwin 1995; Grasley 2003). The silicate gel is capable of absorbing a large amount of moisture, and because it has a large surface area, it is very susceptible to evaporation and moisture loss once the concrete has hardened (Schmitt and Darwin 1995). While the basic cause of drying shrinkage is known, how to analyze the strains due to this shrinkage and how the shrinkage relates to specific concrete mix designs is not well understood.

The distribution of drying shrinkage (and to a smaller extent all shrinkage) strains throughout the thickness of a bridge deck remains ill-defined. In general, it is assumed that the strain is not uniform through the thickness of the bridge deck. The top surface of the deck will dry faster than the remainder of the deck, and will therefore have the tendency for larger shrinkage strains. The specific distribution throughout the remainder of the deck is unclear. It is generally recommended that this distribution be assumed as linear (Krauss and Rogalla 1996). If the formwork is removed, the strain due to drying alone should be similar in both the top and bottom surface (neglecting the effects of thermal drying). The increased use of stay in place formwork (fiber reinforced polymer and other types) will also create further doubts with regard to the distribution of shrinkage strains throughout the concrete deck thickness.

It has been reported that drying shrinkage is strongly influenced by w/c ratio, volume to surface ratio, and cement type (Saadeghvaziri and Hadidi 2002). Other researchers have suggested that critical parameters are aggregate size and the combined volume of water and cement (Schmitt and Darwin 1995). Despite the varying opinions with regard to concrete mix design, it is generally agreed that slump, cement content, air content, and temperature are critical to characterizing the tendency for drying shrinkage to cause cracking in bridge decks. In addition, it is believed that proper curing practice substantially reduces cracking caused by strains induced in a bridge deck through drying shrinkage. It has been theorized that if the concrete is allowed to gain sufficient strength as shrinkage strains occur, the concrete will be able to withstand the additional stresses without cracking (PCA 1970).

Thermal Contraction After Hydration

The hydration process (cement forming chemical bonds with water or water aids generating chemical bonds between fine and coarse aggregates) results in the temperature of concrete rising after placement. In addition, the modulus of elasticity of the concrete continues to rise as the concrete cures. If the concrete is restrained during the hydration process the cooling of concrete that follows the hydration process can produce tensile stresses (Saadeghvaziri and Hadidi 2002; Schmitt and Darwin 1995). These stresses are thought to produce hard-to-detect micro-cracking, which could weaken the early-age concrete thereby contributing to cracking later in the life of the concrete component (Krauss and Rogalla 1996). Low heat of hydration cement is often used to remedy this problem. However, if low heat cement

generates a rapid early rise in the modulus of elasticity of the concrete, it may not prevent cracking (Saadeghvaziri and Hadidi 2002).

If concrete hardens at a relatively warm temperature, early thermal stresses are increased (Krauss and Rogalla 1996). This is thought to result from the fact that warm temperatures essentially "lock in" stresses into the concrete. As the concrete component cools and attempts to match the surrounding temperature, restraints preventing free movement of the components fibers may lead to cracking.

To ensure protection from thermal contraction, researchers suggest that concrete should be protected (covered) from sudden temperature changes, providing slower cooling rates (Schmitt and Darwin 1995). It has been recommended that the maximum temperature drop during the first 24 hours following the mandatory protection period should not exceed 50°F (Schmitt and Darwin 1995). Others suggest that controlling the mix design is of significance. It is believed that low alkali cement, coarsely ground with high sulfate content, lowers the tendency for thermal contraction (Saadeghvaziri and Hadidi 2002).

Ambient Temperature

Whenever there is restraint imposed on a given volume that attempts to change size or shape, stresses will be developed in the volume if that volume has a material with stiffness. In the case of a bridge deck, ambient temperature can cause both uniform and linear volume changes across its thickness. When seasons change, the ambient air temperature variation will cause a somewhat uniform shrinkage or expansion throughout the entire deck and bridge components. However, the sun will typically heat the surface of the deck more than any other part. As a consequence, the effects of the sun will cause linear variations of strain throughout the deck thickness, with the top of the deck (exposed to the sun) tending to expand more than the rest of the deck.

The concrete deck is therefore exposed to internal restraints, as differing levels within the concrete deck thickness expand or contract at different rates based on their location in the thickness of the deck. In this case, decks would be subject to internal stresses regardless of external restraint. Figure 2.3 shows a plot of an assumed temperature gradient throughout a composite deck and girder (Saadeghvaziri and Hadidi 2002). As shown, there is a steeper gradient in temperature at the top of the deck presumably due to thermal heating, while there is little to no variation in temperature over the height of the girder.

Creep

Creep causes concrete to deform with time under sustained loading (or stress). As a result, it could be surmised that creep reduces deck cracking. It is believed that concretes with high w/c ratios, low strength,

and soft aggregates produce concrete with high creep (Saadeghvaziri and Hadidi 2002). Creep, however, is a long-term effect, and even though some believe the effects of creep can be seen in the first few months after casting, if the cracking occurs in the first few days, creep may be ineffective at reducing cracking.

Despite the long-term effects, creep is believed to dissipate most strains caused by increased temperatures due to hydration (Krauss and Rogalla 1996). Even if creep helps to limit cracking in bridge decks and other concrete components, it would seem counterproductive to develop a concrete solely to encourage creep as a result of detrimental effects on reducing concrete cracking (e.g. increased permanent deformation in the component as a result of flexure).

CRACK CLASSIFICATION

Based on the orientation of cracking in bridge decks, cracks are commonly characterized into five major categories (Schmitt and Darwin 1995): transverse, longitudinal, diagonal, pattern or map, and random. Within bridge decks, transverse cracking is seen as the predominant form of cracking, while longitudinal and diagonal cracks are seen most commonly on slab and bridges with skew, respectively. Map and random cracks are commonly seen on all types of bridge structures.

Transverse Cracks

Transverse cracks, which are roughly perpendicular to the bridge longitudinal axis, are the predominant form of cracking within bridge decks (PCA 1970; Ramey et al. 1997). These cracks appear soon after the casting, and commonly form at the top surface of the bridge deck under which the transverse reinforcement is placed (i.e., the transverse crack is at the same location of transverse reinforcement) (Schmitt and Darwin 1995; Saadeghvaziri and Hadidi 2002). The location of these cracks is quite devastating to the life of the bridge deck. Due to the transverse cracks' location directly over the steel reinforcement, water and deicing chemicals can easily access the reinforcing steel, increasing the steel's rate of corrosion, and therefore decreasing the service life of the bridge. The location of the transverse reinforcing steel near the surface of the deck and the steel's restraint of concrete movement is believed to increase the tensile stress in the concrete at this location, increasing the likelihood of cracking (PCA 1970).

Longitudinal Cracks

Longitudinal cracks are the cracks parallel to the traffic direction. Some researchers observed that longitudinal cracks occur primarily in solid and hollow slab bridges (Schmitt and Darwin 1995). Similar to the transverse cracks, longitudinal cracks tend to form above the top layer of longitudinal steel in solid-

slab bridges, and the restraint provided by the rebar is believed to be a main factor in this form of cracking (PCA 1970).

Diagonal Cracks

Diagonal cracks are commonly associated with bridges with skewe, as the cracks are generally observed in areas of the deck with acute angles (PCA 1970). It is believed that the combined effects of restraint provided at the end of the bridge along with concrete shrinkage, plays a large role in the creation of diagonal cracks.

Pattern/Map Cracks

Pattern or map cracking is a very common form of cracking seen on all types of decks and bridges. Map cracks are often attributed to improper curing (ACI 1990; PCA 1970). As the deck cures, surface moisture is allowed to evaporate too quickly and volumetric change through shrinkage is incited. The restraint against free volumetric change provided by girders and abutments results in prevention of this free volume change and tensile stresses develop. Cracks result and these cracks are usually very shallow in depth and fine in width. It has been suggested that heir limited depth and width leads to cracks that have little effect on the long-term durability of bridges (Schmitt and Darwin 1995). However, this does not take into consideration the possible secondary effects of delamination and concrete spalling that may occur after initial cracking.

VARIABLES CONTRIBUTING TO BRIDGE DECK CRACKING

The factors that contribute to bridge deck cracking still are not fully understood from an analytical perspective. However, the dominant variables felt to contribute most to cracking in bridge decks have been grouped into five categories: material properties, site conditions, construction procedures, design specifications, and traffic and age. Of the five categories, some studies show that concrete properties have the largest affect on deck cracking (Krauss and Rogalla 1996).

Material Properties

The constituent properties of the concrete are the first parameters to be discussed. Variations in these properties can lead to increased shrinkage and the tendency for cracking to form. Each property of concrete will be addressed within the context of generating increased tendency for cracking.

Cement

Many studies have shown that an increase in cement content has a direct correlation to an increase in deck cracking (Krauss and Rogalla 1996; Kochanski et al. 1990). In general, these studies have shown that the maximum amount of cement used should be limited to 600 lb/yd^3 (of concrete), which correlates to at 28-

day unconfined compression strength near 4.5 ksi (Kochanski et al. 1990; Krauss and Rogalla 1996). Several studies have analyzed the effects of varying cement types on deck cracking. It has been accepted that Type II cement helps reduce cracking (Krauss and Rogalla 1996). Researchers generally believe that Type II cement is successful in reducing cracking due to its reduction in early thermal gradient and shrinkage (Saadeghvaziri and Hadidi 2002).

Slump

Despite significant research into the affects of concrete slump on cracking, researchers have yet to identify any definitive trends. Some have found that slump is not related to deck cracking, while others have found that increasing slump actually decreases cracking (Cheng and Johnson 1985). Additionally, in analyzing cracking patterns in existing bridges, it has been found that cracking increases with an increase in slump (Schmitt and Darwin 1995; Krauss and Rogalla 1996). It is assumed that this relationship is based on the effects of higher water/cement content, which correspond to an increase in slump (PCA 1970). The conflicted conclusions in different research indicate that the relationship between concrete slump and deck cracking is unclear and further research is needed.

Admixtures

The effects of concrete admixtures still are not fully understood. In the case of set retarders, researchers have reached different conclusions. While some see no relationship between set retarders and cracking, others encourage their use, believing that the reduced rate of early temperature rise and early gain of modulus of elasticity will help reduce deck cracking (Saadeghvaziri and Hadidi 2002; Krauss and Rogalla 1996). The conflicted conclusions on retarder and some other factors may be due to that the researchers only considered one or few factors. In reality, many other factors were affecting the volumetric change of concrete besides of the factors which were evaluated in those researches. In examining existing bridges, albeit on a very small sample size, some researchers have seen a trend of increased cracking with use of set retarder (Schmitt and Darwin 1995). It is generally agreed that the used of silica fume can greatly increase the occurrence of cracking (Krauss and Rogalla 1996). This is most likely due to the silica fume's tendency to reduce bleeding within the concrete (Schmitt and Darwin 1995).

w/c Ratio

Reduced cracking has frequently been linked to a reduction in w/c ratio (Schmitt and Darwin 1999 and 1995). Water to cement ratios near 0.4 have been recommended as a maximum (Kochanski et al. 1990; Krauss and Rogalla 1996). To help reduce the w/c ratio, some suggest the use of water-reducing admixtures (Saadeghvaziri and Hadidi 2002). However, it has been noted that these water reducers can themselves increase cracking, and therefore they may not be an adequate solution. Moreover, the w/c

ratio vs. cracking relationship is relatively weak, and a correlation to cracking is better seen in a relationship between % volume of water and cement (Schmitt and Darwin 1995).

In existing bridges, much higher levels of cracking have been observed with increased percentage of water and cement total volume. Specifically, cracking drastically increases when the % volume exceeds 27.5% (Schmitt and Darwin 1995). This cracking is most likely correlated to a combination of increased moisture loss, early modulus of elasticity, and restraint of free volumetric change resulting from shrinkage.

Air Content

While air content is considered quite important in cooler climates to help with freezing and thawing, it has also been found that increased air content can reduce deck cracking in warmer climates (Cheng and Johnson 1985). More specifically, a large decrease in cracking has been found when the air content exceeds 6% (Schmitt and Darwin 1995). In general, this should come as no surprise, as an increase in air content most likely comes with a reduction in water content, therefore reducing the drying shrinkage.

Compressive Strength

Increased concrete compressive strength is commonly suggested to be a significant cause of deck cracking (Saadeghvaziri and Hadidi 2002). The correlation between cracking and compressive strength appears to be a reasonable assumption. Increased unconfined compression strength is usually associated with increased cement content, cement paste volume (water and cement), and higher hydration temperatures (Saadeghvaziri and Hadidi 2002; Schmitt and Darwin 1995). An early increase in compression strength is also accompanied by an early rise in modulus of elasticity that would make the concrete more susceptible to cracking in its early stages as shrinkage occurs. Shrinkage strains are generated as the concrete cures and higher compression strength implies higher w/c ratio or cement content and therefore, higher hydration rates thereby consuming water more rapidly. Shrinkage strains can be sufficient to generate stress large enough to crack the concrete, if the modulus of elasticity is large enough thereby leading to sufficient concrete stiffness. The early rise in modulus of elasticity is especially important in early-strength concretes that may achieve their 28-day compressive strength in three to seven days (Krauss and Rogalla 1996).

Poisson's Ratio

With the use of higher strength concrete, there comes an increase in Poisson's ratio. The increase in Poisson's ratio in turn has been shown to cause increased deck stresses (Krauss and Rogalla 1996). Therefore, a decrease in Poisson's ratio would reduce the likelihood of cracking. However, Poisson's ratio for concrete generally ranges from 0.15 to 0.20, with higher-strength concretes having a higher

Poisson's ratio (Krauss and Rogalla 1996). Based on this relationship, it is apparent that a reduction in Poisson's ratio would require a reduction in compressive strength (by decreasing cement content), which would in itself cause a reduction in cracking. Therefore, it is unclear that Poisson's ratio directly increases the tendency for cracking. Furthermore, it seems unlikely that Poisson's ratio could be controlled independently of the 28-day unconfined compression strength.

Aggregates

Type, size, and relative volume of aggregates can all have a large impact on the cracking characteristics of concrete (Saadeghvaziri and Hadidi 2002). As aggregates in concrete help reduce shrinkage, studies show that using the largest possible aggregates (Krauss and Rogalla 1996, PCA 1970), maximizing aggregate volume (Kochanski et al. 1990), and using low shrinkage (low water absorption) aggregate all help to reduce cracking (Krauss and Rogalla 1996, PCA 1970, Saadeghvaziri and Hadidi 2002). In addition, thermally conductive aggregates (aggregates that have been shown to reduce hydration heat and cyclical daily thermal gradients) may lower thermal stresses by lowering the temperature gradient within the concrete, and therefore help reduce cracking (Krauss and Rogalla 1996). In altering the aggregate content of concrete, however, one must keep in mind the minimum compressive strength required of the concrete.

Thermal Diffusivity

Thermal diffusivity in concrete is a measure of how readily heat flows through concrete. A larger value represents quicker heat conduction (Krauss and Rogalla 1996). A concrete with high diffusivitywould have smaller temperature gradients, and in turn lower thermally-induced stresses. Studies have determined that quartzite and limestone aggregate cause the highest diffusivity (Krauss and Rogalla 1996) as shown in Table 2.1.

Epoxy Coated Rebar

Steel reinforcement is often epoxy coated to help prevent corrosion from deicing chemicals, should cracking occur. But research has shown that epoxy coating is often damaged when cracks develop over transverse reinforcement (Kochanski et al. 1990). However, chloride penetration has been shown to have a much more significant effect on epoxy coating. Chloride penetration has been shown to deteriorate the adhesion between the bars and the epoxy; therefore some have suggested the epoxy coating is ineffective, at least as the sole solution to concrete deck cracking (Kochanski et al. 1990).

Site Conditions

Site conditions are also felt to increase the tendency for bridge deck cracking. Site conditions conspire to make controlled curing of the concrete difficult. Controlling the heat and rate of hydration during curing

can be made more difficult through site conditions. Each environment related condition thought to contribute to the likelihood of concrete bridge deck cracking is discussed in the following.

Ambient Temperature

It is logical to assume the ambient temperature range at the time of casting and curing will have an effect on deck cracking as a result of differential shrinkage and thermal contraction. Researchers have noted a significant increase in cracking when the daily temperature range increases, and therefore the following guidelines have been generated to inhibit cracking. The maximum concrete temperature at placement should not exceed 80°F (PCA 1970; Krauss and Rogalla 1996). The minimum ambient temperature should not drop below 45°F (Cheng and Johnson 1985). Sunshades are often used to help regulate these temperatures immediately following casting. In extremely cold temperature ranges, the following recommendations have been provided for durable, high-strength concrete (Cheng and Johnston 1985). Each recommendation is intended to either generate or preserve heat during the hydration process. First of all, the cement content can be increased. This will result in the hydration process being accelerated and more heat being generated. The mixing water can also be heated to provide initial heat for the hydration process. The aggregates can also be preheated. Finally, the forms can be insulated to maintain heat of hydration levels throughout curing.

Concrete Temperature

For different ambient temperatures, minimum mix temperatures should be required to produce good quality of concrete in order to reduce the cracking. Cheng and Johnston (1985) suggest the minimum concrete temperatures for various ambient weather conditions as shown in Table 2.2. It should be noted that the 60 degree Celsius temperature in the lower right hand corner of the table should be 60 degrees Fahrenheith.

Relative Humidity

Some researchers suggest that there is no relationship between relative humidity and deck cracking (Schmitt and Darwin 1995). However, plastic shrinkage is related to evaporation rates and concrete bleeding and therefore, it is possible that low humidity will increase evaporation rates and thus increase plastic shrinkage (Saadeghvaziri and Hadidi 2002). It is imperative curing compounds are not applied before bleeding has ceased and that the procedures designed to facilitate curing are begun immediately following the placement of the concrete (Schmitt and Darwin 1995).

Wind Velocity

Wind velocity is very similar to relative humidity as it relates to concrete cracking. It is theoretically possible that an increase in wind velocity would increase cracking due to an increase in evaporate rate. In

practice, however, wind breaks are used over the surface of concrete, and no relationship has been seen between wind velocity and deck cracking (Schmitt and Darwin 1995).

Evaporation Rate

As previously discussed, evaporation of concrete can play a strong role in plastic shrinkage. It is therefore recommended that the concrete be placed under low ambient evaporation rates. Kochanski et al. (1990) suggests that concrete decks not be poured when a theoretical evaporation rate exceeds 0.25 $lb/ft^2/hr$. The theoretical evaporation rate can be determined from Figure 2.4.

Time of Casting

Several studies have found that mid-evening or night casting can reduce cracking. This may be due to the cooler temperatures experienced at night (PCA 1970; Krauss and Rogalla 1996).

Construction Procedures

Construction procedures can also affect the tendency for cracking in bridge decks. This section outlines conditions related to construction practice that can increase the tendency for deck cracking and outlines past recommendations for controlling cracking in bridge decks.

Curing

At least one study has found that adequate and timely curing is a key factor in reducing cracking (Saadeghvaziri and Hadidi 2002). In general, transportation agencies suggest at least 14 days of moist curing (Krauss and Rogalla 1996). Cracking at this stage is often related to plastic shrinkage, and therefore, PCA (1957) findings are again emphasized:

1. Apply a membrane curing compound, as early as possible. Kochanski et al. (1990) recommends that any membrane be permeable to help reduce temperature.
2. Protect the concrete with temporary coverings or apply a fog spray during any appreciable delay between placing and finishing. During curing it is crucial to keep the concrete moist, and therefore it is suggested that water be sprinkled on the surface of the concrete (PCA 1970), or wetted burlap sacks be placed over the concrete surface (Krauss and Rogalla 1996).
3. Erect windbreaks to reduce the wind velocity over the surface of the concrete.
4. Provide sunshades to control the temperature at the surface of the concrete.

Pour Sequence

It is often difficult to evaluate the effects of pour sequence on bridge decks. In general, when sections of concrete are initially placed, they may be thought of as “cantilever” sections. When these sections are

made "continuous," the stresses in each section will redistribute (Issa 1999). Accordingly, special attention must be paid to the pouring sequence.

Although pouring sequences are specified in bridge plans, contractors nevertheless often employ their own pouring sequence (Schmitt and Darwin 1995). These new sequences must be approved by the engineers, but frequently they are not recorded. Given the limited data available on the subject, researchers have found varying levels of importance in pouring sequence and its relationship to cracking.

Some research suggests that deck cracking in continuous superstructure systems is most likely to occur in the positive moment region of the first span poured (Cheng and Johnston 1985). Some researchers credit this phenomenon to the fact that, when the concrete is poured in the second span, the deflection in the first span will actually be reduced, and therefore the original span is subject to an initial deflection larger than the final deflection as shown in Figure 2.5. It is also possible that this change in deflection combined with the increasing modulus of elasticity of the concrete will contribute to cracking. Issa (1999) has also hypothesized that initially placing concrete in positive moment regions will also reduce deck cracking over interior supports. In the case of multiple-span bridges, research has been done to determine the order in which the positive regions of the spans should be poured (see Figure 2.6).

The pouring sequence accepted by the Wisconsin DOT is shown in Figure 2.7. Finite element analysis has shown that increasing the length of the initial concrete pour (in positive moment regions) can reduce the residual dead load deck stresses by up to 70% throughout the deck, and has been shown to leave a majority of the deck in residual compression, as opposed to tension (Cheng and Johnston 1985).

Pour Rate

Kochanski et al. (1990) recommends that concrete should be placed at a rate greater than 0.6 span lengths per hour. He theorizes that the pouring of adjacent concrete could cause a change in curvature of the girder, therefore disturbing the previously poured concrete after it has already begun to set. If the concrete is poured too slowly, the concrete will gain a significant amount of strength, and therefore be subject to larger stresses due to imposed deformations.

Some research has shown that increasing pour length causes an increase in the number of cracks per pour. Table 2.3 provides observations assembled by Cheng and Johnston (1985). The data in Table 2.3, however, can be quite deceiving. A longer pour, by their definition, will cover a larger portion of the deck, and therefore it is to be expected that a larger portion of deck will contain more cracks. Accordingly, it is more beneficial to focus on the number of cracks per lineal foot of concrete, rather than

pour length. Table 2.4 indicates that there is no correlation between pour length and cracking (Cheng and Johnston 1985).

During placement and finishing, concrete tends to consolidate within the formwork and around reinforcing steel. During this consolidation, voids and cracks may form in areas in which reinforcing bars or formwork prevents the concrete from freely consolidating (Krauss and Rogalla1996). Testing has shown that, to prevent these voids and cracking, a minimum of three vibrators should be used for placement rates averaging 22 m^3/hr (Krauss and Rogalla 1996). This recommendation, however, seems rather arbitrary.

Deck Formwork

Researchers have had difficulty determining the effects of form type on deck cracking. In general it has been found that there is no significant difference between stay in place (SIP) forms and removable forms in terms of cracking (Cheng and Johnson 1985). But other research has suggested there may be increased cracking with SIP forms due to a non-uniform shrinkage profile (Krauss and Rogalla). At the same time, however, those researchers acknowledge that removable forms allow for an increased drying rate (drying from both sides) which may cause additional cracking.

Superstructure Configuration

Superstructure configuration parameters have also been examined with regard to the tendency for cracking to form in bridge decks. This section outlines past research that examined the role of these parameters in increasing the tendency for bridge deck crack formation.

Girder Type

Past research efforts suggest that decks on steel girders crack more frequently than decks supported by concrete (reinforced or prestressed) girders (Krauss and Rogalla 1996; PCA 1970; Cheng and Johnson 1985). In general, concrete girders conduct heat more slowly than their steel counterparts. As a result, there are lower temperature gradients throughout the superstructure height, and in turn, lower thermal stresses generated. Some researchers suggest that cast-in-place concrete girders in particular have the best crack performance of all girders (Krauss and Rogalla 1996). However, cracking occurs on decks supported by all types of girders, and therefore girder type is only one of many factors that may affect cracking.

Overlays

Past research suggest that there has been no appreciable difference in cracking when comparing monolithic deck and the deck with concrete overlay in existing structures (Schmitt and Darwin 1995).

Deck Thickness

A reduction in cracking can be seen with an increase in deck thickness. Researchers recommend decks with a thickness of at least 6 ¼ in (French et al. 1999), and more specifically a thickness of between 7 ½ and 9 in (Kochanski et al. 1990; Krauss and Rogalla 1996). These recommendations are consistend with WisDOT's current practice. Theoretically, this increased thickness will provide more concrete area to resist tensile forces and require less transverse steel (Kochanski et al. 1990). The increased deck thickness will also lower the volume of steel used, when compared to the volume of concrete. The lower ratio of steel to concrete volume will also allow the deck to become less congested, and therefore it will have a better chance to consolidate properly.

Deck Top Cover

There appears to be a strong correlation between top cover and cracking. However, it is a rather complicated mechanism and still not fully understood. An increase in top cover would help reduce the possibility of settlement cracking, however at the same time it would also increase the distance of the steel from the surface, therefore reducing its effectiveness in controlling the width of cracks that form. While researchers cannot agree on a proper cover depth, departments of transportation often recommend a minimum and maximum cover of 1.5 in. and 3.0 in. respectively, while Schmitt and Darwin (1995) and Ramey et al. (1997) concur that a cover of 2.5 in. minimizes cracking. The Wisconsin Department of Transportation currently recommends a top cover of 2.5 in., which agrees with the previous findings.

Reinforcement

Researchers have found that bar size, spacing, and distribution all affect the cracking tendency of concrete decks (Saadeghvaziri and Hadidi 2002). In general, increased bar sizes and spacing tends to result in increased cracking (Schmitt and Darwin 1995). However, the increase in cracking due to spacing may simply represent the fact that increased spacing implies increased bar sizes. A maximum top transverse bar size of No. 5 (Kochanski et al. 1990; Ramey et al. 1997), or even No. 4 (Krauss and Rogalla 1996) is recommended at a spacing less than 6 in. (Schmitt and Darwin 1995). In fact, research has shown that the top reinforcement does not contribute (significantly) to the strength of the deck (Newhook et al. 2002), and therefore minimizing bar size and maximizing spacing is a higher priority (French et al. 1999). Current U.S. design specification (AASHTO 2006) provisions for crack control have been established with maximum bar spacing provisions designed to limit crack width.

Longitudinal bars are believed to help control deck stresses, and therefore it is advantageous to increase the amount of longitudinal steel (Krauss and Rogalla 1996; PCA 1970; Kochanski et al. 1990). If large stresses develop while the concrete is still in a plastic state, the longitudinal steel is of little value.

In addition, to gain any true benefit with respect to cracking, this increase in longitudinal steel must be done without increasing bar size, i.e., the increase of total steel area should be done by increasing the number of rebars with small diameter instead of using larger rebars. Contrary to the previous findings, Saadeghvaziri and Hadidi (2002) actually found that any increase in longitudinal steel increases deck stresses and cracking. In either case, special attention should be paid to rebar at splice locations, as these effectively act as an increase in bar size (PCA 1970).

Skew

No direct relationship between deck skew and cracking has been obtained. However, an increase in cracking has been seen when the transverse steel is placed parallel to the deck skew (Kochanski et al. 1990). Skew angle can result in acute angles in the concrete deck and cracking has been observed when this angle results in adhesion resisting free shrinkage during curing. Cracking related to skew angle is limited to these acute-angle corner locations in the deck.

Span Length

There appears to be no relationship between bridge superstructure span length and cracking in bridge decks (Saadeghvaziri and Hadidi 2002; Schmitt and Darwin 1995). However, modern precast concrete girders are resulting in span lengths never seen prior to the year 2000. These increased span lengths may require evaluation of this parameter.

Flexibility

Research has generally shown that flexibility of the bridge superstructure has no effect on the formation of transverse and other cracks (PCA 1970; Cheng and Johnston 1985; Kochanski et al. 1990). However, finite element modeling illustrated that increasing the ratio of girder moment of inertia to deck moment of inertia (maintaining an equivalent composite section moment of inertia) can increases deck stresses (Saadeghvaziri and Hadidi 2002). Therefore, some researchers recommend the relative flexibility between the deck and girder may play a role in deck cracking.

Span Type

Figure 2.8 illustrates fundamental superstructure configurations often used in bridges. Research efforts have been undertaken to evaluate the effects of simply supported bridge superstructures versus vs. continuous bridge superstructure configurations (Keller 2004).

Simply supported girder configurations (Figure 2.8) have large positive moments near girder mid-span. Theoretically, the bending moment decreases to zero as one moves toward the end supports. Continuous superstructure configurations include girders that act as continuous beams over multiple

interior supports. The continuous superstructure configuration includes a reduction in the positive moment near mid-span of the girders when compared to simply supported superstructure configurations. However, there is a large negative moment created in the girders over the intermediate supports. These negative moments cause tensile stresses in the deck, which can cause deck cracking when vehicle loads are present. Therefore, researchers suggest the use of simple span superstructure configurations as opposed to a continuous bridge design (Keller 2004; Krauss and Rogalla 1996; Schmitt and Darwin 1995).

The usual construction practice for precast, prestressed concrete girders includes simple spans during deck placement that then become continuous under vehicle loading. The increasing length of spans feasible with deep precast girders (e.g. 72'', 80'') may result in increased rotational demand at the ends of these girders during deck placement. This increased span length combined with standard practice that includes concrete pilasters at interior piers cast integrally with the concrete deck suggests that deck cracking over interior piers may become more prevalent.

Girder Spacing

Finite element models have shown that increasing girder spacing will reduce cracking, due to the reduction of restraints (i.e. girders) at the base of the deck (Saadeghvaziri and Hadidi 2002). However, analysis of existing bridges has shown that there is a strong correlation between an increase in transverse beam spacing and an increase in the severity of deck cracking (Keller 2004). Researchers attribute this correlation to the additional stress generated from increased flexural bending (Buckler et al. 2000). However, if reduced spacing implies additional girders, it would also make sense that the more restraints (i.e. girders) that are present, the higher the level of stress that will develop, as the girders will prevent expansion or contraction of the concrete at the base of the deck.

Supports and Restraint

It is generally accepted that the more restraint the end conditions apply, the more cracking that will occur (e.g. decks on "fixed-end" girders crack more than pin-ended girders). In this case, a "fixed-end" girder is meant to imply that the end of the girder is built into the abutment wall, and the end diaphragm is cast around the girders. Therefore, there is a relatively larger restrain on the girder. However, it is still considered as simply supported in design and analysis of the bridge. Figure 2.9 illustrates such a "fixed-end" girder.

Characterizing the restraint characteristics at the ends of girders in bridge superstructures has been done using a beta (β) ratio (French et al. 1999). This restraint coefficient is defined as the ratio of cross-sectional area of a steel girder, to the effective area of the concrete slab. β values less than 0.05 indicate limited restraint (low probability of premature deck cracking), while β values greater than 0.12

indicate substantial girder restraint, and therefore a much higher probability of premature deck cracking (French et al. 1999). Figure 2.10 illustrates the restraint coefficient beta (at midspan) vs. the cracking condition of steel girder bridges.

The rating scale used in the Figure 2.10 was developed using the following guidelines (French et al. 1999):

- 9—no cracks;
- 8—few single cracks < 0.75 mm (0.03 in.) wide;
- 7—single cracks with a crack width < 0.75 mm (0.03 in.) and crack spacing greater than approximately 1.82 m (6 ft);
- 6—areas with high crack density; crack width < 0.75 mm (0.03 in.) and crack spacing between approximately 0.91 m (3 in.) and 1.82 m (6 ft) [or single transverse cracks with a crack width > 0.75 mm (0.03 in.)];
- 5—areas with a high crack density and a large crack width; crack width > 0.75 mm (0.03 in.) and crack spacing closer than 0.91 m (3 ft).

Figure 2.10 illustrates a general trend of increased cracking with increased β values (i.e. increased end restraint). However, one should note that the low-correlation coefficients in Figure 2.10 were not unexpected, as transverse bridge cracking is assumed to be the result of a combination of variables.

Construction Joints

For construction joints to be effective, they must be designed to properly transfer tensile forces from traffic loading. When concrete barriers are cast and placed, the bridge deforms, creating a given curvature in the barriers. Due to the barriers' added height, the barrier deforms with a larger curvature, and therefore larger tensile stresses. In negative moment regions especially, if the joint is not properly able to transfer the tensile forces, the forces are simply transferred to the deck at the locations of the joint, hence helping to increase cracking (Kochanski et al. 1990). The weight of typical barriers and the fact that all girders in the superstructure will act compositely during barrier placement suggest this is not the case.

Support Bearing

In general, girders bear on either steel bearings or elastomeric pads. Previous research suggests that girders with elastomeric bearing pads are more likely to crack (Saadeghvaziri and Hadidi 2002). However, in analyzing the different bearing pads, researchers noted that elastomeric pads were usually used in conjunction with end diaphragms cast around girders (Saadeghvaziri and Hadidi 2002).

Consequently, it is difficult to determine if the additional cracking was simply caused by the end restraints resulting from the diaphragms/pilasters.

Traffic Loading and Age

Past research efforts suggest that there is a weak correlation between increased annual average daily traffic (AADT) and increased cracking (Schmitt and Darwin 1995). As previously discussed, it is possible that the traffic loading in conjunction with the residual stresses built into the concrete during construction may result in additive tensile stresses that, when combined, exceed the tensile strength of the concrete. At such an early age, creep would not have a chance to "relax" some of the residual tensile stresses (Schmitt and Darwin 1995).

SUMMARY

Previous research shows that both direct and indirect (restraint) loading cause tensile stresses within the concrete, which may exceed the tensile strength of the concrete. When the tensile strength is exceeded, cracks will begin to develop. Based on bridge deck exposure to deicing chemicals, cracks may allow harmful chemicals to easily penetrate the deck, corroding the rebar and increasing the maintenance and life-cycle cost of the bridge structure.

The cracks in bridge decks are categorized into five major groups: transverse; longitudinal; diagonal; map; and random. While the factors that contribute to bridge deck cracking still are not fully understood, the variables thought to causing cracking can be grouped into five categories: material properties; site conditions; construction procedures; design specifications; traffic and age. Material properties play the largest role in concrete cracking. It is crucial that concrete be properly cured. This includes the application of curing compounds, covering of the concrete to prevent excessive evaporation, wind breaks, and sunshades. If cured properly, plastic shrinkage can essentially be eliminated.

While increased compressive strength may be beneficial in bridge design, the increase in cement associated with additional compressive strength has been shown to be a major factor in deck cracking. It is therefore suggested that the amount of cement be limited to 600 lb/yd^3 of concrete. In addition, it is suggested that the water/cement ratio not exceed 0.4. However, current research has also suggested that it may be more crucial to limit the total volume percentage of cement and water. With this in mind, it is suggested that the total percent cement and water not exceed 27.5%.

A significant increase in cracking has also been seen with increased air content. Therefore, to reduce cracking, total air content should not exceed 6%. It is also suggested that the theoretical

evaporation rate not exceed 0.25 lb/ft^2/hr. Currently, the Wisconsin Department of Transportation limits this value even further, suggesting a maximum evaporation rate of 0.15 lb/ft^2/hr.

The Wisconsin Department of Transportation has recommended that while pouring the concrete deck in superstructure configurations that include steel girders, the positive moment regions of the deck should be poured first. In addition, in these steel girder configurations it is suggested that the rate of placing concrete shall equal or exceed 1/2 the span length per hour, but need not exceed 100 cubic yards per hour. The pour rate and pour sequence regulations are implemented due to the hardening and variation in curvature of the deck during the pouring process.

It has been seen that bridge decks in a wide variety of superstructure configurations can all exhibit premature or early age cracking. However, simply-supported bridge superstructures appear to have a reduced tendency for early age cracking in the deck. A top reinforcement clear cover of 2.5 inches is also suggested (as recommended in AASHTO 2006). It should be noted that increasing and decreasing clear cover from frequently recommended values have both been shown to exhibit increased tendency for cracking.

REFERENCES

AASHTO (2006). *AASHTO LRFD Bridge Design Specifications*, 2006 Interim Revisions, 3rd Edition, Washington D.C.

ACI (1995). *Control of Cracking in Concrete Structures (AC1 224R-90)*, Manual of Concrete Practice, Part 3, American Concrete Institute, Detroit MI, 43 pp.

Buckler, J.G., Barton, F.W., Gomez, J.P., Massarelli, P.J., and McKeel, W.T. (2000). *Effect of Girder Spacing on Bridge Deck Response*, VTRC 01-R6, Virginia Transportation Research Council, Charlottesville, VA, 2000.

Cheng, T.T.H. and Johnston, D.W. (1985). *Incidence Assessment of Transverse Cracking in Concrete Bridge Decks: Construction and Material Considerations*, Report No. FHWA/NC/S5-002 Vol. 1, North Carolina State University at Raleigh, Department of Civil Engineering, 232 pp.

French, C., Eppers, L., Le, Q., and Hajjar, J.F. (1999). "Transverse Cracking in Concrete Bridge Decks", *Transportation Research Record*, No. 1688, p 21-29.

Grasley, Z.C. (2003). "Relative Humidity, Drying Stress, Gradients, and Hygrothermal Dilation of Concrete," PCA R&D Serial No. 2625, University of Illinois at Urbana-Champaign, Portland Cement Association.

Holt, E.E. (2001) "Early Age Autogenous Shrinkage of Concrete," Technical Research Centre of Finland, VTT Publications, University of Washington.

Issa, M.A. (1999). "Investigation of Cracking in Concrete Bridge Decks at Early Ages", *Journal of Bridge Engineering*, Vol. 4, No. 2, p 116-124.

Keller, W.J. (2004). "Effect of Environmental Conditions and Structural Design on Linear Cracking in Virginia Bridge Decks," Virginia Polytechnic Institute and State University.

Koch, G.H., Po, M., Broongers, H., Thompson, N.G., Virmani, Y.P., and J. H. Payer, *Corrosion Cost and Preventive Strategies in the United States*, Report No. FHWA-RD-01-156, Federal Highway Administration, McLean, VA.

Kochanski, T., Parry, J., Pruess, D., Schuchardt, L., and Ziehr, J. (1990). *Premature Cracking of Bridge Decks Study*, Wisconsin Department of Transportation.

Krauss, P.D., and Rogalla, E.A. (1996). *Transverse Cracking in Newly Constructed Bridge Decks*, NCHRP Report 380, Transportation Research Board, Washington, DC.

Newhook, J., Tadros, G., Hussan, T., and Kroman, J. (2002). "Improving the Durability of Concrete Bridge Deck Slabs".

Paillere, M., Buil, M., and Serrano, J.J. (1989). "Effect of Fiber Addition on the Autogenous Shrinkage of Silica Fume Concrete", *ACI Material Journal*, Vol. 86, No.2, pp. 139-144.

PCA (1970). *Durability of Concrete Bridge Decks*, Final Report, 35 pp.

PCA 1957. *Plastic Shrinkage*, Bulletin 81.

Ramey,G.E., Wolff, A.R., and Wright, R.L. (1997). "Structural design actions to mitigate bridge deck cracking", *Practice Periodical on Structural Design & Construction*, Vol. 2, No.3, pp. 118-124.

Saadeghvaziri, M. and Hadidi, R. (2002). *Cause and Control of Transverse Cracking in Concrete Bridge Decks*, Final Report, FHWA-NJ-2002-19.

Schmitt, T.R. and, Darwin, D. (1995). *Cracking in Concrete Bridge Decks*, Report No. K-TRAN: KU-94-l, Final Report, Kansas Department of Transportation.

Schmitt, T.R. and, Darwin, D. (1999). "Effect of Material Properties on Cracking in Bridge Decks", *Journal of Bridge Engineering*, Vol. 4, No. 1, pp. 8-13.

Table 2.1 Aggregate Effect on Diffusivity (Krauss and Rogalla 1996)

Coarse aggregate	Diffusivity of concrete m^2/day (ft^2/day)
Quartzite	0.129 (1.39)
Limestone	0.113 (1.22)
Dolomite	0.111 (1.20)
Granite	0.096 (1.03)
Rhyolite	0.078 (0.84)
Basalt	0.072 (0.77)

Table 2.2 Minimum Concrete Temperatures (Cheng and Johnston 1985).

Weather Condition	Minimum Mixing Temperature		
	Thin Sections (4"-8") (100 to 200 mm)	Moderate Sections (8"-24") (200 to 600 mm)	Mass Sections (> 24") (> 600 mm)
30°F to 40°F -1°C to 4°C	60°F 16°C	55°F 13°C	50°F 10°C
0°F to 30°F -18°C to -1°C	65°F 18°C	60°F 16°C	55°F 13°C
Below 0°F Below -18° C	70°F 21°C	65°F 18°C	60°C 16°C

Table 2.3 Average Cracking Based on Pour Length (Cheng and Johnston 1985).

Average Number of Cracks Per Pour As A Function of Pour Length

"Avgcrack" = Average No. of Cracks in Each Length Group
"Avgcrack" = Major Crack + Minor Crack/4.0

POUR LENGTH GROUP	OBSERVATIONS	MEAN	STANDARD DEVIATION	MINIMUM VALUE	MAXIMUM VALUE
30	53	1.207	3.035	0	14.500
50	68	1.603	4.711	0	28.500
70	91	3.498	5.846	0	33.500
90	63	6.607	7.489	0	33.000
110	32	3.828	5.768	0	24.500
130	14	4.750	7.320	0	28.250
150	6	4.875	2.893	1.000	8.750
170	1	7.000	-	7.000	7.000
190	2	14.750	1.061	14.000	15.500
310	2	12.125	13.258	2.750	21.500

Table 2.4 Cracks per Linear Foot Based on Pour Length (Cheng and Johnston 1985).

Transverse Cracks Per Linear Foot vs. Pour Length for All Pours Observed

Pour Length Group	Observations	Mean	Standard Deviation	Minimum Value	Maximum Value
30	53	0.037	0.095	0	0.414
50	68	0.030	0.084	0	0.511
70	91	0.048	0.079	0	0.440
90	63	0.074	0.083	0	0.362
110	32	0.036	0.054	0	0.222
130	14	0.036	0.058	0	0.225
150	6	0.032	0.019	0.006	0.057
170	1	0.040	-	0.040	0.040
190	2	0.074	0.005	0.070	0.078
310	2	0.040	0.044	0.009	0.071

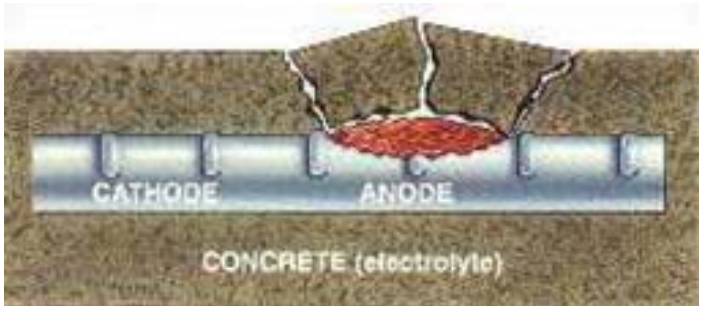

Figure 2.1 Concrete Cover Deterioration (Keller 2004).

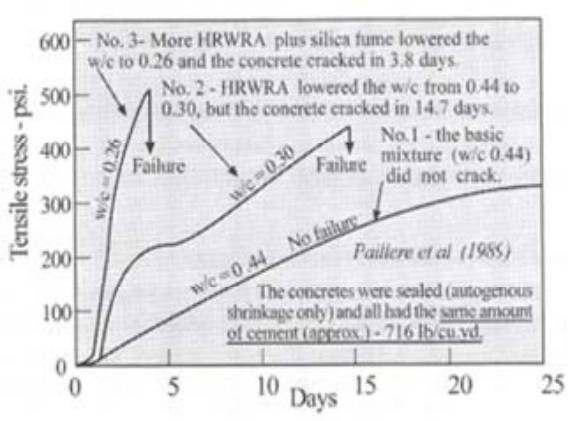

Figure 2.2 Effect of Varying w/c ratio on Cracking (Paillere et al. 1989).

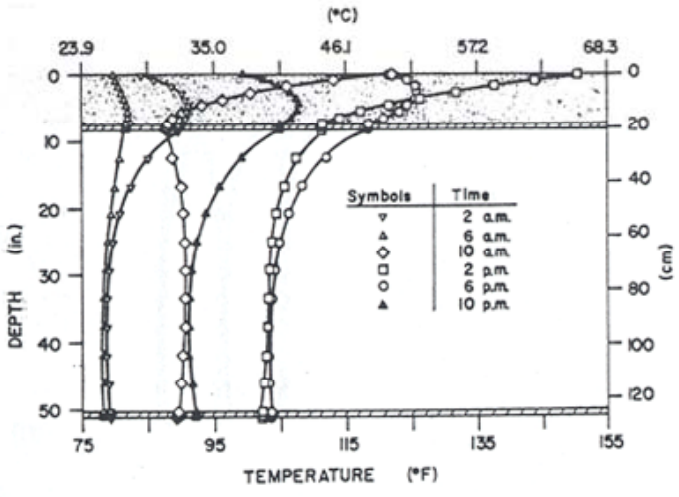

Figure 2.3 Thermal Gradient (Saadeghvaziri and Hadidi 2002).

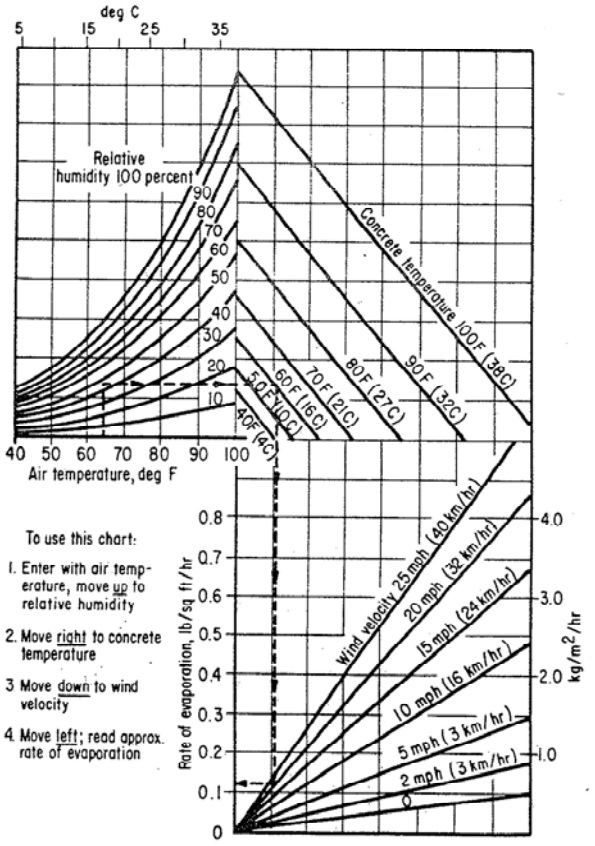

Figure 2.4 Evaporation Rate Chart (Kochanski et al. 1990).

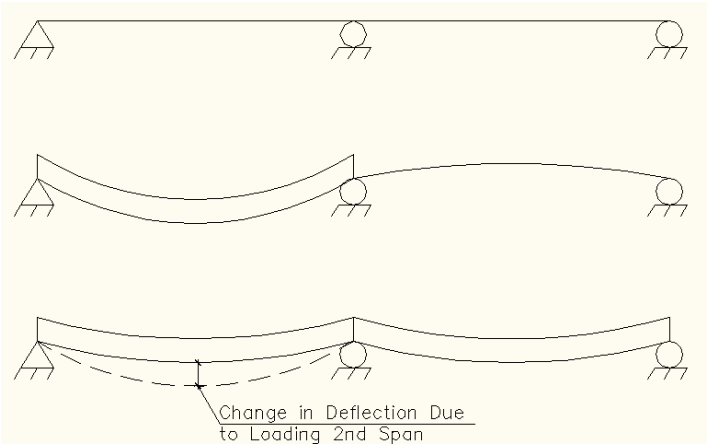

Figure 2.5 Deck Deflection due to Pour Sequence (Cheng and Johnston 1985).

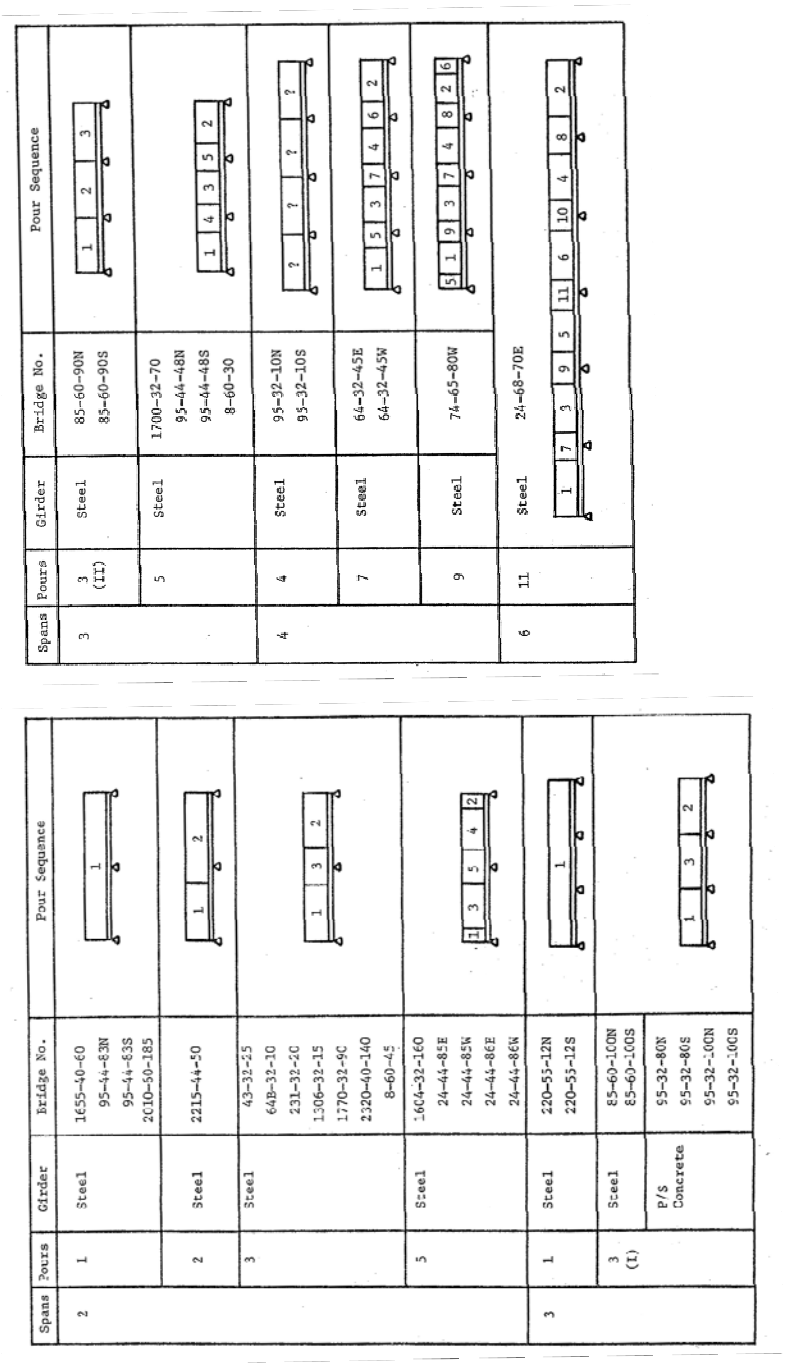

Spans	Pours	Girder	Bridge No.	Pour Sequence
2	1	Steel	1655-40-60 95-44-83N 95-44-83S 2C10-50-185	1
	2	Steel	2215-44-50	1 2
	3	Steel	43-32-25 64B-32-10 231-32-2C 1306-32-15 1770-32-9C 2320-40-140 8-60-45	1 3 2
	5	Steel	1604-32-160 24-44-85E 24-44-85W 24-44-86E 24-44-86W	1 3 5 4 2
3	1	Steel	220-53-12N 220-53-12S	1
	3 (I)	Steel	85-60-100N 85-63-100S	1 3 2
		P/S Concrete	95-32-80N 95-32-80S 95-32-100N 95-32-100S	
3	3 (II)	Steel	85-60-90N 85-60-90S	1 2 3
	5	Steel	1700-32-70 95-44-48N 95-44-48S 8-60-30	1 4 3 5 2
4	4	Steel	95-32-10N 95-32-10S	? ? ? ?
	7	Steel	64-32-45E 64-32-45W	1 5 3 7 4 6 2
	9	Steel	74-65-80W	5 1 9 3 7 4 8 2 6
6	11	Steel	24-68-70E	1 7 3 9 5 11 6 10 4 8 2

Figure 2.6 Pour Sequence (Cheng and Johnston 1985).

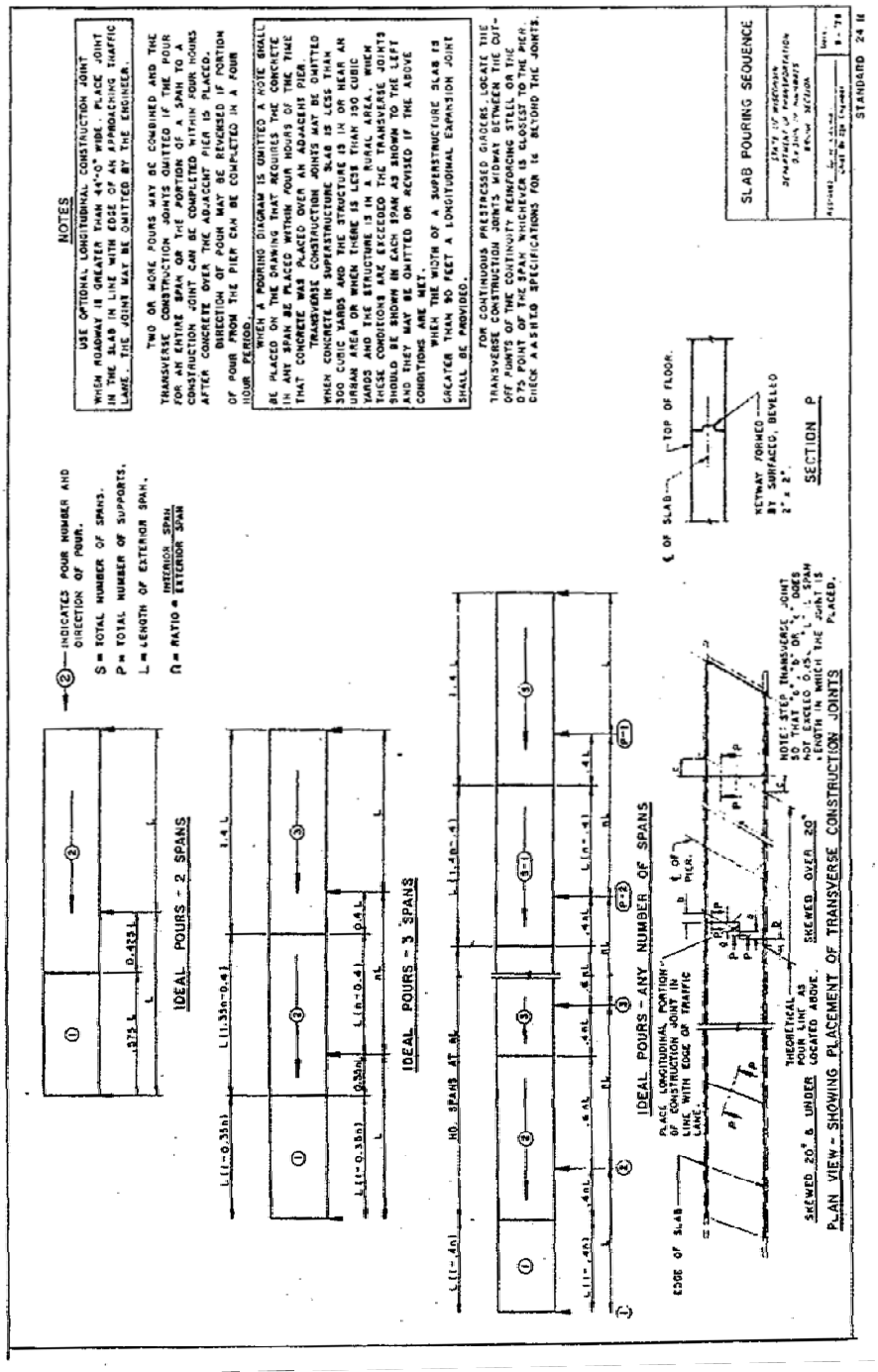

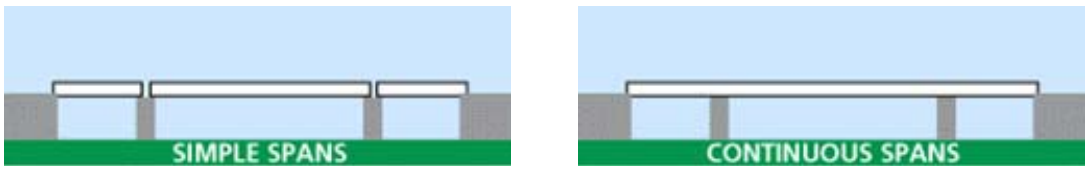

Figure 2.8 Span Configurations (Keller 2004).

Figure 2.9 **"**Fixed End" Restraint (Saadeghvaziri and Hadidi 2002).

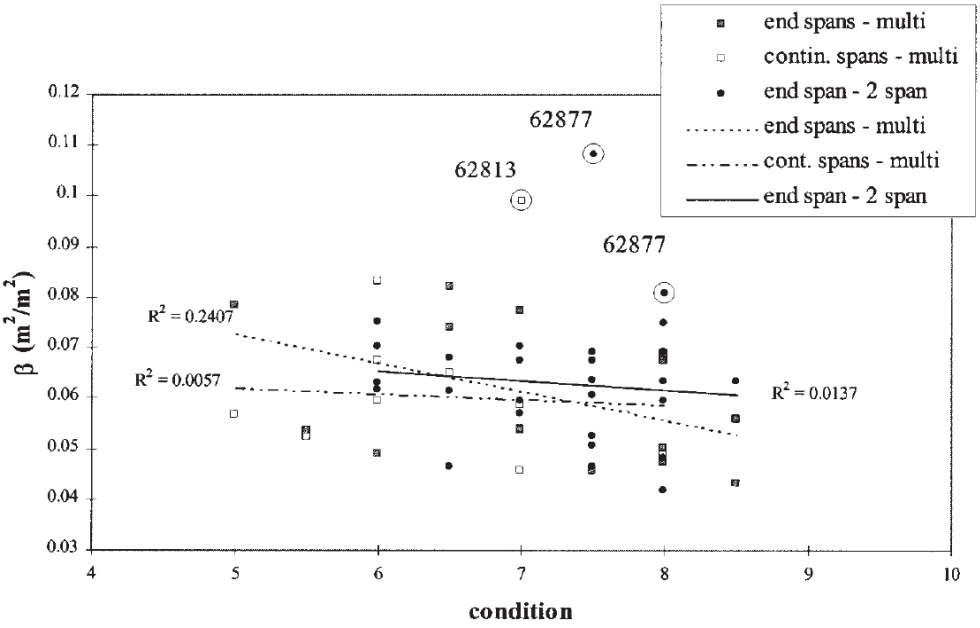

Figure 2.10 Restraint Coefficient Beta (French et al. 1999).

This page has intentionally been left blank.

Chapter 3
Marquette Interchange Data Synthesis

INTRODUCTION

This chapter provides evaluation of the effects of the bridge variables discussed earlier on the level of deck cracking seen in 15 bridge superstructures located in the Marquette Interchange in Milwaukee, Wisconsin. The variables however, do not include all material property variables, as mix design specifics were unavailable. The bridge superstructure data were collected from the Wisconsin Department of Transportation bridge plans, and the site conditions were determined from field reports obtained through WisDOT. Crack data were obtained through the lineal footage of cracks that required sealing (feet of cracking per bridge) after initial construction. Unfortunately, data regarding the specific location, or type of crack on each bridge super-structure was unavailable. However, once gathered, all data were correlated to a specific bridge such that each variable could be independently analyzed with respect to the level of cracking. This procedure allows for the determination of what, if any, role the variable played in the cracking seen on the decks in the Marquette Interchange bridge super-structures.

BACKGROUND

In May of 2008, the Wisconsin DOT finished construction on the Marquette Interchange. The core of the interchange consisted of 20 individual bridge structures. Figure 3.1 illustrates the Marquette Interchange project, specifically the core structures. Initially, very little cracking was observed in the bridge decks, however immediately following the opening of the interchange, significant amounts of cracking in the decks was observed.

In this study, crack data were recorded for 17 of the 20 bridge structures. Data were recorded as a length of cracking over the entire bridge structure (e.g. linear feet of cracking per bridge). The design and construction specifications were available for an additional 17 structures (not corresponding to the 17 structures for which crack data were available). When the crack data were combined with the design/construction data, it was possible to analyze and compare 15 of the bridge super-structures with respect to the cracking observed. The data for these 15 bridges are shown in Table 3.1.

The concrete used in all bridge decks on all 15 structures consisted of WisDOT MC 330 mix design as shown in Table 3.2. The values shown in Table 3.2 were the specifications for each mix; however, the actual values (including specific admixtures) in the corresponding bridge structures are unknown. It was therefore assumed that concrete mix for each bridge deck was approximately equal to

MC 330. In addition, it was assumed that the MC 350 mix design was used for the 2 inch overlay found on each of the decks.

To obtain data corresponding to each structure, the Wisconsin DOT bridge plans were utilized, along with field notes made by the construction team. Figure 3.2 represents a sample of the notes used to complete the study. The 15 structures were analyzed using the following 21 variables: Cracks/ft, Cracks/ft^2, Span Type, Curved vs. Straight, Number of Spans, Bridge Length, Average Span Length, Average Deck Width, Deck Area, Mix Design (MC 330), Air Entrainment, Concrete Slump, Placement Rate, Air Temperature, Humidity, Wind, Concrete Temperature, Evaporation Rate, Deck Thickness, Girder Type, and Bearing.

VARIABLES AFFECTING DECK CRACKING IN MARQUETTE INTERCHANGE

Each variable or parameter described above was considered in detail with respect to its likely effect on cracking in the Marquette Interchange bridge decks. This section outlines a review of each parameter and its likely role in facilitating early-age cracking.

Cracks/ft and Cracks/ft^2

Once significant cracking was observed, the cracks were sealed with TK-9030 Crack and Joint Repair (Low Viscosity Urethane/Polyurea Hybrid). The crack data therefore, were compiled based on the lineal footage of cracking that was sealed. As such, it is important to make several observations. Initially, it is possible that some cracks were not amenable to sealing, and/or additional cracking developed since the original cracks were sealed. In addition, when analyzing the lineal footage of cracking, it is impossible to determine what type of cracking occurred, over which sections of the bridge the cracking occurred, or at what spacing interval the cracking occurred.

Initially, the crack data were normalized. In analyzing the linear footage of cracking over a bridge deck, it is logical that a very long and wide bridge would have more cracking than a small 2-lane bridge. This rationale is based on the increased area over which cracking can occur. Therefore, the lineal footage of cracking was converted to feet of cracking per longitudinal centerline length of bridge deck (ft/ft) and feet of cracking per area of bridge deck (ft/ft^2).

Figure 3.3 displays the results for the 15 structures in terms of feet of cracking, based on length, width, and area. As shown in Figure 3.3, the length, width, and area of bridge deck played little to no role (no apparent trends), in the total length of cracking over a given bridge. When the total amount of cracking is evaluated in non-normalized and normalized format, it can be seen that the results are independent of the normalization process as shown in Table 3.3. Based on Figure 3.3 and Table 3.3, it

would appear that no normalization is required, as the three levels of cracking compare quite favorably, and any normalization may inadvertently skew the data.

Continuous vs. Simple Span

The Marquette Interchange core is made up of 20 continuous bridge super-structures. However, each structure is separated by a modular expansion device as shown in Figure 3.4. As such, adjacent continuous superstructures can be considered independent. In analyzing each independent bridge structure, it was assumed that the bridge was continuous unless a specific detail for an expansion joint was noted in the bridge plans. If an expansion joint detail existed, the location of the joint(s) was recorded. In general, the structures were almost exclusively continuous, and therefore it was impossible to compare levels of cracking using this as an evaluation parameter.

In-Plane Girder Curvature

Due to the elaborate nature of the Interchange, quite a few of the structures appear curved (in plan). However, often this curvature was achieved through several straight segmental girder spans. Therefore, a structure is labeled as curved only when the bridge plans specifically denote “curved girders”.
Once again, a majority of the structures were not curved, and curvature in plan was not used as a variable in the analysis.

Number of Superstructure Spans

The number of spans within a given structure was determined directly off the bridge plans. As shown by Figure 3.5, the number of spans within a bridge appears to have little influence over the total length of cracking observed.

Overall Bridge Length

The overall longitudinal length of a given superstructure was recorded as the centerline distance of the bridge deck. As shown in Figure 3.3, the length of bridge deck appears to play no role in defining the amount of cracking in the bridge deck.

Average Girder Span Length

The average span length was determined by dividing the total length of the bridge superstructure along the bridge centerline by the number of spans (ft/span). As expected, because neither the number of spans nor the total longitudinal length of the bridge superstructure appears to influence cracking, the average span similarly has no influence as shown in Figure 3.6.

Deck Width

The deck widths within the Interchange tend to vary quite significantly over the length of a given bridge superstructure. When a constant width exists, the bridge width was recorded as the total width of the deck (including barrier base dimension). Frequently however, the width of bridge deck would vary within a given span. Engineering judgment was applied when a given span included entrance and exit ramps. A variation in deck width often arose due to the addition or subtraction of a lane. The maximum or minimum deck width was selected based on the average width on the remainder of the structure (e.g. whether the lane was added or subtracted on the remainder of the bridge), as shown in Figure 3.7. Once an "average" width was determined on every span, the width was then multiplied by the length of the span and then divided by the total centerline length of the bridge. This process was completed for all spans, adding the results to develop a total "average width". Figure 3.3 illustrated that the average width appears to have no influence over the level of cracking in the bridge deck.

Deck Area

The deck area was calculated as the total centerline length of the bridge superstructure, multiplied by the average width of the bridge determined using the previously outlined procedure. Once again, as shown in Figure 3.3, the deck area appears to have no influence over the level of cracking seen.

Mix Design

The mix design for the bridge deck was assumed to be the MC 330, as previously discussed. The 2 inch overlay present on all of the structures was not considered, however, some research has shown that the overlay present on a bridge structure slightly increases the frequency of cracking (Schmitt and Darwin 1995). Since the proportion of the constituent materials used by the concrete supplier to satisfy the MC330 mix design specifications was not known, the mix design was not used as a variable in the analysis.

Air Entrainment

For each deck pour, a varying amount of concrete was taken and sampled. The percent air entrainment was recorded as the average air entrainment over all the concrete samples taken from a given deck. In doing so, it is assumed that more samples were taken on larger deck pours, and therefore the average air entrainment on the larger deck pours plays a larger factor in the average. In addition, if no test values were available, the standard 4.5-7.5% air entrainment value was averaged (6%). As shown in Figure 3.8, there appears to be no relationship between bridge deck cracking and air entrainment.

Slump

Concrete slump was averaged and calculated in the same manner as the air entrainment. Once again, if no samples were available, the average or goal values (which varied by structure) were assumed. In general, the slump of concrete in all structures was approximately 3.5 in. Due to the close proximity of the values, it was difficult to compare cracking between the structures, and therefore no relationship between slump and cracking was obtained. Figure 3.9 confirms this.

Placement Rate

Placement rates were recorded in the construction logs. In general, for each deck pour, an initial placement rate goal (yd/hour) ranging from 40-130 (usually varying by 20 yd/hour) was recorded. A peak placement rate was also listed, denoting that the rate of placement would increase during the casting period. An average placement rate was recorded as the average of the minimum and maximum placement rate over a given pier-to-pier span. The average was then combined with all the spans in a given structure to obtain the superstructure average. There were frequent instances where no placement rates were given and complete data sets could not be assembled. Therefore, no analysis was completed to quantify placement rate as an indicator of deck cracking.

Air Temperature, Humidity and Wind Velocity

The air temperature (°F), humidity (%), and wind speed (mph) were all calculated in a similar manner to the air entrainment and concrete slump. In each case, recorded values were simply averaged. It appears as though an increase in air temperature, humidity, and wind may all show a decrease in cracking as shown in Figure 3.10. This finding is counterintuitive, as air temperature, humidity, and wind could all increase drying and/or plastic shrinkage. However, one might also conclude that when conditions that tend to increase drying and plastic shrinkage are present during construction (e.g. increased wind speed), the concrete contractor will take precautions to inhibit the tendency for drying and plastic shrinkage to cause cracking (e.g. install wind breaks). Therefore, it is difficult to isolate these as parameters guilty of causing deck cracking. Furthermore, evaporation rates are computed using these three parameters. As a result, they may actually be more appropriately handled within the context of a single parameter – evaporation rate. In order to accurately validate the apparent “trends” in the data set, more data is required.

Concrete Temperature

Concrete temperature was calculated in a fashion similar to the air temperature, humidity, and wind. In each case, concrete temperatures were recorded for each superstructure, and therefore the values were simply averaged. When the concrete temperature was compared to the length of cracking, it appears as though an increase in concrete temperature may cause a decrease in cracking, as shown in Figure 3.11.

However, this trend was loosely obtained over a relatively small sample size. In addition, very little research has been developed on the relationship between concrete temperature and cracking, and therefore it is difficult to validate this finding.

Evaporation Rate

The evaporation rate during the deck pour was calculated by the field crew at the construction site. The calculations were based on Figure 2.4 contained in the previous literature review, and take into consideration air temperature, relative humidity, concrete temperature, and wind velocity. Figure 3.12 compares the evaporation rate with the total amount of cracking recorded. It indicates that there is no direct relationship between evaporation rate and cracking. At larger evaporation rates however, it appears that there is a decrease in cracking. This is quite counterintuitive, as an increase in evaporation rate would tend to increase drying shrinkage. This trend is most likely due to the small sample size, and can be explained by the slight trend seen in air temperature, humidity, and wind, which all play a role in the evaporation rate calculation. One can also theorize that when the evaporation rates were predicted to be higher in the field, the construction personnel took precautions to inhibit drying shrinkage (e.g. erected windbreaks) and this inhibited cracking.

Deck Thickness

Deck thicknesses were recorded to the nearest half inch. In general, a given structure had a uniform deck thickness (within a small tolerance). However, in some cases the deck actually varied in thickness depending on a given deck pour/section. In this case, an averaging process similar to the averaging process used for the air entrainment was implemented. Figure 3.13 indicates that in general, deck thickness has no relationship to cracking. However, it can be noted that on the largest deck thickness (over 10.5 inches), the most significant cracking occurs. The figure also illustrates that there can be significant variability in cracking for any given thickness (e.g. 9 inches and 10 inches). Without more data, it is impossible to identify any trends.

Girder Type

Girders were divided into three categories: prestressed concrete girders (Ps-C), steel plate girders (S-PG), and steel box girders (S-BG). In two structures (structures B-40-1312 and B-40-1412), the structure was made of seven continuous “units”. In each case, six of the units consisted of prestressed concrete girders, while the remaining unit consisted of steel plate girders. For the analysis process, the entire structure was assumed to be composed of prestressed concrete girders. In general, it would be beneficial to analyze each type of structure (prestress/plate/box) individually to determine if any of the previous factors affect one type of bridge in particular. Currently however, the sample data is far too small to divide the data into individual segments, as each category of girder would consist of three to four data points.

Bearing Condition

Bearing conditions were determined through analyzing the bridge drawings. In general, four bearing conditions were identified: rocker, guided, fixed, and elastomeric bearing pad. Several of the bearing conditions could be present in a single structure. Therefore, each bearing condition was given a respective numerical value. Previous research, suggests that deck cracking increases with an increase in restraint at girder (or span) ends (Saadeghvaziri and Hadidi 2002).

The corresponding numerical label was assigned an increasing value as the girder end rotational restraint characteristics increased. For example, the rocker base restraint was given a numerical value of "1", as it is the closest restraint to an idealized pin support (applying the least restraint). The detail for a rocker can be seen in Figure 3.14. The guided support appears somewhat equivalent to a rocker support, however it is assumed that the guiding plates would apply additional restraint (Figure 3.15). The guided support was therefore given a numerical value of "1.5". The fixed support (Figure 3.16) was given a numerical value of "2.0", due to the increased restraint. Previous studies have shown that bearing pads tend to cause the most cracking due to their increased restraint (Issa 1999). Therefore, the elastomeric bearing pads (Figure 3.17) were given a numerical value of "2.5".

The numerical value of each restraint was added over the course of a structure, at which point the total was divided by the number of supports. Therefore, an overall value of 1 represented a structure consisting of all rocker supports, and a value of 2.5 represented a structure consisting of all elastomeric bearing pads. All other values would fall within this limiting range. At this point, it is also important to note that only the restraint due to bearing conditions is being considered. The fixity or restraint due to diaphragms, or girders being directly cast into piers is being neglected.

When the previously described numerical values were calculated and compared to the corresponding cracking values, Figure 3.18 was obtained. Contrary to previous research, it would appear as though the bearing condition or configuration has no effect on the cracking of a given bridge structure (at least for the small sample size considered here). Figure 3.18 does indicate, however, that there is significant variability in the extent of deck cracking for a given averaged support characteristic (e.g. bearing value of approximately 1.5 and 2.5).

SUMMARY AND CONCLUSIONS

From the data gathered, it appears to be impossible to definitively identify the variables that play a significant role in concrete deck cracking in the Marquette Interchange superstructures. Of the 21 variables analyzed, only concrete temperature appears to be a weak indicator of deck cracking. However, the limited number of data points makes definitive statements regarding this parameter ill-advised.

To properly determine the cause of deck cracking, additional data will be required and it is likely that some degree of simulation will be required (e.g. FE simulation of bridge superstructures under traffic loading or simulation of the effects of shrinkage induced strains). The 15 data points alone are not enough to develop proper relationships with the crack data. In addition, the 15 structures analyzed are all quite similar in construction and design. Therefore, it is crucial to know what types of cracks occur and at what locations they occur to properly determine their causes.

Traffic data and structure age are beneficial in analyzing the crack data. In the case of the Marquette Interchange, the structures were built and opened over a four-year window. As such, each structure was subject to varying traffic loads, and freezing/thawing periods. It is possible that either of these variables may increase deck cracking.

While additional data are required, it may be more significant to obtain specific mix design information used by concrete contractors to satisfy the WisDOT specified mixes and concrete properties at early ages to supplement the data that has already been collected. Currently, concrete material properties are believed to be the most significant cause of deck cracking, as they relate to plastic and drying shrinkage (Schmitt and Darwin 1995). Without specific constituent material information and concrete properties, it is impossible to accurately examine the effects of concrete on cracking, and therefore the most significant cause of deck cracking may be neglected.

REFERENCES

Issa, M.A. (1999). "Investigation of Cracking in Concrete Bridge Decks at Early Ages", *Journal of Bridge Engineering*, Vol. 4, No. 2, p 116-124.

Saadeghvaziri, M. and Hadidi, R. (2002). *Cause and Control of Transverse Cracking in Concrete Bridge Decks*, Final Report, FHWA-NJ-2002-19.

Schmitt, T.R. and, Darwin, D. (1995). *Cracking in Concrete Bridge Decks*, Report No. K-TRAN: KU-94-l, Final Report, Kansas Department of Transportation.

Wisconsin Department of Transportation (WisDOT) (2006). *MC330 Mix Design*, Milwaukee, WI.

Wisconsin Department of Transportation (WisDOT) (2008). *Marquette Interchange Bridge Plans*, Milwaukee, WI.

	Continous	Curved?	Number of Spans	Average Span Length (ft)	Average Width (ft)	Structure Length (ft)	Area (ft^2)	Mix Design
B-40-1322	Yes	No	4	118.25	42.90	473	20291.70	MC330
B-40-285	Yes	No	4	116.25	33.63	465	15635.63	MC330
B-40-1231	Joint at Pier 8	No	12	117.79	42.90	1413.5	60639.15	MC330
B-40-1132	Yes	No	4	137.03	30.00	548.1	16443.00	MC330
B-40-1221	Joint at Pier 5	No	10	204.12	29.90	2041.2	61031.88	MC330
B-40-1111	Yes	No	12	149.19	58.90	1790.24	105445.14	MC330
B-40-1122	Yes	Yes	6	178.26	29.90	1069.5625	31975.46	MC330
B-40-1422	Expansion Joint between span 5 and 6	Yes	9	172.32	42.90	1550.9	66533.61	MC330
B-40-1321	Yes	No	8	187.00	42.90	1496	64178.40	MC330
B-40-1131	Yes	Yes	5	184.29	29.90	921.4375	27550.98	MC330
B-40-1421	3 spans and 6 spans	No	9	131.64	29.90	1184.75	35424.03	MC330
B-40-1123	2-6 Span Continuous Sections	No	12	197.80	44.90	2373.54	106571.95	MC330
B-40-1412	Each unit Continuous	No	41	121.58	64.17	4984.62	319854.28	MC330
B-40-1312	Expansion Joints between units	No	34	107.28	63.45	3647.6333	231434.23	MC330
B-40-1311	No (expansion joint detail, but no location)	No	15	103.73	57.70	1556	89781.20	MC330

	Air Entrainment (%)	Slump (in)	Placement Rate (yds/hr)	Air Temp (°F)	Humidity (%)	Wind (mph)	Conc. Temp (°F)	Evaporation Rate (lb/ft^2hr)
B-40-1322	5.73	3.83	85	50.75	73.75	3.75	70.50	0.0725
B-40-285	6.11	3.48		47.20	82.40	4.80	63.00	0.0520
B-40-1231	6.06	3.33		51.43	61.00	7.00	69.00	0.1100
B-40-1132	6.08	3.33		61.00	68.50	4.00	72.00	0.0600
B-40-1221				40.50	76.50	8.50	65.00	0.0950
B-40-1111	6.05	3.55	89	57.75	60.27	3.32	69.17	0.0538
B-40-1122	6.11	3.58	75	78.78	44.33	3.00	72.17	0.0417
B-40-1422	6.44	3.70		56.10	72.20	7.10	68.40	0.0922
B-40-1321	6.39	3.69	85	55.71	74.57	2.29	67.43	0.0315
B-40-1131	5.86	3.23	80	76.00	72.00	5.50	73.00	0.0400
B-40-1421	5.89	3.23	77.5	53.20	73.80	2.60	73.00	0.0608
B-40-1123	6.23	3.21	80	47.23	65.15	4.92	67.15	0.0785
B-40-1412	6.10	3.43	91	66.69	54.10	4.50	72.00	0.0655
B-40-1312	6.36	3.59	98	63.15	65.14	3.77	71.82	0.0563
B-40-1311	6.63	3.89	96	56.02	67.85	3.91	67.25	0.0540

	Deck Thickness (in)	Girder Type	Bearing	Cracks (ft)	Cracks (ft/ft)	Cracks (ft/ft^2)		
B-40-1322	9.00	Ps-C	1.00	2399	5.072	17.024		
B-40-285	9.00	S-PG	1.50	3760	8.086	34.629		
B-40-1231	9.71	S-PG	1.58	1859	1.315	4.415		
B-40-1132	9.50	S-PG	1.60	200	0.365	1.752		
B-40-1221	9.00	S-BG	1.64	5005	2.452	11.809		
B-40-1111	10.55	S-PG	1.64	23757	13.270	32.443		
B-40-1122	10.00	S-BG	1.64	2303	2.153	10.371		
B-40-1422	10.00	S-BG	1.65	6876	4.434	14.882		
B-40-1321	10.00	S-BG	1.67	11018	7.365	24.722		
B-40-1131	10.00	S-BG	1.67	6624	7.189	34.621		
B-40-1421	9.80	S-PG/BG	1.70	1939	1.637	7.882		
B-40-1123	10.00	S-BG	1.77	14087	5.935	19.034		
B-40-1412	9.05	Ps-C (Unit 4 Steel I-Girders)	2.50	500	0.100	0.225		
B-40-1312	9.36	Ps-C (Unit 4 Steel I-Girders)	2.50	12818	3.514	7.975		
B-40-1311	9.00	Ps-C	2.50	14759	9.485	23.672		

Table 3.2 MC330 Mix (WisDOT 2006)

Mix Design Listing
Actual Batch Weights

Mix #	Description	Cement	Flyash	Water	Sand#1	Sand#2	Stone#1	Stone#2	Admixtures	Air
MC 325	5000# 30% SUPERSTRUCTURE	460 Type I	200 Class "C"	27.0	1,280 Torpedo	0	1,199 Limestone	646 Limestone	Air 5.0 Water Reducer 26	6%
MC 350	5000# OVERLAY	460 Type I	200 Class "C"	27.0	1,401 Torpedo	0	1,647 Limestone	0	Air 5.0 Water Reducer 26	6%
MC 330	5000# 30% SUPERSTRUCTURE	428 Type I	183 Class "C"	27.0	1,297 Torpedo	0	1,217 Limestone	655 Limestone	Air 4.6 Water Reducer 24	6%

Table 3.3 Ranking for Normalized and Non-Normalized Crack Data.

Structure	Cracks (ft)	Cracks/length (ft/ft)	Cracks/area (ft/ft^2)	Ranking (ft)	Ranking (ft/ft)	Ranking (ft/ft^2)
				(Least cracking = 1)	(Least cracking = 1)	(Least cracking = 1)
B-40-1132	200	0.365	1.752	1	2	2
B-40-1412	500	0.100	0.225	2	1	1
B-40-1231	1859	1.315	4.415	3	3	3
B-40-1421	1939	1.637	7.882	4	4	4
B-40-1122	2303	2.153	10.371	5	5	6
B-40-1322	2399	5.072	17.024	6	9	9
B-40-285	3760	8.086	34.629	7	13	15
B-40-1221	5005	2.452	11.809	8	6	7
B-40-1131	6624	7.189	34.621	9	11	14
B-40-1422	6876	4.434	14.882	10	8	8
B-40-1321	11018	7.365	24.722	11	12	12
B-40-1312	12818	3.514	7.975	12	7	5
B-40-1123	14087	5.935	19.034	13	10	10
B-40-1311	14759	9.485	23.672	14	14	11
B-40-1111	23757	13.270	32.443	15	15	13

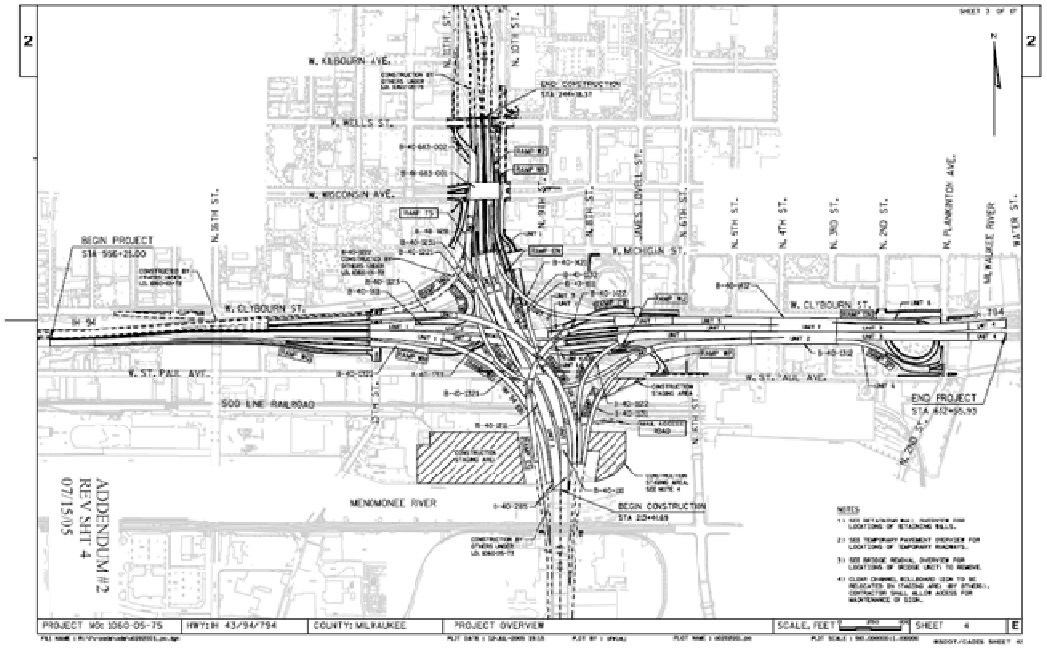

Figure 3.1 Marquette Interchange Core (WisDOT 2008).

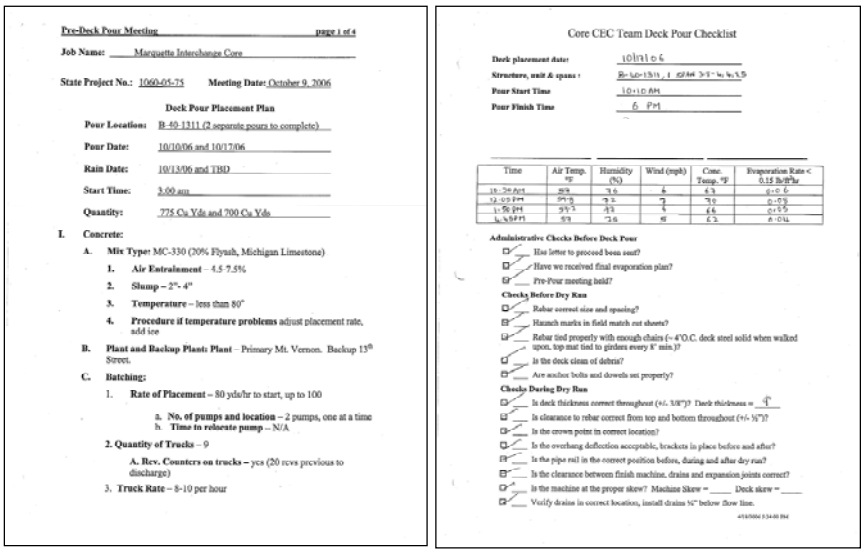

Pre-Deck Pour Meeting page 1 of 4

Job Name: Marquette Interchange Core

State Project No.: 1060-05-75 Meeting Date: October 9, 2006

Deck Pour Placement Plan

Pour Location: B-40-1211 (2 separate pours to complete)

Pour Date: 10/10/06 and 10/17/06

Rain Date: 10/13/06 and TBD

Start Time: 3:00 am

Quantity: 775 Cu Yds and 700 Cu Yds

I. Concrete:

A. Mix Type: MC-330 (20% Flyash, Michigan Limestone)

1. Air Entrainment – 4.5 7.5%
2. Slump – 2"- 4"
3. Temperature – less than 80°
4. Procedure if temperature problems adjust placement rate, add ice

B. Plant and Backup Plants: Plant – Primary Mt. Vernon. Backup 13th Street.

C. Batching:

1. Rate of Placement – 80 yds/hr to start, up to 100

a. No. of pumps and location – 2 pumps, one at a time
b. Time to relocate pump – N/A

2. Quantity of Trucks – 9

A. Rcv. Counters on trucks – yes (20 revs previous to discharge)

3. Truck Rate – 8-10 per hour

Core CEC Team Deck Pour Checklist

Deck placement date: 10/11 to 6

Structure, unit & spans: B-40-1311, 1 span 3-3-4.4.5

Pour Start Time 10:10 AM

Pour Finish Time 6 PM

Time	Air Temp. °F	Humidity (%)	Wind (mph)	Conc. Temp. °F	Evaporation Rate < 0.15 lb/ft²/hr
10:30 AM	85	36	6	63	0.06
12:00 PM	91	32	7	70	0.09
1:30 PM	95	32	5	66	0.09
3 PM	93	36	10	63	0.04

Administrative Checks Before Deck Pour

- Has letter to proceed been sent?
- Have we received final evaporation plan?
- Pre-Pour meeting held?

Checks Before Dry Run

- Rebar correct size and spacing?
- Haunch marks in field match cut sheets?
- Rebar tied properly with enough chairs (~ 4'O.C. deck steel solid when walked upon, top mat tied to girders every 8' min.)?
- Is the deck clean of debris?
- Are anchor bolts and dowels set properly?

Checks During Dry Run

- Is deck thickness correct throughout (+/- 3/8")? Deck thickness = 9"
- Is clearance to rebar correct from top and bottom throughout (+/- ½")?
- Is the crown point in correct location?
- Is the overhang deflection acceptable, brackets in place before and after?
- Is the pipe rail in the correct position before, during and after dry run?
- Is the clearance between finish machine, drains and expansion joints correct?
- Is the machine at the proper skew? Machine Skew = ____ Deck skew = ____
- Verify drains in correct location, install drains ½" below flow line.

Figure 3.2 Field Reports of Marquette Interchange.

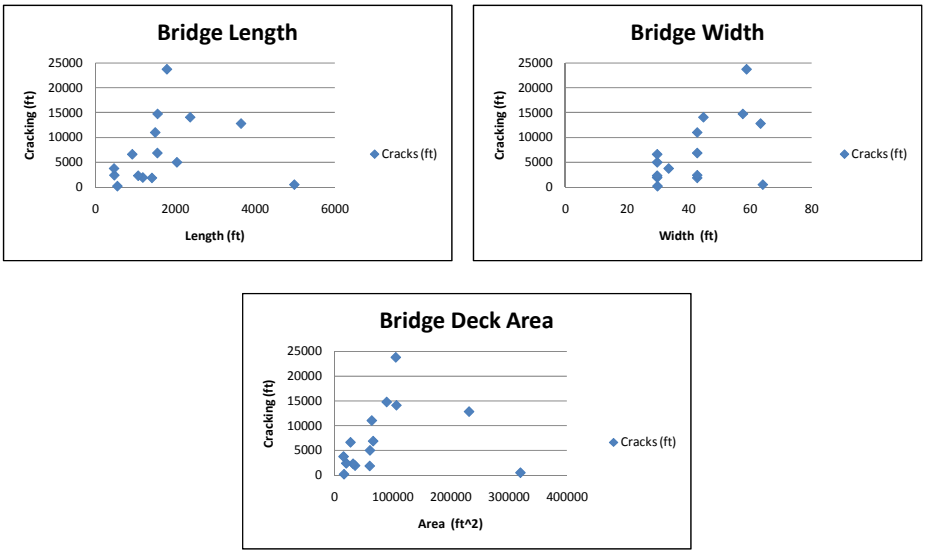

Figure 3.3 Cracking Based on Length, Width, and Area.

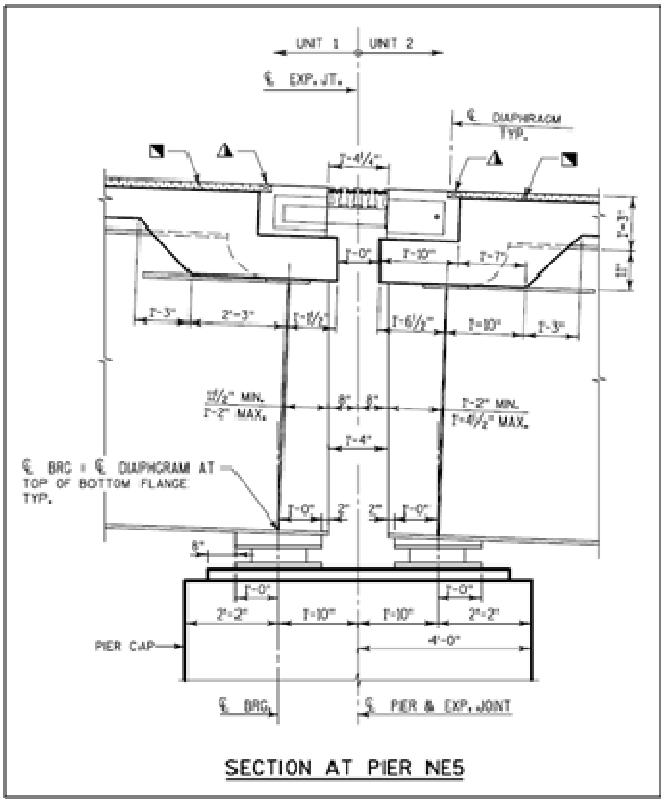

Figure 3.4 Modular Expansion Device (WisDOT 2008).

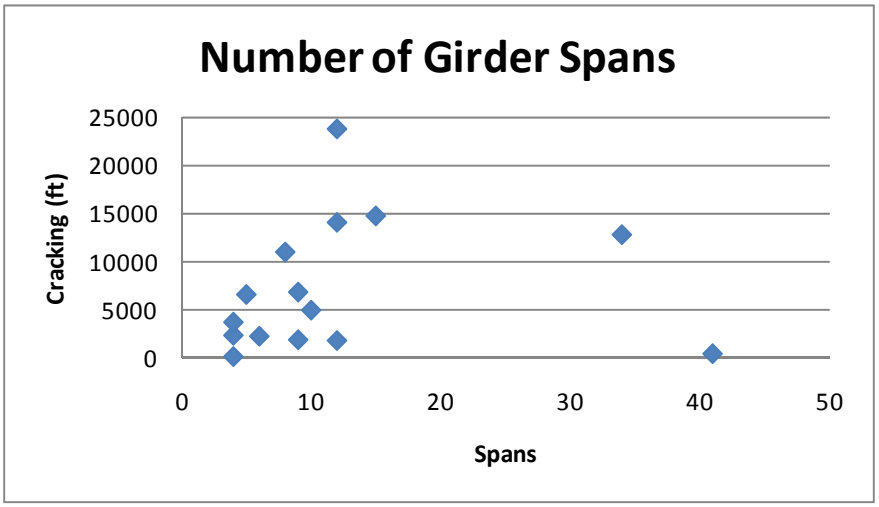

Figure 3.5 Cracking vs. Number of Superstructure Spans.

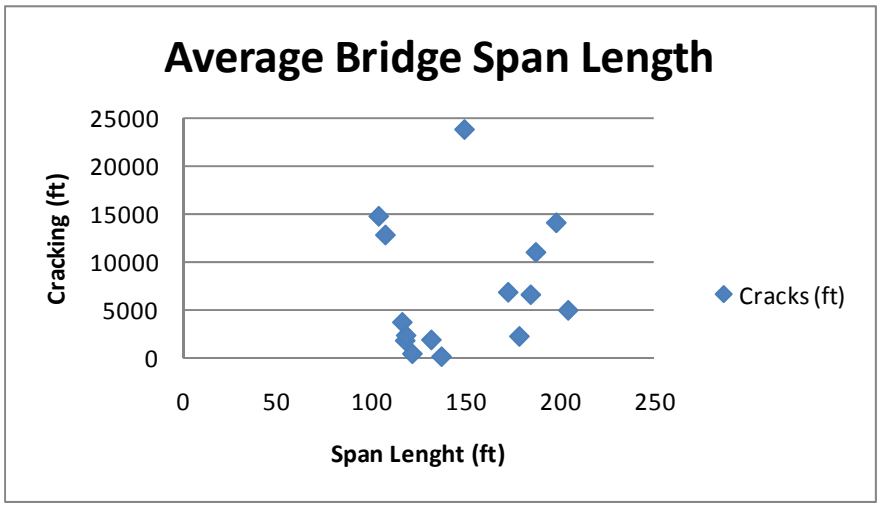

Figure 3.6 Cracking vs. Average Span Length.

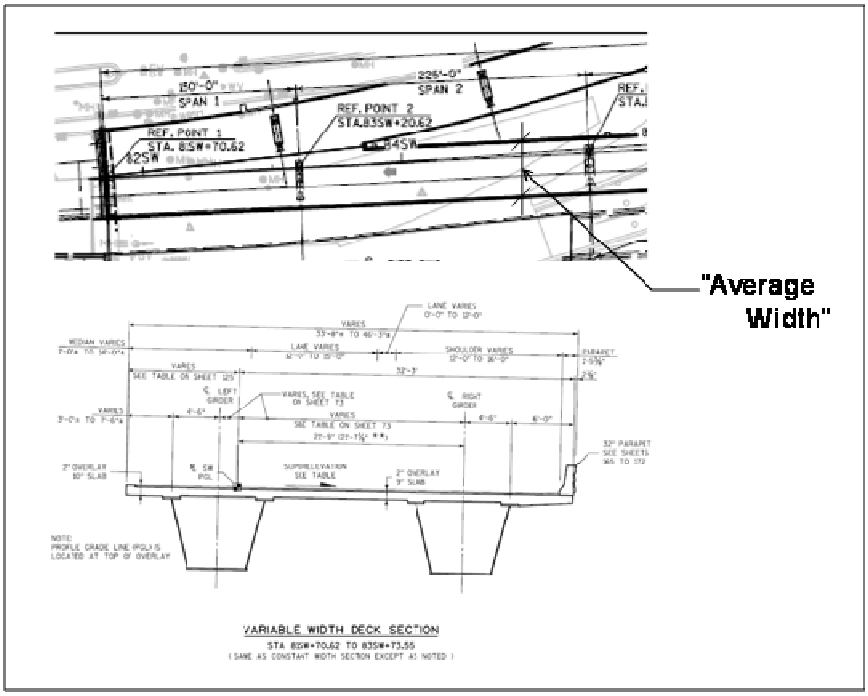

Figure 3.7 Variation in Deck Width (WisDOT 2008).

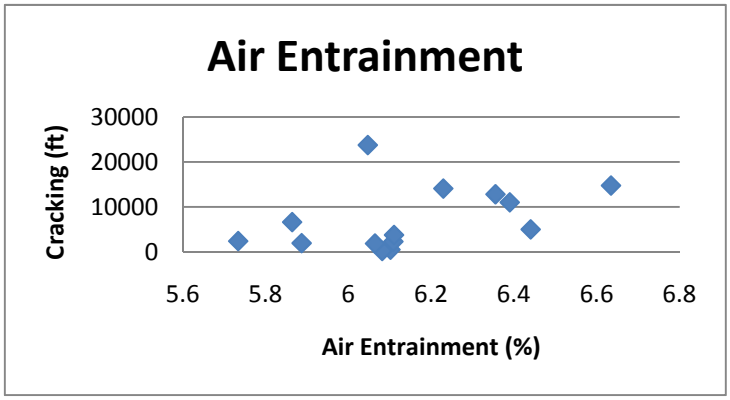

Figure 3.8 Cracking vs. Air Entrainment.

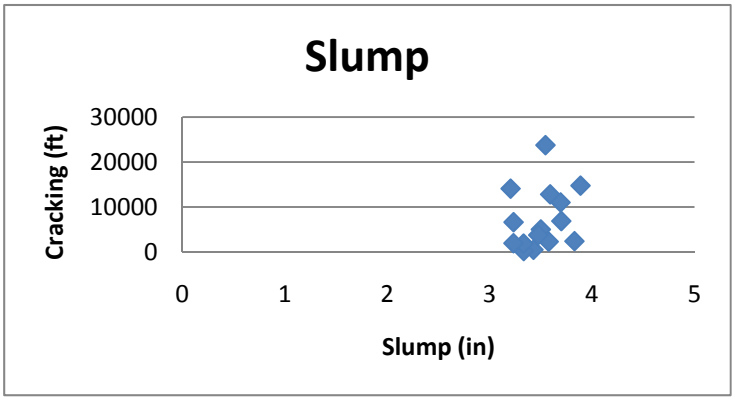

Figure 3.9 Cracking vs. Slump.

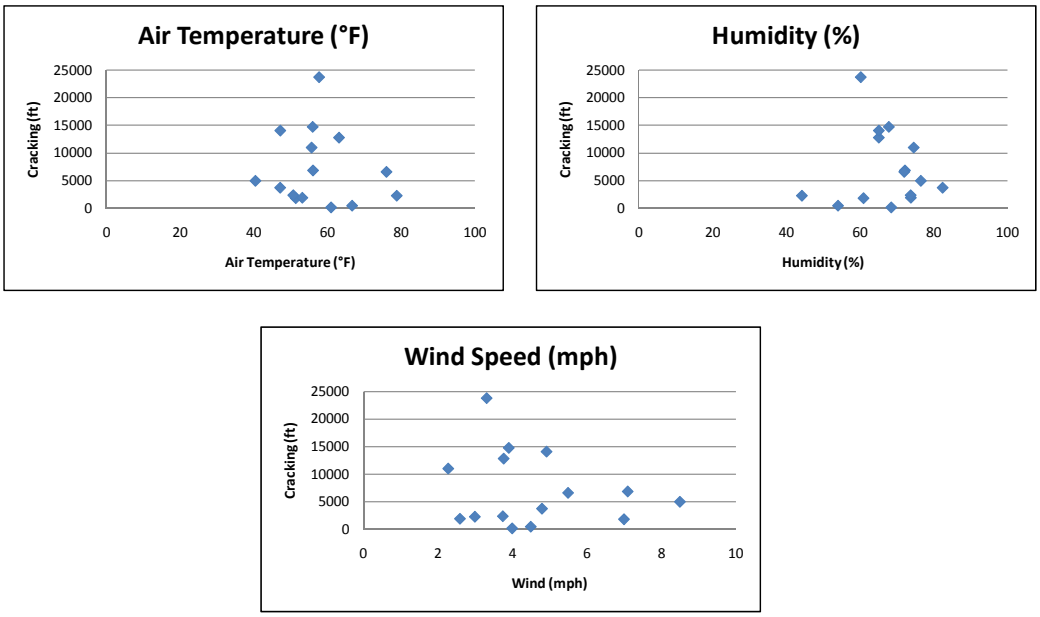

Figure 3.10 Cracking vs. Air Temperature, Humidity, and Wind.

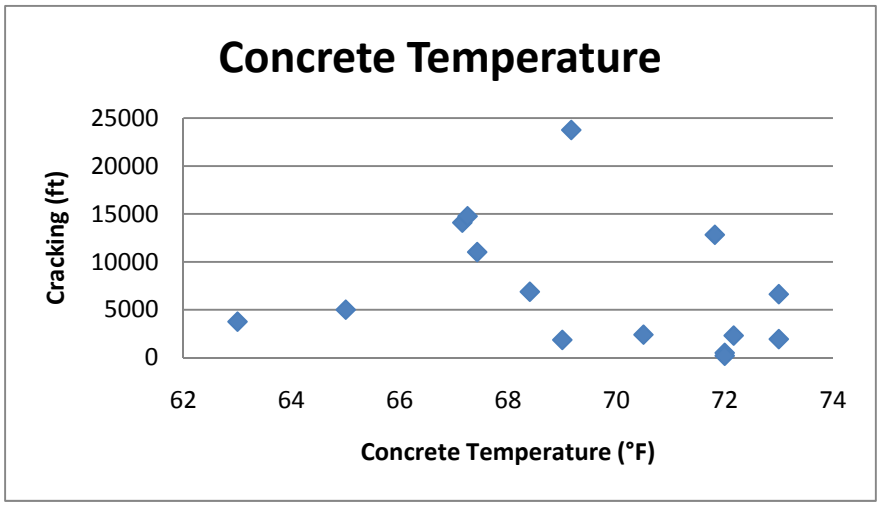

Figure 3.11 Cracking vs. Concrete Temperature.

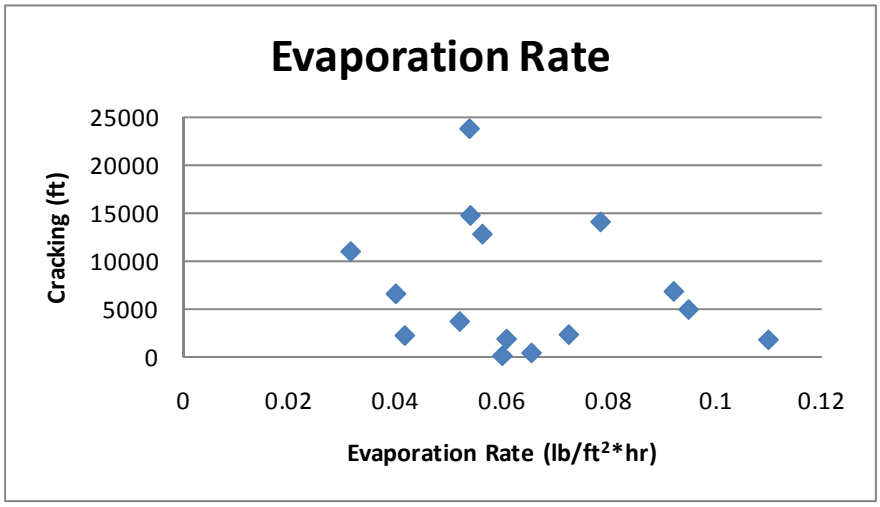

Figure 3.12 Cracking vs. Evaporation Rate.

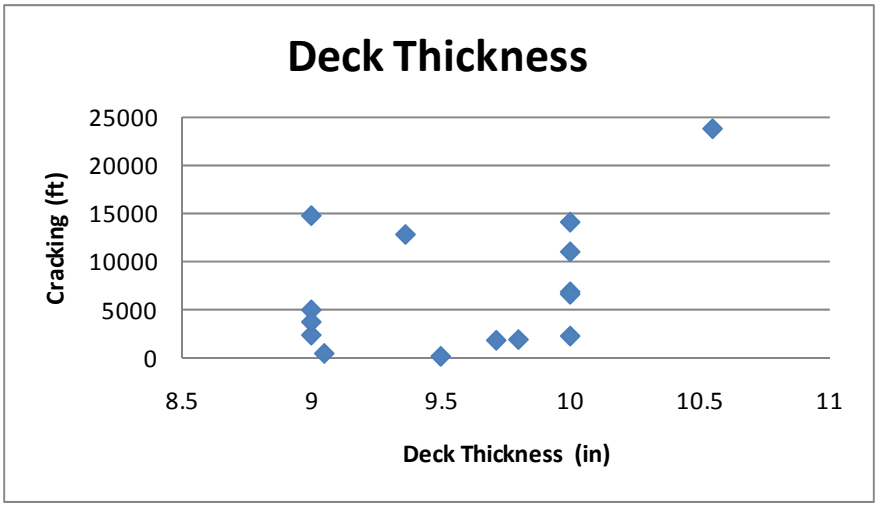

Figure 3.13 Cracking vs. Deck Thickness.

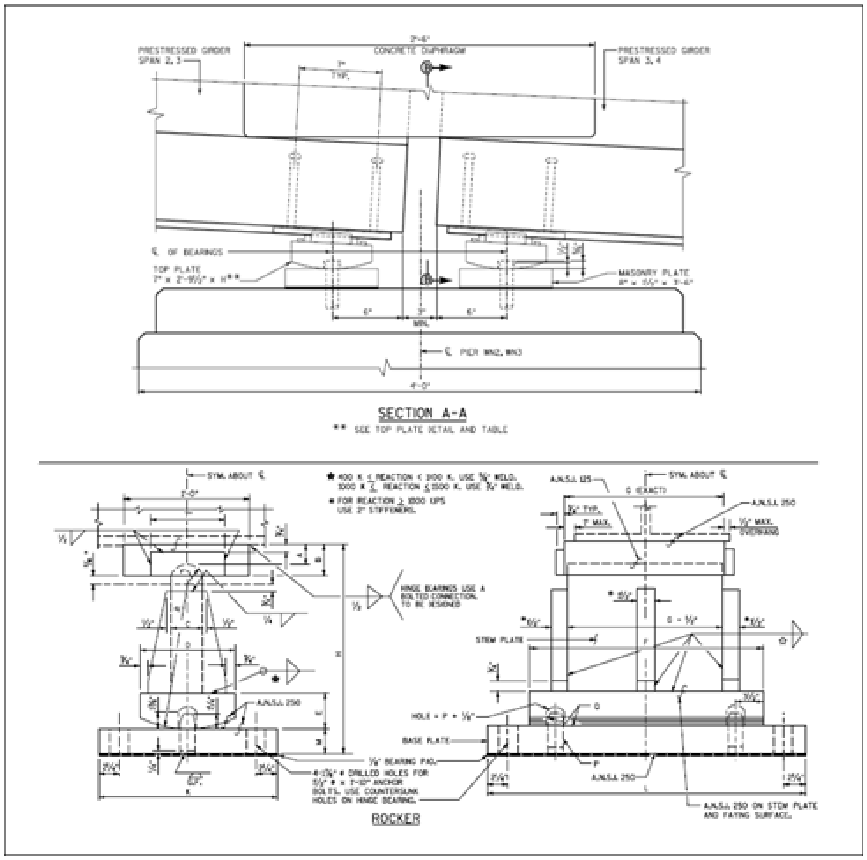

Figure 3.14 Rocker Support (WisDOT 2008).

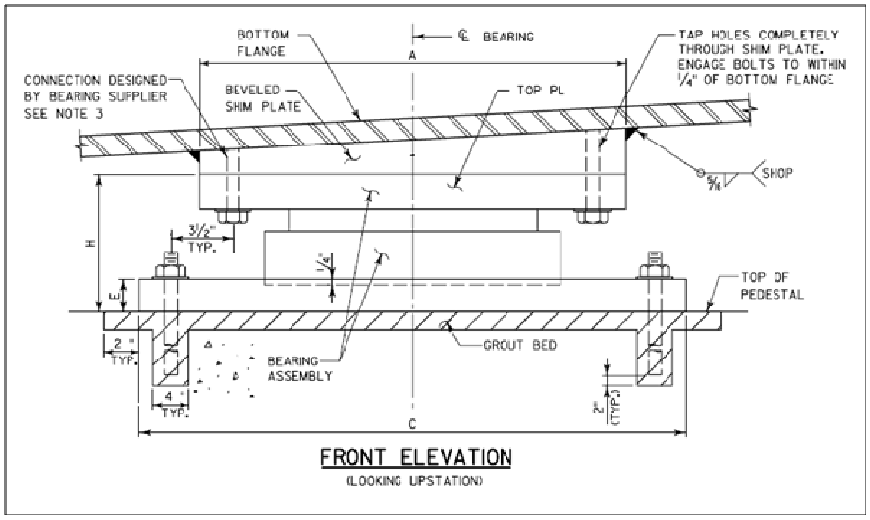

Figure 3.15 Guided Support (WisDOT 2008).

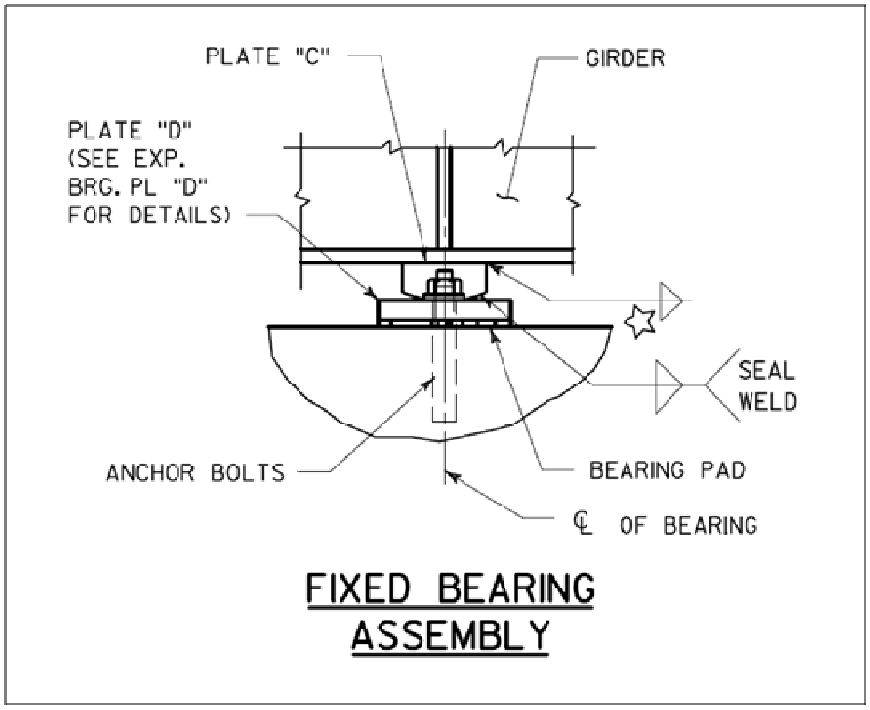

Figure 3.16 Fixed Support (WisDOT 2008).

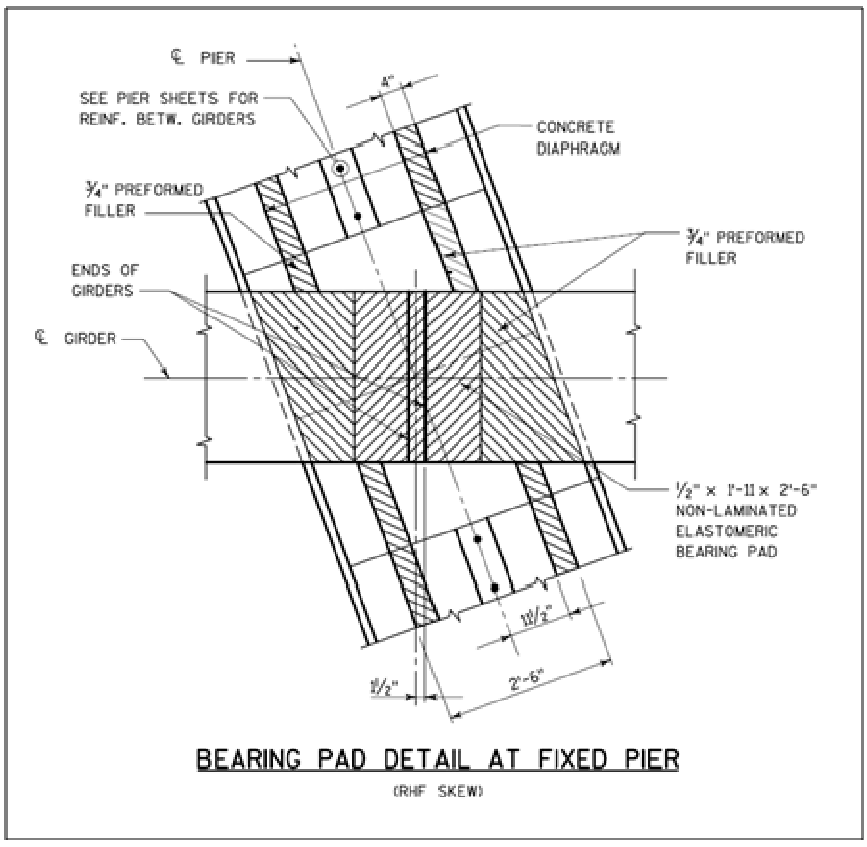

Figure 3.17 Elastomeric Bearing Pad (WisDOT 2008).

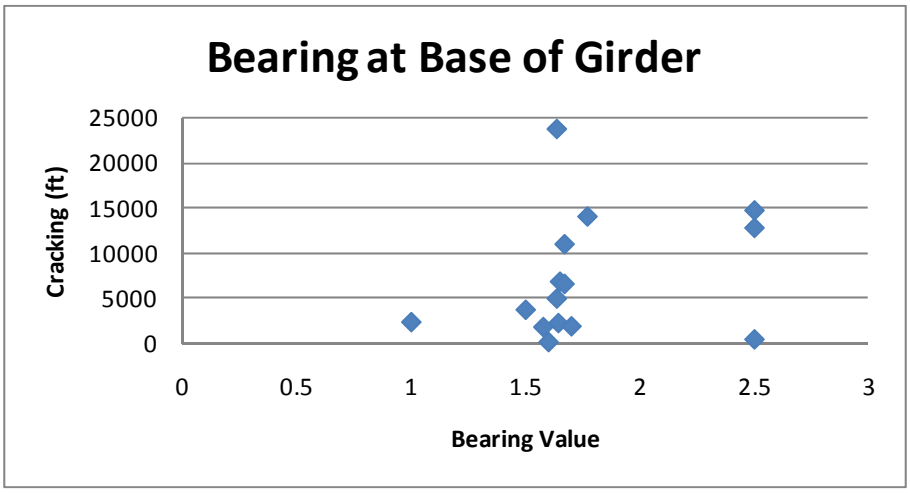

Figure 3.18 Cracking vs. Bearing.

This page has intentionally been left blank.

Chapter 4
Field Investigation of Deck Cracking in Milwaukee Area

INTRODUCTION

The research team worked with WisDOT to identify bridges with different levels of deck cracking problems around the metro-Milwaukee. These bridges were then the subject of field inspections. All of selected bridges were built or re-decked in a similar period to that of Marquette Interchange construction. The following bridges were selected for these field inspections. The bridge deck cracking classifications are also provided for reference.

Serious Deck Cracking

- B-40-692, W Walnut St over I-43
- B-40-686, W Highland Ave over I-43
- B-40-689, W Winnebago St over I-43

Medium Cracking Levels in Deck

- B-67-293, I-43 SB over Moorland Rd
- B-67-294, I-43 NB over Moorland Rd
- B-67-296/297, I-43 over Beloit Rd

No or Minor Cracks in Deck

- B-40-57, N 25th St over I-94
- B-40-34, W St Paul Ave - N 26th St over I-94
- B-51-078, STH 36 over Fox River

The research team visited these bridges on June 1 and 17, 2009. During the trips to these bridges, two other bridges not in the original list above were also investigated. These were B-67-134/135 (I-43 over W Beloit Rd) and B-40-429 (State Hwy 145 over W Fond Du Lac Ave). For each bridge, the structure information and previous inspection reports were obtained through WisDOT HSI system website. The cracking type and spacing were inspected during the visit. A brief summary was made for each bridge.

BRIDGES WITH SEVERE CRACKS

There were four bridges determined to have cracking at levels that could be described as severe. A description of the research team's findings following visual inspection of these bridges follows.

Bridge B-40-692

Bridge B-40-692 is 2-span continuous bridge with prestressed concrete girder built in 2006. The plan view, elevation and typical cross section are shown in Figure 4.1. The structure information and most recent WisDOT inspection report are summarized in Table 4.1. The deck of B-40-692 has cracked seriously including longitudinal cracks, transverse cracks, diagonal cracks and map cracks. A majority of longitudinal cracks occur 64 in. from the face of the curbs as shown in Figure 4.2 (a) and a majority of transverse cracks are located over interior piers as shown in Figure 4.2 (b). There are also map cracks (Figure 4.2 (c)) and severe transverse cracks (as seen in Figure 4.2 (d)) were observed at 3-4 foot intervals over the sidewalk.

Bridge B-40-686

Bridge B-40-686 is 2-span continuous bridge with prestressed concrete girders built in 2006. The plan view, elevation and typical cross section are shown in Figure 4.3. The structure information and most recent WisDOT inspection report are summarized in Table 4.2. The deck of B-40-686 has cracked seriously. There were a significant level of map cracks observed as shown in Figure 4.4(a) and transverse cracking was centered over 60 feet (longitudinally) in the vicinity of the interior support as shown in Figure 4.4(b). Diagonal cracking was observed over the acute angle at the west support as shown in Figure 4.4 (c). However, no cracking was observed over the acute angle at the east support as shown in Figure 4.4 (d).

Bridge B-40-689

Bridge B-40-689 is 5-span continuous bridge with prestressed concrete girder built in 2006. The plan view, elevation and typical cross section are shown in Figure 4.5. The structure information and most recent WisDOT inspection report are summarized in Table 4.3. The deck of B-40-689 has cracked seriously. Figure 4.6(a) shows the severity of some of transverse cracks, as the cracks span the entire width of the bridge, and then penetrate and continue throughout the pedestrian walkway. Transverse cracking increases in severity over pier locations. Longitudinal cracks appear to be concentrated half way between the edge of the walkway and dashed white line as shown in Figure 4.6(b). The longitudinal cracks were also more prevalent on the raised (superelevated) side (south) of the deck. Bridge B-40-689 suffered from significant map cracking, which appeared to be focused near walk-way joints as shown in Figure 4.6(c). The walk-way itself also showed significant transverse and map cracking as shown in

Figure 4.6(d). Some of the cracks penetrate the entire depth of the walk-way, and in some cases continue throughout the bridge deck.

Bridge B-40-689 appeared to have one construction joint at approximately 1/3 of the bridge length (from the east end of the bridge). There appeared to be significant longitudinal cracking at the joint location as shown in Figure 4.7. Figure 4.8 depicts the diagonal cracking near the piers on the underside of the deck. In addition, the super elevation of the deck can be seen in the "steps" shown below the girders.

Bridge B-40-429

Bridge B-40-429 is 3-span continuous bridge with steel I-beam built in 1983. The plan view, elevation and typical cross section are shown in Figure 4.9. The structure information and most recent WisDOT inspection report are summarized in Table 4.4. Bridge B-40-429 was subject to severe transverse cracking as shown in Figure 4.10, as seen from both the top and underside of the deck. The transverse cracks were spaced at approximately 6 feet. Despite the large level of transverse cracking, there was relatively little (no) map cracking.

BRIDGES WITH MEDIUM AMOUNT OF CRACKS

There were three bridges determined to have cracking at levels that could be described as medium. A description of the research team's findings following visual inspection of these bridges follows

Bridges B-67-293/294

Bridges B-67-293/294 are slab bridges built in 2008. They are I-43 SB and NB over Moorland Rd. The plan view, elevation and typical cross section are shown in Figure 4.11. The structure information and most recent WisDOT inspection report are summarized in Table 4.5. Because these bridges are on highway I-43, the inspection was performed from beneath the bridges. There were medium amount of cracks seeing from the bottom of the deck. The longitudinal cracking appeared to be due to rebar corrosion as shown in Figure 4.12(a). Some transverse cracks and diagonal cracks were also observed as shown in Figure 4.12(b) and (c), respectively. Figure 4.12 (d) shows that the bridge pier caps also suffered from corrosion problems.

Bridges B-67-296/297

Bridges B-67-296/297 are single span bridge superstructures with prestressed concrete girders built in 2007. The plan view, elevation and typical cross section are shown in Figure 4.13. The structure information and most recent WisDOT inspection report are summarized in Table 4.6. Because these bridges are on highway I-43, the inspection was again performed from beneath the bridges. There were

transverse and diagonal cracks seen from the bottom of the decks as shown in Figure 4.14. Small amount of longitudinal cracks were also observed. Most of diagonal cracks appeared at the acute angle location of external abutment supports for the bridges. It seems that the different pouring segments had different levels of cracks as shown in Figure 4.14 (d).

Bridges B-67-134/135

Bridges B-67-134/135 are 3-span continuous bridges with steel beams. These bridges were built in 1968 and re-decked in 1992. The plan view, elevation and typical cross section are shown in Figure 4.15. The structure information and most recent WisDOT inspection report are summarized in Table 4.7. The undersides of structures B-67-134 and 135 showed uniform transverse cracking throughout the entire middle span as shown in Figure 4.16(a), with small amounts of transverse cracking throughout the remaining two spans. Some transverse cracks penetrated full depth through the thickness of the deck and barriers as shown in Figure 4.16(b). Medium amount of longitudinal cracks (Figure 4.16(c)) were observed and there were low levels of map cracking (Figure 4.16(d)) near exterior supports.

BRIDGES WITH MINOR CRACKS

There were three bridges determined to have cracking at levels that could be described as minor. A description of the research team's findings following visual inspection of these bridges follows

Bridges B-40-57

Bridge B-40-57 is a two-span continuous bridge with steel beams. This bridge was originally built in 1960 and new superstructure was built in 2006. The plan view, elevation and typical cross section are shown in Figure 4.17. The structure information and most recent WisDOT inspection report are summarized in Table 4.8. No deck cracks were observed in this bridge.

Bridges B-40-34

Bridge B-40-34 is a three-span continuous bridge with steel beams. This bridge was originally built in 1957 and new deck was built in 2006. The plan view, elevation and typical cross section are shown in Figure 4.18. The structure information and most recent WisDOT inspection report are summarized in Table 4.9. There was very little cracking on bridge structure B-40-034. Only very minor transverse cracking was seen over interior piers as shown in Figure 4.19.

Bridges B-51-78

Bridges B-51-78 is a four-span continuous bridge with prestressed concrete girders which was built in 1996. The plan view, elevation and typical cross section are shown in Figure 4.20. The structure

information and most recent WisDOT inspection report are summarized in Table 4.10. Both top and bottom of the deck were observed and no cracks were found in this bridge.

SUMMARY AND CONCLUSIONS

In this chapter, visual inspections of 16 bridges (including three pairs of twin bridges) were described. These investigations were centered on evaluating levels and severity of deck cracking. The superstructures sampled include continuous span superstructures, simple span bridges (B-67-296/297), and two slab bridges (B-67-293/294). Simple span superstructures appeared to suffer from medium levels of cracking. All bridges found to have serious crack levels were continuous superstructures and three of four seriously cracked bridges have precast prestressed concrete girders. Among the three bridges with minor or no cracks, two of them are incorporate steel girders.

Many of the factors likely to affect the levels of deck cracking in the sixteen superstructures considered were not available for further investigation. Only the superstructure configuration was considered. Because these important factors or parameters (e.g. concrete properties, traffic, etc.) were not available and the number of bridges investigated is relatively small, no definitive conclusion can be drawn. However, this part of investigation indicates that the bridge structure type is definitely a factor affecting the deck cracking.

Table 4.1 Bridge B-40-692 Structure Information.

Year Built	Girder Type	Girder Spacing (ft)	Lanes	Deck Area (ft^2)
2006	Prestressed Concrete	16 @ 6.4	4	30180
Span Type	**Span Length (ft)**	**Skew/Curvature Radius (°/ft)**	**Expansion Joint**	
2 Continuous	134.0	6°	N.A.	N.A.
	134.0			
Top Deck Condition State:		3		
	Numerous fine longit & trans cracks, med trans cracks at moderated density, Fn pattern cracking			
Under Deck Condition State:		1		
	Fine trans cracks w/leeching, few longit & diag cracks @ Abuts.			
NBI Rating (Initial, Most recent):		8,8 (2007)		

Table 4.2 Bridge B-40-686 Structure Information.

Year Built	Girder Type	Girder Spacing (ft)	Lanes	Deck Area (ft^2)
2006	Prestressed Concrete	2 @ 8.33	2	15825
		3 @ 9.25		
		2 @ 8.33		
Span Type	**Span Length (ft)**	**Skew/Curvature Radius (°/ft)**	**Expansion Joint**	
2-Span	85.0	N.A.	Steel Strip	East Abut
	123.2		Steel Strip	West Abut
Top Deck Condition State:		2		
	Extensive HL Pattern cracking, HL/Fn Trans cracks @ mod density			
Under Deck Condition State:		1		
	Trans cracks w/leeching.			
NBI Rating (Initial, Most recent):		9,7 (2008)		

Table 4.3 Bridge B-40-689 Structure Information.

Year Built	Girder Type	Girder Spacing (ft)	Lanes	Deck Area (ft^2)
2006	Prestressed Concrete	7 @ 7.2	4	32804
Span Type	**Span Length (ft)**	**Skew/Curvature Radius (°/ft)**	**Expansion Joint**	
5-Span	85.7	1273.24 ft	Strip Seal	W Abut
	91.4			
	120.6			
	120.6			
	95.7			
Top Deck Condition State:		3		
	Extensive pattern cracking, longit and trans cracks mod size & density.			
Under Deck Condition State:		1		
	Some trans cracks w/leeching, some diag cracks @ piers.			
NBI Rating (Initial, Most recent):		9,7 (2008)		

Table 4.4 Bridge B-40-429 Structure Information.

Year Built	Girder Type	Girder Spacing (ft)	Lanes	Deck Area (ft^2)
1983	Steel I Beam	6 @ 9.5	2	25472
Span Type	**Span Length (ft)**	**Skew/Curvature Radius (°/ft)**	**Expansion Joint**	
3 Continuous	121.3	62°	Sliding Plate Steel	North Abut
	148.3		Sliding Plate Steel	South Abut
	123.3			
Top Deck Condition State:		3		
	Transverse cracks of moderate size and density.			
Under Deck Condition State:		2		
	Transverse cracks w/leaching, Some rust stains along longit constr joint.			
NBI Rating (Initial, Most recent):		6,6 (2007)		

Table 4.5 Bridge B-67-293/294 Structure Information.

Year Built	Girder Type	Girder Spacing (ft)	Lanes	Deck Area (ft^2)
2008	Slab Bridge	-	3	14943
Span Type	**Span Length (ft)**	**Skew/Curvature Radius (°/ft)**	**Expansion Joint**	
2 Continuous	117.0	41°	-	-
	117.0			
Top Deck Condition State:		1		
	Transverse Hairline crks @ over piers			
Under Deck Condition State:		1		
NBI Rating (Initial, Most recent):		9		

Table 4.6 Bridge B-67-296/297 Structure Information.

Year Built	Girder Type	Girder Spacing (ft)	Lanes	Deck Area (ft^2)
2007	Concrete Girder	5 ft	4	10945
Span Type	**Span Length (ft)**	**Skew/Curvature Radius (°/ft)**	**Expansion Joint**	
1 Span	134.0	39°	-	-
		4583.66 ft		-
Top Deck Condition State:		1		
Under Deck Condition State:		1		
	Most of deck not stripped at time of inspection.			
NBI Rating (Initial, Most recent):		9		

Table 4.7 Bridge B-67-134/135 Structure Information.

B-67-134				
Year Built	**Girder Type**	**Girder Spacing (ft)**	**Lanes**	**Deck Area (ft^2)**
1968	Steel I Girder	12	2	10178
1992				
Span Type	**Span Length (ft)**	**Skew/Curvature Radius (°/ft)**	**Expansion Joint**	
3 Continuous	56.0	50°	Steel Strip	South Abut
	110.0	2864.8 ft	Lewis Engr W300-L	North Abut
	45.0			
Top Deck Condition State:		3		
	Unsealed trans cracks @ Moderate density, most prevelant on E 1/2 of deck.			
Under Deck Condition State:		1		
	Transv cracks w/leaching, Span 2, <2%; Diag cracks @ Abuts.			
NBI Rating (Initial, Most recent):		6,7 (2008)		
B-67-135				
Year Built	**Girder Type**	**Girder Spacing (ft)**	**Lanes**	**Deck Area (ft^2)**
1968	Steel I Girder	12.3	2	12245
1992				
Span Type	**Span Length (ft)**	**Skew/Curvature Radius (°/ft)**	**Expansion Joint**	
3 Continuous	68.0	55°	Steel Strip	South Abut
	124.0		Steel Strip	North Abut
	48.5			
Top Deck Condition State:		2		
	Numerous HL/Fn transv cracks, diagonal cracks @ S. Abut.			
Under Deck Condition State:		1		
	Leaching transv cracks in Span 2, some diag cracks @ Abuts, <2%.			
NBI Rating (Initial, Most recent):		7,7 (2008)		

Table 4.8 Bridge B-40-57 Structure Information.

Year Built	Girder Type	Girder Spacing (ft)	Lanes	Deck Area (ft^2)
1960	Steel I Beam	(St.Paul)	4	11520
2006		1 @ 7.5		
(New Super Structure)		2 @ 7.33		
		1 @ 7.5		
		3 @ 7.33		
		(North 26th)		
		5 @ 6.7		
Span Type	**Span Length (ft)**	**Skew/Curvature Radius (°/ft)**	**Expansion Joint**	
2 Continuous	92.5	N.A.	Steel Strip	East Abut
	99.5		Steel Strip	Pier
			Steel Strip	West Abut
			Steel Strip	North Abut
Top Deck Condition State:		1		
Under Deck Condition State:		1		
NBI Rating (Initial, Most recent):		9,9 (2007)		

Table 4.9 Bridge B-40-34 Structure Information.

Year Built	Girder Type	Girder Spacing (ft)	Lanes	Deck Area (ft^2)	
1957	Steel I Beam	5 @ 8.4	2	7670	
2006					
Span Type	**Span Length (ft)**	**Skew/Curvature Radius (°/ft)**	**Expansion Joint**		
3 Continuous	57.3	22°	Steel Strip	North Abut	
	57.2		Steel Strip	South Abut	
	32.0				
Top Deck Condition State:		1			
	Fine trans cracks				
Under Deck Condition State:		1			
	Trans cracks w/leeching, most prevelant in Span 2.				
NBI Rating (Initial, Most recent):		8,8 (2007)			

Table 4.10 Bridge B-51-78 Structure Information.

Year Built	Girder Type	Girder Spacing (ft)	Lanes	Deck Area (ft^2)
1996	Prestressed Concrete	4 @ 8'-10"	2	13398
Span Type	**Span Length (ft)**	**Skew/Curvature Radius (°/ft)**	**Expansion Joint**	
4 Continuous	76.0	35°	Steel Strip	South Abut
	76.7		Steel Strip	North Abut
	76.7			
	76.0			
Top Deck Condition State:		1		
Under Deck Condition State:		1		
NBI Rating (Initial, Most recent):		8,8 (2008)		

(a) B-40-692

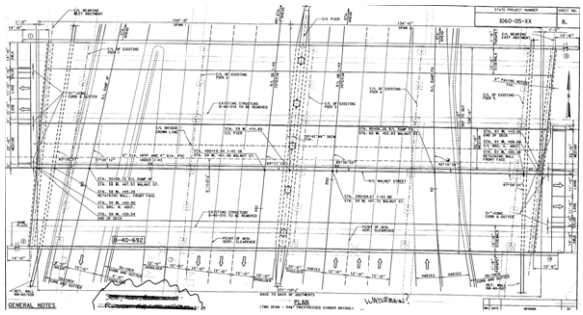

(b) B-40-692 Plan View

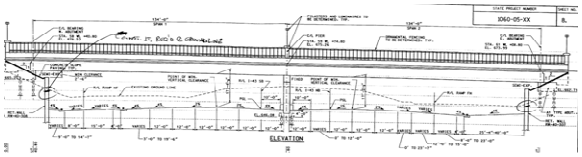

(c) B-40-692 Elevation

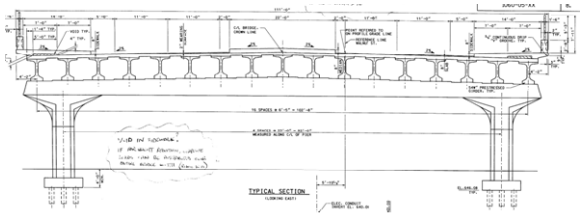

(d) B-40-692 Typical Cross Section

Figure 4.1 Bridge B-40-692 plan view, elevation and typical cross section.

(a) B-40-692 Longitudinal Cracks

(b) B-40-692 Transverse Cracks

(c) B-40-692 Map Cracks

(d) B-40-692 Cracks in Sidewalk

Figure 4.2 Bridge B-40-692 Deck Cracking.

(a) B-40-686

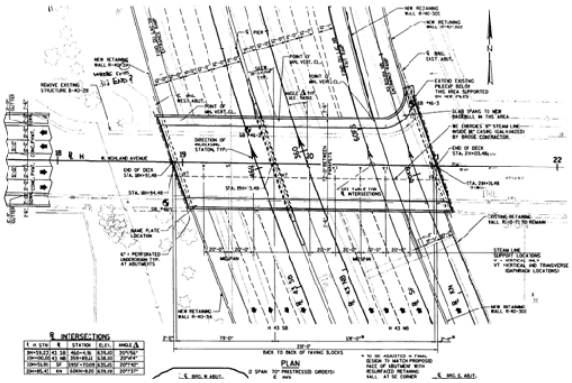

(b) B-40-686 Plan View

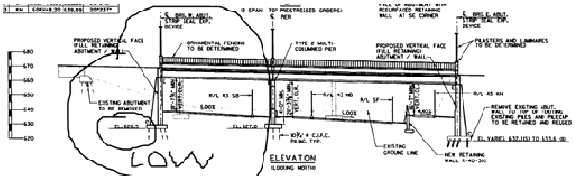

(c) B-40-686 Elevation

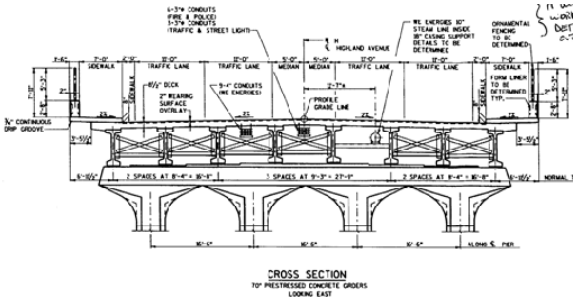

(d) B-40-686 Typical Cross Section

Figure 4.3 Bridge B-40-686 plan view, elevation and typical cross section.

(a) B-40-686 Map Cracks

(b) B-40-686 Transverse Cracks

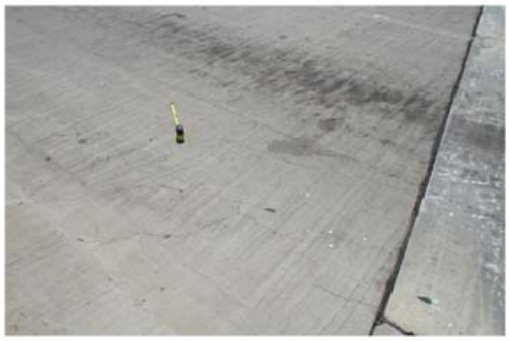

(c) B-40-686 Diagonal Cracks at West Support

(d) B-40-686 East Support (No Cracks)

Figure 4.4 Bridge B-40-686 Deck Cracking.

(a) B-40-689

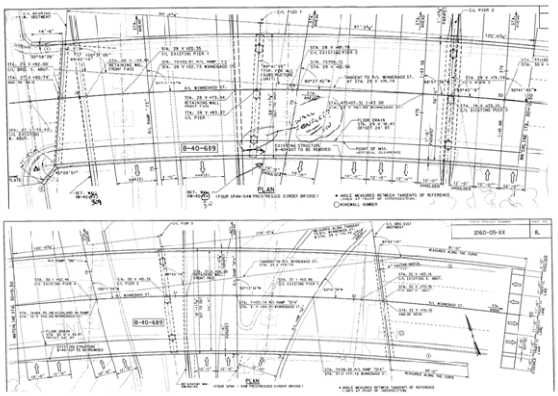

(b) B-40-689 Plan View

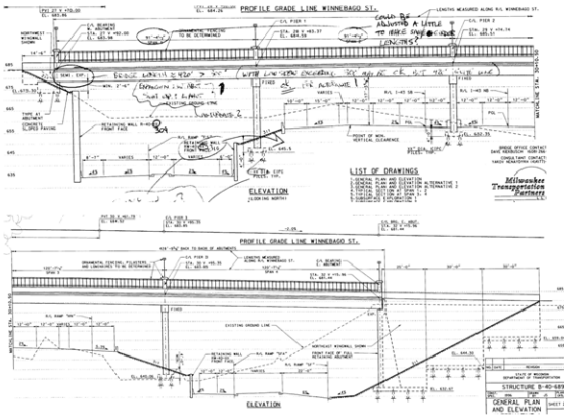

(c) B-40-689 Elevation `

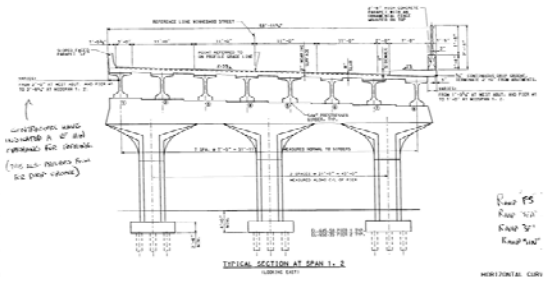

(d) B-40-689 Typical Cross Section

Figure 4.5 Bridge B-40-689 plan view, elevation and typical cross section.

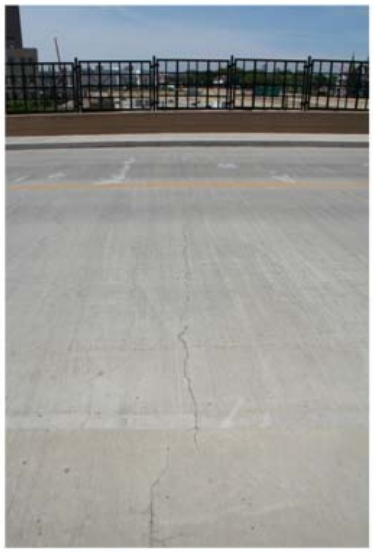

(a) B-40-689 Transverse Cracks

(b) B-40-689 Longitudinal Cracks

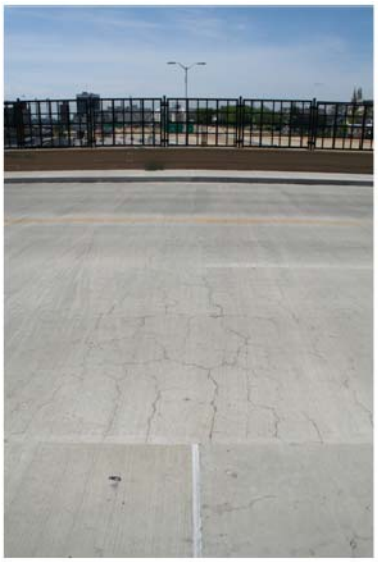

(c) B-40-689 Map Cracks

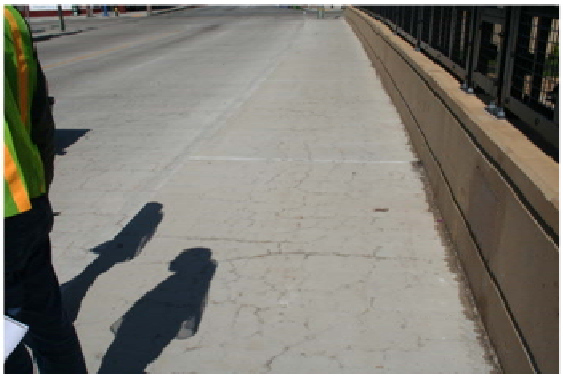

(d) B-40-689 Walk-Way

Figure 4.6 Bridge B-40-689 Deck Cracking.

Figure 4.7 Bridge B-40-689: Longitudinal Cracks at the Construction Joint.

Figure 4.8 Bridge B-40-689: Diagonal Cracks at the piers.

(a) B-40-429

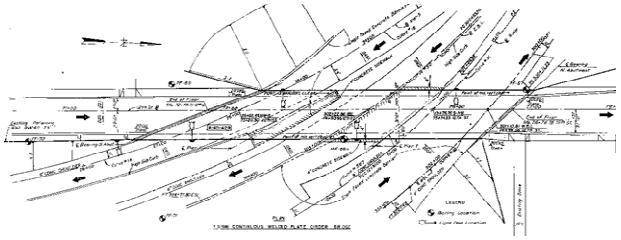

(b) B-40-429 Plan View

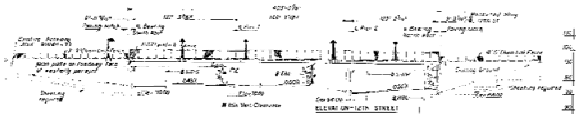

(c) B-40-429 Elevation `

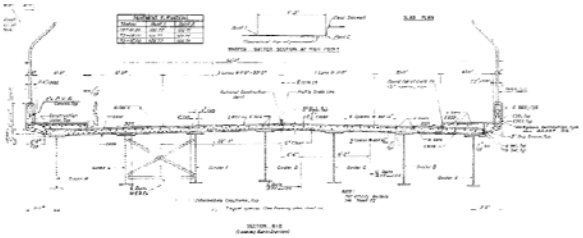

(d) B-40-429 Typical Cross Section

Figure 4.9 Bridge B-40-429 plan view, elevation and typical cross section.

(a) B-40-429 Transverse Cracks on Top

(b) B-40-429 Transverse Cracks on Bottom

Figure 4.10 B-40-429 Deck Cracking.

(a) B-67-293/294

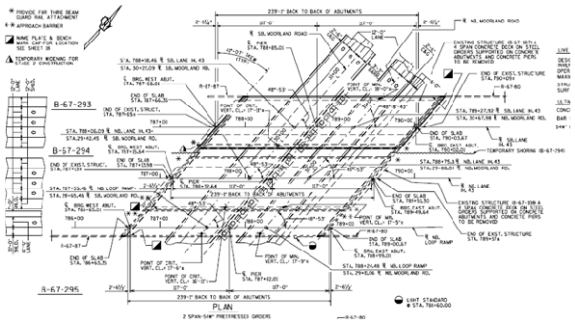

(b) B-67-293/294 Plan View

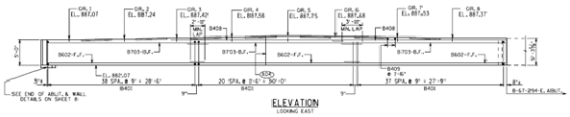

(c) B-67-293/294 Elevation

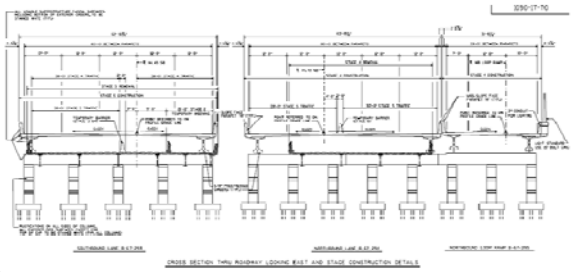

(d) B-67-293/294 Typical Cross Section

Figure 4.11 Bridge B-67-293/294 plan view, elevation and typical cross section.

(a) B-67-293/294 Longitudinal Cracks

(b) B-67-293/294 Transverse Cracks

(c) B-67-293/294 Diagonal Cracks

(d) B-67-293/294 Pier Cap

Figure 4.12 Bridge B-67-293/294 Deck Cracking.

(a) B-67-296/297

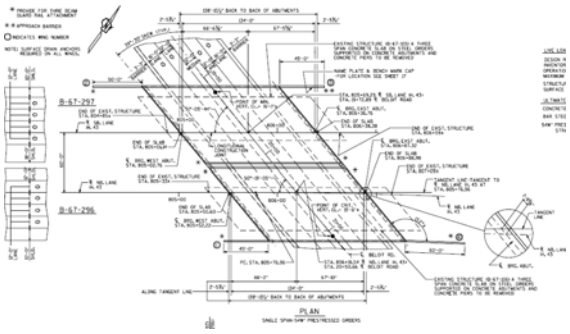

(b) B-67-296/297 Plan View

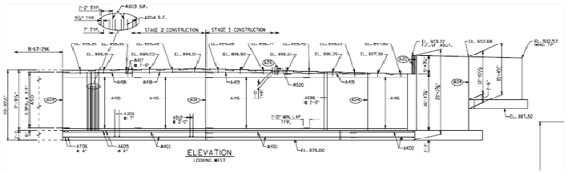

(c) B-67-296/297 Elevation

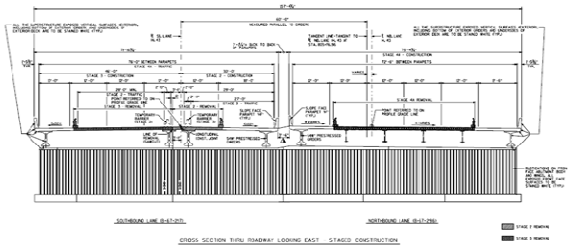

(d) B-67-296/297 Typical Cross Section

Figure 4.13 Bridge B-67-296/297 plan view, elevation and typical cross section.

(a) B-67-296/297 Longitudinal Cracks

(b) B-67-296/297 Transverse Cracks

(c) B-67-296/297 Diagonal Cracks

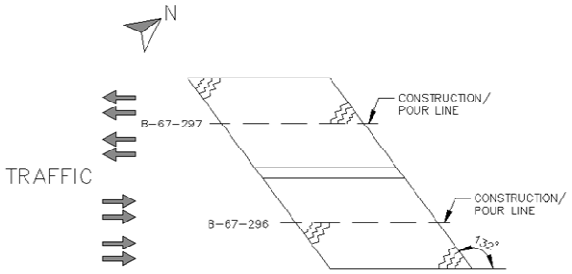

(c) B-67-296/297 Diagonal Cracks Location

Figure 4.14 Bridge B-67-296/297 Deck Cracking.

(a) B-67-134/135

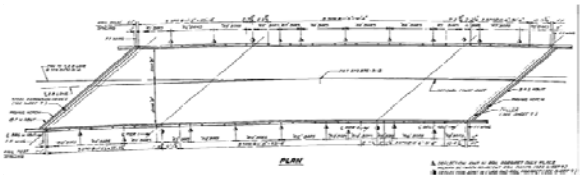

(b) B-67-134 Plan View

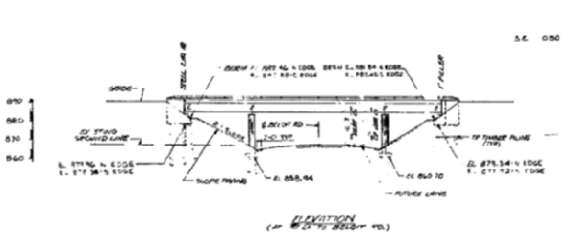

(c) B-67-134 Elevation

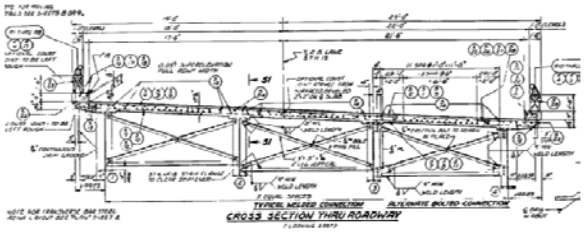

(d) B-67-134Typical Cross Section

Figure 4.15 Bridge B-67-134/135 plan view, elevation and typical cross section.

(a) B-67-134/135 Transverse Cracks

(b) B-67-134/135 Transverse Cracks at Barriers

(c) B-67-134/135 Longitudinal Cracks

(c) B-67-134/135 Map Cracks

Figure 4.16 Bridge B-67-134/135 Deck Cracking.

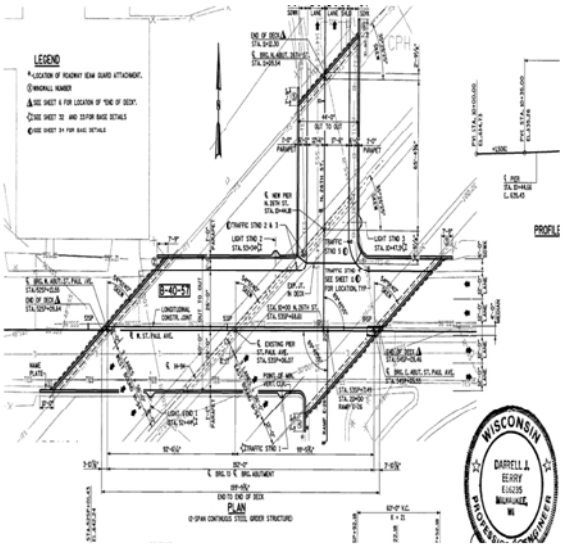

(a) B-40-57 Plan View

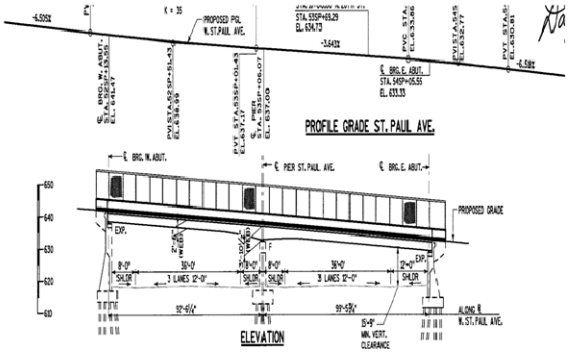

(b) B-40-57 Elevation

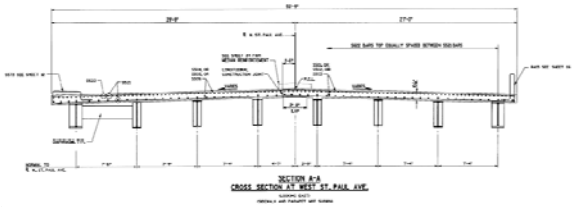

(c) B-40-57 Typical Cross Section

Figure 4.17 Bridge B-40-57 plan view, elevation and typical cross section.

(a) B-40-34

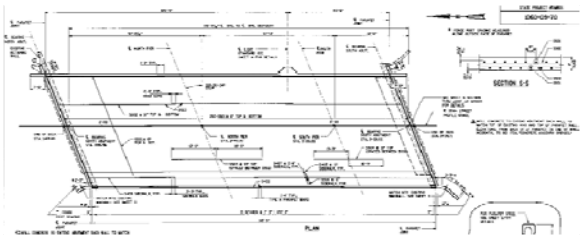

(b) B-40-34 Plan View

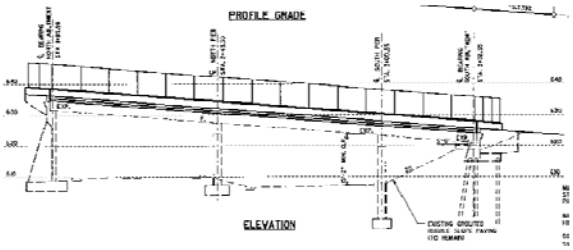

(c) B-40-34 Elevation

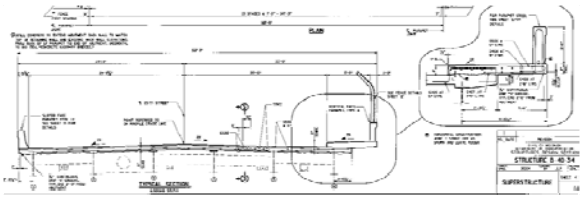

(d) B-40-34 Typical Cross Section

Figure 4.18 Bridge B-40-34 plan view, elevation and typical cross section.

Figure 4.19 Bridge B-40-34 Deck Cracking (Transverse Cracks).

(a) B-51-78

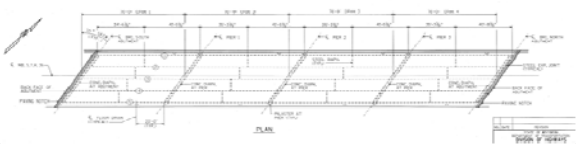

(b) B-51-78 Plan View

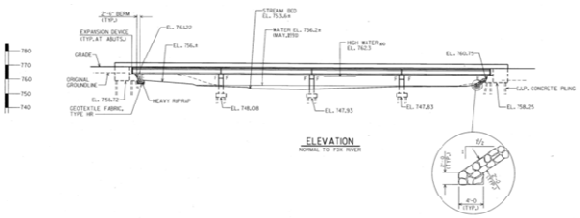

(c) B-51-78 Elevation

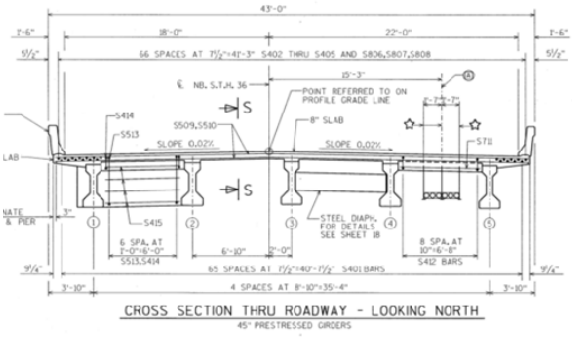

(d) B-51-78 Typical Cross Section

Figure 4.20 Bridge B-51-78 plan view, elevation and typical cross section.

Chapter 5
Finite Element Analysis

INTRODUCTION

The previous discussion indicates that the tensile stresses in a bridge deck due to direct and indirect loads should be analyzed in order to identify potential (major) causes of deck cracking. Shrinkage-induced cracking in bridge decks has not been systematically evaluated for precast concrete girder superstructures. Furthermore, the combination of shrinkage-induced strains along with strains superimposed by traffic loading has yet to be fully evaluated. Therefore, in order to quantify the tendency for shrinkage and traffic induced strains to cause cracking in bridge decks of continuous superstructures containing precast concrete girders, a finite element simulation of a typical precast-concrete two-span continuous bridge superstructure was conducted. The prototype for the numerical model is bridge structure B-20-133/134, located in Waupun, Wisconsin. The bridge was modeled using the ANSYS finite element analysis software system (ANSYS 2007). The model was created with the use of 2-dimensional link elements for rebar and steel diaphragms, as well as 3-dimensional brick elements used in the creation of bearing plates, girders, barriers, concrete diaphragms, and the concrete deck (Komp 2009). All trial runs were linear elastic, and all results from the finite element simulations were based upon "nodal solutions". Values of interest were averaged between nodes around the target locations.

BRIDGE PROTOTYPE

The State of Wisconsin recently constructed a highway bridge with a novel deck system as part of the FHWA Innovative Bridge Research and Deployment (IBRC) Program. One of the IBRC bridges is the bridge B-20-133 in Waupun, Wisconsin. The bridge (Figure 5.1) consists of a superstructure composed of precast prestressed concrete I-girders that act compositely with the concrete bridge deck. The deck employs novel fiber-reinforced polymer stay-in-place (FRP-SIP) formwork that serves as positive flexural reinforcement and FRP I-bars to serve as negative flexural reinforcement in the deck across the interior piers. Two in-situ load tests were performed on this bridge as part of a long-term monitoring program. The first load test was performed in the summer of 2007 and the other was in the summer of 2009. Further details regarding the instrumentation and load testing can be found in Foley, et al (2010). The load tests consisted of positioning a wheel of a tri-axle dump truck with calibrated loading at a series of target locations in a line parallel to the girders at mid-span of the deck. Portable strain sensors developed as part of the long-term monitoring effort were used to determine the distribution of the wheel loads within the FRP-SIP bridge deck and draw-wire transducers were used to measure deck deflections (Schneeman 2006; Foley et al. 2010).

A visual inspection on B-20-133/134 was performed on October 27, 2005 and a crack map was created as shown in Figure 5.2 (Martin 2006). It can be seen that most of the cracks are concentrated around the negative moment regions above the central piers. Both bridges exhibit similar cracking patterns. B-20-133 is the IBRC bridge with SIP FRP reinforcement, and B-20-134 is the traditional steel reinforced bridge. Hairline cracks in the bridge decks have propagated to and through the parapet with efflorescence showing on the underside of the overhang on the southern side of each bridge deck shown in Figure 5.3. As seen in Figure 5.2, cracking on both bridges is primarily located near the abutments and the central pier. Bridge B-20-133 appears to have less frequent cracking at mid-span between the abutment and central pier. This may be a result of the SIP FRP formwork restraining shrinkage of the deck as well as the tight spacing of the FRP grillage. Both the innovative and traditionally constructed twins have significant efflorescent cracks in the bridge deck overhang. Both bridges appeared to have very similar crack patterns and either would be suitable prototypes for the FE simulations.

In order to test the response under truck loads, the B-20-133 was instrumented with portable strain sensors which was developed and calibrated by MU-IBRC team (Schneemen 2006; Foley, et al 2010). Two sensor lines were utilized. The first is designated as TW1. This sensor array is located at the centerline of the exterior deck span. The second sensor array designated as TW2 is located along the centerline of the first interior span of the bridge deck. Detailed locations of the sensor arrays relative to the abutment face are shown in Figure 5.4.

During the in-situ load test, a calibrated truck (Figure 5.5) was slowly brought onto the superstructure and temporarily stopped at the first sensor location. The truck then proceeded forward at a slow (controlled) pace with additional stops at locations corresponding to the remaining four strain sensors and one draw wire transducer (DWT). These stops were essentially 17.5 inches (444 mm) apart. Table 5.1 provides a synopsis of the corrected strain values obtained via the field load test. The shaded areas represent values that were obtained based on symmetry of the strain gauges, rather than actual strain gauge readings. Further details of the load test can be found in Foley, et al (2010).

FINITE ELEMENT MODEL OF BRIDGE B-20-133/134

The creation of the bridge finite element model began with using planar elements to generate a planar model with the cross sectional (x-y plane) dimensions given in the bridge drawings. The bridge cross-section was then extruded (z-direction) into solid elements to create volumes representing the entire bridge. To create the skew, each girder and associated deck/barrier was staggered by 1500 mm (z-direction), as shown in Figures 5.6 and 5.7. 1500 mm was chosen, as the element depth was already set at

150 mm, and therefore the staggering was equivalent to 10 elements, giving an acceptable representation of the skew (Komp 2009).

Once completed, each of the major constituents of the bridge model (girder, deck, barrier, base plates, and diaphragms) was given individual material properties. In doing so, individual parts of the bridge could be independently manipulated. The deck elements were given a Poisson's ratio of 0.2 and a modulus of elasticity consistent with a given compressive strength. Because the concrete compressive strength and modulus of elasticity increase with time at the early age, these values were dependent on time. The linear-elastic analysis was carried out until first cracking occurred. First cracking in the model was defined as a situation when the maximum tensile stress in the concrete deck was larger than the modulus of rupture for the concrete from which was composed. In general, it is relatively accurate to assume linear behavior to the tensile stress level of the modulus of rupture (Kachlakev, et al. 2001). Rebar was not added to the deck during analyses involving temperature gradients which represented the concrete shrinkage strains. While the steel would tend to slightly reduce the stress within the concrete elements, the slight gains in accuracy are far outweighed by the computing memory required to add rebar throughout the deck. Due to the size of the bridge model, it was not possible to analyze the convergence of stress and strain results, with respect to the bridge mesh within the finite element package. However, at this time it is assumed the mesh is fine enough to gather the desired level of accuracy on the bridge deck with the use of nodal averaging.

FINITE ELEMENT MODEL CALIBRATION

Once completed, the finite element (FE) model of the bridge was subjected to the loading of a tri-axle truck used during the field load test in 2007 (Foley, et al. 2008; Foley, et al 2010) to calibrate the model. In the FE model, the load of each tire as shown in Figure 5.5 was converted to pressures, which act over the contact area of each tire. These pressures were applied to the upper surface of the elements corresponding to the top surface of the deck, as shown in Figure 5.8. Although the exact distances and dimensions of the truck and the strain gauge locations were slightly altered as a result of the finite element model mesh, every effort was made to maintain model locations that were close to the actual locations, as shown in Figures 5.9 and 5.10.

An initial linear elastic structural analysis was run to simulate response corresponding to the first truck stop (TW1-W2 location as shown in Figure 5.4). While the bridge structure would include bending behavior, only transverse deck strains were considered in this analysis (Komp 2009). However, using a finite element model of the entire bridge superstructure to obtain data about a relatively small portion of the bridge is quite inefficient. To save memory and computation time, it was desirable to model only a portion of the bridge superstructure.

If the bridge was analyzed as a two span continuous beam, it would be evident that the moment throughout the "beam" would reach an inflection point. If the inflection point location was identified, appropriate constraints could be applied at that location and only a fraction of the bridge would require modeling, without altering the strain distribution throughout the remainder of the bridge. MASTAN2 (Ziemian 2007) was utilized to generate and study a two-span continuous beam model. The beam was used to once again represent the loading scenario where concentrated loads equivalent to the tri-axle truck loads were applied at locations with respect to the center girder of the actual bridge, as shown in Figure 5.11. A first-order linear elastic frame analysis was performed in MASTAN2 to get the moment diagram as shown in Figure 5.12. From the moment diagram, the inflection point (at which there is zero moment) locates at the distance of 26,471 mm to the right of the left support.

In the finite element model, each girder (and corresponding deck/barrier) was modeled with a longitudinal length equal to 26,700 mm as shown in Figure 5.13. Because the inflection point has zero moment, a roller support can used at the inflection point without affecting the stress results in the part of bridge model subjected to the truck load. In the FE model, the support-to-support distance was 26,500 mm (instead of 26,471 mm from the MASTAN2 analysis).

A linear elastic structural analysis was conducted using the partial finite element model. As expected, there were no significant differences between the deck stresses found in partial model and those found in full bridge model (Komp 2009). While the partial bridge segment shown in Figure 5.13 would be appropriate, it might not be 100 percent accurate to model other loading scenarios because the point of inflection on the moment diagram would vary with the movement of the truck loads. However, if the same bridge segment were used for all 10 loading scenarios, the global stiffness matrix within ANSYS would only need to be evaluated once, thereby requiring much less computational memory and time. Because the load locations in the field test only varied by 450 mm (less than 1.4% of the span length) with each change in position, it is logical that the point of inflection on the moment diagram would have little movement. Therefore, the partial bridge with a support-to-support distance of 26,550 mm as shown in Figure 5.13 was used for the remainder of the tri-axle dump truck load test simulations.

With the knowledge that the partial bridge accurately represented the transverse strains at the base of the bridge deck, steel re-bars were added into the deck of the FE model as the bridge B-20-134. Because the load test was performed on B-20-133 which uses FRP stay-in-place formwork instead of steel rebar, the stiffness of the actual deck using FRP and the stiffness of the deck model using steel rebar should be calculated to determine if the FE model results can represent the bridge B-20-133 subjected to truck load. Stiffness was represented solely by cross-section rigidity, EI, for both the mild-steel scenario

and the FRP-SIP configuration. The calculations for the FRP-SIP bridge deck were based on the work of Martin (2006), for an 8 x 36 inch cross section of the FRP-SIP bridge deck. Figure 5.14 includes the calculations of relative stiffness for the two deck configurations and it demonstrates that the stiffness of the mild-steel bridge deck is within 3% of the actual FRP-SIP bridge deck. This is because that the modulus of the FRP-SIP formwork and FRP reinforcement used in bridge B-20-133 is very close to that of the concrete, and the area of steel reinforcement used in the bridge B-20-134 and FE model is relatively small when compared to the concrete area. Therefore, the steel reinforcement model used in this study is deemed to be an acceptable representation of the FRP-SIP deck condition.

Ten simulations were run for different load positions. The simulations are labeled using the position of the front truck tire. Therefore, when the front tire was over strain gauge TW1-W2, the trial was labeled "Position1". When the front tire moved over strain gauge TW1-W1, the trial was labeled "Position2." Therefore, positions 1-5 represented the readings over the exterior strain gauges, with Position5 representing the truck at its closest location relative to the "front" abutment. The tests of interior span were similarly labeled Position 6-10, with Position10 representing the truck at its closest location relative to the "front" abutment. Table 5.2 includes the transverse deck strains obtained from the 10 independent linear elastic finite element analyses corresponding to the locations of interest in the field load test.

Figure 5.15 shows the comparison of strain values obtained from finite element analyses and field load test. Except the field data for Position 2 and 8, the finite element simulations and field acquired data show a peak strain directly over the front wheel of the trial-axle truck at each position. When positioning the truck in the field however, the location of the strain gauges was estimated as the truck was very difficult to align and position exactly. Furthermore, it is impossible to position vehicles of the size used in the load test at the locations intended. As a result, strain values are expected to show variance when compared to the finite element simulations.

The actual variance between the strains obtained through the finite element model and the field tests can be observed in Table 5.3 where the ratio between ANSYS FE model results and load test results is calculated. The data suggest that the finite element model underestimates the peak strain in five of the trials, while the remaining five finite element trials overestimate the peak strain. At first glance, it may appear that the variances in strain are random. In looking at the data however, it is apparent that the variance in strain readings between the finite element simulations and the field measured data are directly correlated to the strain gauge (for example TW1-W2) that is collecting the data.

Table 5.4 again shows the variance between finite element simulation and the field acquired data. However, the data are banded into ten groups, with each band representing a different strain gauge. As seen in Table 5.4, the green band (far right band), which spans over the exterior set of strain gauges, indicates the finite element simulation compares quite favorably with field acquired data. In observing the strain gauge that collected the data in the field, it can be seen that in the TW1-W2 trial (Position1), the strain gauge 1800 mm from the front tire would be TW1-E2. However, in the TW1-W1 trial (Position2), strain gauge TW1-E2 is now located at a distance of 1300 mm from the front of the tire. Therefore, the entire green band consists of data collected by strain gauge TW1-E2. In analyzing the yellow band (the band directly to the left of the green band), it can be seen that the results are not as good, with the finite element simulations underestimating the strains by nearly 50%. Similarly, the finite element simulations significantly overestimate the strain readings from strain gauge TW1-W1 (orange band).

It is possible that the strain gauges in the field were calibrated differently, each gauge having a different sensitivity. To gain a better understanding of the variance in strain data between the field data and the finite element simulations, more field data would be required, possibly with the use of different strain gauges. A larger pool of data could then help rule out poorly positioned truck loads or poorly calibrated strain gauges, and help determine if, in fact, the finite element simulations could be used to obtain accurate strain readings. In general however, one must keep in mind that positioning large vehicles exactly and consistently with locations assumed in the finite element simulations is very difficult. There were also concessions made in the finite element modeling that lead the model away from reality. Overall, the comparisons are quite favorable and the model was deemed acceptable to future finite element modeling.

HL-93 INTERIOR MOMENT LOADING

As shown in Figure 5.2, more transverse cracks on the bridge decks are at the location over interior piers. Therefore, a finite element study was developed to determine the relationship between traffic loading on bridge decks, and the possibility of transverse cracking over interior piers. This part of finite element analysis used the full length of the bridge B-20-134 model. To get an accurate representation of the actual traffic loading on the structure, the bridge deck was loaded with two HL-93 trucks. The load and wheel spacing of HL-93 truck are shown in Figure 5.16.

The positioning of the trucks was determined through the use of an influence line for a two span continuous beam. Based on the influence line, it was determined that concentrated loading at 0.6*span length (L) of the first span and 0.4L of the second span would cause the largest negative moment over the interior support (causing tension on the top surface of the deck). To approximate the maximum loading position, the tires on the center axle of each HL-93 truck were placed at the respective peak value

locations (0.6L of the first span and 0.4L of the second span). This loading, as well as the influence line for negative moment over the interior support can be seen in Figure 5.17.

To properly locate the trucks on the finite element model, the left front tires of the trucks were centered at mid-width of the deck surface. Due to the skew of the bridge, the bridge deck was constructed in several "saw-tooth" segments. The center of the deck was therefore determined as the center of the third "tooth" (third of five segments). It should be noted that all span lengths were measured from the center segment of the deck, which was 3,000 mm from the exterior ends of the bridge deck. A plan view of the bridge deck with the HL-93 truck loadings can be seen in Figure 5.18.

The HL-93 concentrated point loads used in typical bridge design were converted into pressures that would act over given tire contact areas. The actual dimensions of the contact patches for HL-93 tires are difficult to quantify, and therefore contact areas similar to those of a tri-axle dump truck used in field load tests were implemented. However, based on the previously developed bridge deck mesh, the size and placement of the contract areas were slightly altered as shown in Figures 5.19 and 5.20.

A linear elastic analysis was run with the given tire pressure loadings. However, it should be noted that due to computational memory restraints, mild steel reinforcement in the bridge deck was neglected in the finite element model for this analysis. In reality, the HL-93 truck loading by itself will not cause cracking within the concrete deck, and therefore the steel rebar would not become "active". Once the linear elastic analysis was completed, the longitudinal (normal) state of stress was examined throughout the top surface of the bridge deck, as shown in Figure 5.21. As one would expect for a continuous structure, areas of tensile stress are concentrated over the supports (specifically the interior support), while the remainder of the top surface is in compression. Under closer examination, it can be seen that centered over the interior pier, the region under tension is approximately 12,000 mm in length (longitudinally), which is equivalent to 0.367 times the span length, as shown in Figure 5.22.

To examine the probability of transverse cracking over the interior pier, nine nodes of the finite element model were selected at the top of the deck surface, over the interior pier of the bridge as shown in Figure 5.23. The normal z-directional (σ_z – longitudinal) stresses were recorded at each of these nine nodal locations as shown in Table 5.5. The results of the linear elastic analysis can also be seen in a contour plot of longitudinal normal stresses at the interior pier (Figure 5.24). As one would expect, the two concentrated areas of peak tensile stress near points 3 and 5 correspond to the transverse (x direction) positioning of the tire loads. The maximum longitudinal tensile stress in the deck is 0.79 MPa which is much less than the concrete modulus of rupture (3.7 MPa as discussed in the next section of this report).

Therefore, it is expected that normal traffic load itself will not cause concrete deck cracking in the Waupun bridges.

SIMULATION OF CONCRETE DECK SHRINKAGE

Drying shrinkage of concrete is defined as a decrease in volume under constant temperature due to loss of moisture after concrete has hardened. Parametric studies conducted by Tadros and Al-Omaishi (2003) focused on water content, type of cement, type of aggregate, ambient conditions (temperature, humidity, and wind velocity) at the time of placement, the curing procedure, the amount of reinforcement, and the volume/surface area ratio of the concrete. Based on these studies, the following empirical equation was created by Tadros and Al-Omaishi (2003):

$$\epsilon_{sh} = -k_{vs}k_{hs}k_f k_{td}(0.48 \times 10^{-3}) \quad (5.1)$$

where $\epsilon_{sh} =$ the strain due to shrinkage of concrete at an exposed surface. The coefficients k_{vs}, k_{hs}, k_f, and k_{td} will be further described in the following.

It should be noted that the value 0.48 x10^{-3} simply represents an estimate for the ultimate shrinkage strain in the concrete. A more accurate estimate of 0.78 x10^{-3} is often used (Saadeghvaziri and Hadidi 2002), and therefore Equation 5.1 was altered. In addition, it is recommended that if the concrete is exposed to drying before five days of curing, the predicted strain should be increased by 20%. Therefore, the final strain equation can be described as Equation 5.2.

$$\epsilon_{sh} = -(1.2)k_{vs}k_{hs}k_f k_{td}(0.78 * 10^{-3}) \quad (5.2)$$

The coefficient k_{vs} is a factor for considering the effect of the volume-to-surface ratio of the concrete. This factor takes into account the fact that relatively thick members do not dry as quickly as thin members, and can be expressed as:

$$k_{vs} = 1.45 - 0.13(V/S) \geq 1.0 \quad (5.3)$$

where V is the volume of concrete and S is the surface area of concrete.

The coefficient k_{hs} is a humidity factor that accounts for the fact that shrinkage tends to be greater in dry climates than humid climates. The humidity factor can be expressed as:

$$k_{hs} = 2.00 - 0.014H \quad (5.4)$$

where H is the relative humidity (%) of the environment. If the humidity at the site is unknown, Figure 5.25 can be used to estimate the humidity.

The coefficient k_f is a factor to take into consideration the effect of concrete strength and can be expressed as:

$$k_f = \frac{5}{1+f'_{ci}} \quad (5.5)$$

where f'_{ci} is the specified compressive strength of concrete at the time of prestressing for pretensioned members and at the time of initial loading for nonprestressed members (ksi). However, because the age of the concrete at the time of loading is unknown, Tadros and Hadidi (2003) suggests the use of $0.80f'_c$. When examining this factor, it can be seen that shrinkage is inversely proportional to concrete compressive strength as seen in Equation 5.5. Tadros and Hadidi (2003) did not take into consideration the effect of the amount of cement used in the concrete. In general, an increase in concrete compressive strength correlates with an increase in cement content. An increase in cement implies an increase in shrinkage. Therefore, this factor is open to some interpretation.

The coefficient k_{td} is a time development factor that can be expressed as:

$$k_{td} = \frac{t}{61 - 4f'_{ci} + t} \tag{5.6}$$

where t is the maturity of the concrete (in days). Maturity is defined as the age of concrete between the end of curing and the time being considered. However, for bridge decks where the curing time may be unknown (or varying), the time immediately following placement is used as an initial time. In analyzing the time development factor, k_{td}, it can be seen that higher strength concretes will produce accelerated early shrinkage as seen in Equation 5.6.

While empirical equation 5.2 provides an estimate as to the shrinkage strain in concrete, this shrinkage is only representative of exposed concrete surfaces. Therefore, while the strain in the concrete at the top and bottom surface can be estimated, nothing is known about values of shrinkage strain across the thickness of the deck, or its variation. Unfortunately, very little research has been done to describe the variation of shrinkage strains throughout the thickness of concrete.

Some research suggests that the shrinkage strains can be analyzed as linear across the thickness of concrete with the top surface having the largest value of strain (Krauss and Rogalla 1996). However, other research shows that drying strains (neglecting the effects of ambient thermal heating) within the deck will be equal at the exposed surfaces (top and bottom), thereby creating compression stresses at the center of the deck (Tadros and Hadidi 2003). Assuming the concrete deck forms will remain in place for some finite amount of time during the concrete hardening, the linear strain distribution appears logical. To determine the slope of the strain distribution, the humidity at the center of the deck was obtained through field testing (Foley, et al 2010). Because k_{hs} is dependent on humidity, the strain was recalculated based on Equation 5.2. These two points of strain helped develop a shrinkage strain gradient throughout the top portion of the deck, and were interpolated throughout the remaining thickness as shown in Figure 5.26.

Equation 5.2 attempts to estimate strains resulting from concrete shrinkage. It is important to understand the limitations of this equation/model. Tadros and Hadidi (2003) defined shrinkage as "a decrease in volume under constant temperature due to loss of moisture after concrete has hardened". A "hardened" state immediately implies that plastic shrinkage, autogenous shrinkage, and settlement cracking are all ignored, as all three happen when concrete is in a plastic (non-hardened) state. In addition, "constant temperature" implies that solar (linearly varying) heating of the deck is ignored. By eliminating these factors, large tensile stresses may be neglected. As such, Tadros and Hadidi (2003) suggest that shrinkage strains could exceed -0.0008 in./in., especially for relatively thick sections of concrete, in which case the equation may be off by as much as 50%. However, the ultimate shrinkage was already adjusted to -0.00078 (Equation 5.2) to compensate for these additional strains. In addition, the effects of creep (reducing stresses over time) were ignored in the analysis.

The modulus of elasticity was determined assuming that the concrete was normal weight (145 lb/ft^3) and therefore, Young's Modulus, E, could be calculated as:

$$E = 57{,}000\sqrt{f_c'} \tag{5.7}$$

where the compressive strength, f'_c, has units of psi. Based on typical concrete strength gain and logarithmic interpolation, the compressive strengths and Young's modulus were determined for different ages (unit: days) as shown in Table 5.6 (Komp 2009). Figure 5.27 shows the variation of shrinkage strain and compressive strength used in the finite element analysis.

Komp (2009) demonstrated that concrete shrinkage strains can be accurately represented by applied temperature loadings within finite element analysis using the following equation:

$$\epsilon = \alpha \Delta T \tag{5.8}$$

where ε is the concrete shrinkage strain; α is the coefficient of thermal expansion; and ΔT is the change of temperature. In general, the coefficient of thermal expansion of concrete ranges from 5 to 9x10^{-6} /°F. Because the temperature loads in this analysis are simply representing the concrete shrinkage strain values, the major role of the coefficient of thermal expansion is to simply "convert" the temperatures into strains. Therefore, the concrete was assumed to have a constant coefficient of thermal expansion (α) equal to 6.6x10^{-6} /°F in this research. Figure 5.28 depicts an example of the varying temperature loads applied within the finite element model.

As previously mentioned, several simplifying assumptions were made in the development of the current finite element model. These assumptions include neglecting mild steel reinforcement and bridge self weight, and removal of the bridge barriers. The validation of these simplifying assumptions is discussed in detail elsewhere (Komp 2009).

Figure 5.29 shows the longitudinal stress contour in the deck due to concrete shrinkage at the location of piers. Table 5.7 provides the results obtained from the finite element simulation for the first 10 days after casting, taking into consideration normal stresses in the z-direction (longitudinal direction) and their potential for causing transverse cracking. The nodes in Table 5.7 are same as those nodes used in HL-93 truck load analysis (Figure 5.23). Several observations can be made from the z-directional normal stresses obtained from the finite element model. First of all, there is an increase in stress on the bridge deck directly over girders (nodes 1, 3, 5, 7, and 9). The five points directly over the girders have nearly 15% more stress than their four counterparts located in-between the girder spacing. In general, the girders provide restraint from volume change, and therefore it comes as no surprise that the stresses above the girders are slightly larger.

While the purpose of this trial was to analyze the effects of shrinkage strains on creating stresses that cause transverse cracking (z-direction stresses), it is also possible to analyze the stresses that would cause longitudinal cracking (due to x-direction stresses). Figure 5.30 provides a representative finite element stress contour of the normal x-stresses at the center of the deck.

There are several areas of peak stress represented by red in Figure 5.30. In each case, these areas are centered just to the right (or left) of a girder, and are elongated in the longitudinal (z) direction. This is most likely caused by the modeling of the concrete diaphragms or pilasters at the center pier in the bridge superstructure. The diaphragm would most likely be cast at an angle, with the pier consistent with the skew of the bridge superstructure. However, in the finite element model, the diaphragms at the central pier and abutments were modeled with displacement restraint conditions in the transverse (x) direction (Komp 2009). The restraint directions were parallel to the x-axis instead of to parallel to the skew. As a result, it appears as though the increased stress contours tend to be distorted in a longitudinal direction, as they follow the skewed shape of the bridge. Therefore, the modeling of the diaphragms may cause a slight increase in stress at those locations.

The deck deflects with a concave upward shape due to the shrinkage strains (Komp 2009). Therefore, the top of the deck near the exterior edges will be in compression as seen in Figure 5.30. This also implies that the bottom of the deck will be in tension. Figure 5.31 illustrates normal typical transverse stress contour at the underside of the bridge deck. The transverse stresses at the bottom of the deck can be quite large, specifically at locations where the concrete diaphragm, girder, and deck meet. For the strains that develop over day four alone, there is a peak tensile stress of near 2.8 MPa. It should be stressed that a relatively coarse mesh was used in the finite element analysis, and the peak stress location is directly on an edge between the girder, diaphragm, and deck. This is a location that likely

contains a very complicated strain and stress field. Due to memory and computing constraints, no further (more detailed) analysis with refined meshes could be carried out for the bridge. It is recommended that sub-modeling be investigated to further study stresses in these areas.

The yellow areas on the contour map in Figure 5.31(slightly removed from the edge) are more representative of the stresses seen in the actual deck. However, these areas still represent a tensile stress of 0.5 MPa, which is still quite significant. These transverse tensile stresses on the underside of the deck are larger than the longitudinal (z) tensile stresses on the top of the deck, and therefore it is possible that longitudinal cracking may occur on the underside of the deck before the transverse cracks are seen on the top of the deck.

CRACKING ANALYSIS

Normal (non-high performance) concrete gains a majority of its strength (90%) in the first 14 days, while a majority of shrinkage strains (80%) develop in the first 100 days. Therefore, it makes sense that the maximum stresses due to concrete shrinkage would occur early in the life of the bridge deck. Table 5.7 shows that these maximum stresses will occur during the fourth day after casting. Therefore, the large early stresses seen in the finite element simulations suggest a need for special attention during the days immediately following casting to control shrinkage strains.

A summation of the stresses from the individual finite element simulations is included in Table 5.8. The total stress is the summation of the average stress (of the nine reference points) up to, and including the stresses that develop on that day. In order to determine if the deck cracks at a specific age, the modulus of rupture at that age should also be calculated. The modulus of rupture was calculated by 10% of the corresponding concrete compressive strength and Equation 5.9;

$$f_r = 0.75\sqrt{f_c'} \tag{5.9}$$

The information in Table 5.8 suggests that if 10% of the concrete's compressive strength were used to define the concrete's tensile strength, the concrete would crack (tensile stress exceeds tensile strength) after four days. If the modulus of rupture was used to characterize the tensile rupture strength of the concrete, it appears that deck cracks would appear after eight days. Therefore, the finite element simulations indicate that transverse cracking in the bridge deck over the interior pier could be expecting 4-8 days after casting due to concrete shrinkage. The type, location, and time frame of cracking all agree with actual results as shown in Figure 5.2.

The transverse stresses are generally less than 50% of the longitudinal stresses. However, this does not imply that the transverse stresses are not important. In fact, it is likely that while not in the same

direction, the longitudinal and transverse stresses in combination will cause the deck to crack earlier than either would predict on their own. In analyzing the principle tensile stress over the center girder on the fourth day, it can be seen that there is a stress of 0.45 MPa. Therefore, the principle tensile stress is approximately 4% larger than the longitudinal stress at that same location. The deck will most likely initiate cracks at an angle (neither perfectly transverse nor longitudinal). However, it is clear that the longitudinal stresses (causing transverse cracking) are still the predominant stresses in the deck.

It should be emphasized that the true cracking "strength" of the concrete is unknown. In this case, the modulus of rupture of the concrete was used as an estimate of the concrete cracking strength. However, the concrete may not be in pure bending, and therefore the modulus of rupture is only an estimate.

As mentioned in the previous section, the HL-93 truck loads itself will not cause deck cracking. Therefore, the effects of the HL-93 truck loading should be analyzed in combination with the shrinkage strains. The following analysis helps compare the effects of both traffic loading and concrete shrinkage on deck cracking. This example examines the state of stress likely to be present at 10 days after casting (assuming 28 MPa (4 ksi) concrete);

$$\sigma_{shrinkage} = 4.074\ MPa$$

$$\sigma_{HL-93} = 0.791\ MPa$$

$$f_r = 3.665\ MPa$$

$$\sigma_{shrinkage} + \sigma_{HL-93} = 4.865\ MPa > f_r = 3.665\ MPa$$

$$\sigma_{HL-93} \approx 0.216\ f_r$$

$$\sigma_{HL-93} \approx 0.194\ \sigma_{shrinkage}$$

The example computations above illustrates that the HL-93 loading causes tensile stress approximately equal to 21.6% of the modulus of rupture (used to represent the cracking strength) for the concrete, and 19.4% of the stress caused by concrete shrinkage. In modeling the traffic loading, only two HL-93 trucks were statically placed on the deck's surface. In reality, varying traffic loading would have a dynamic component as vehicles move across the bridge deck. Therefore, even if the deck is not cracked due to concrete shrinkage, the combination of traffic load and concrete shrinkage does appear to have the potential to cause transverse cracking in the bridge deck over the interior support as is seen in the Bridge B-20-133/134.

REFERENCES

ANSYS (2007). *ANSYS User's Manual*, Academic Research Release 11.0, ANSYS Inc.

Foley, C.M., Wan, B., Schneeman, C., Barnes, K., Komp, J., Liu, J., Smith, A. (2010). *In-Situ Monitoring and Testing of IBRC Bridges in Wisconsin*, Final Report, Wisconsin Highway Research Program, Wisconsin Department of Transportation, Madison, WI.

Foley, C.M., Wan, B., and Liu, J. (2008). "Wheel Load Distribution in Concrete Bridge Decks with FRP Stay-In-Place Forms", *FRP Stay-In-Place Forms for Concrete Structures, ACI SP-257*, American Concrete Institute, Farmington Hills, MI, pp. 33-52.

Kachlakev, D., Miller, T., and Yim, S. (2001). *Finite Element Modeling of Reinforced Concrete Structures Strengthened with FRP Laminates*, Final Report, Oregon Department of Transportation Research Group.

Komp, J.T. (2009). *Evaluation of Premature Cracking in Concrete Bridge Decks Using Finite Element Analysis*, Master's Thesis, Marquette University, Milwaukee, WI.

Krauss, P.D., and Rogalla, E.A. (1996). *Transverse Cracking in Newly Constructed Bridge Decks*, NCHRP Report 380, Transportation Research Board, Washington, DC.

Martin, K.E. (2006). *Impact of Environmental Effects on, and Condition Assessment of IBRC Bridge Decks in Wisconsin*, Master's Thesis, Marquette University, Milwaukee, WI, 2006.

Saadeghvaziri, M. and Hadidi, R. (2002). *Cause and Control of Transverse Cracking in Concrete Bridge Decks*, Final Report, FHWA-NJ-2002-19.

Schneeman, C.L. (2006). *Development and Evaluation of a Removable and Portable Strain Sensor for Short-Term Live Loading of Bridge Structures*, Master's Thesis, Marquette University, Milwaukee, WI.

Tadros, M.K. and Al-Omaishi, N. (2003). *Prestress Losses in Pretensioned High-Strength Concrete Bridge Girders*, Report 496, National Cooperative Highway Research Program.

Ziemian, R.D. and McGuire, W. (2007). *MASTAN2*, Wiley.

Table 5.1 Strain Readings Recorded During Field Loading Tests.

Span and	Location Relative to Truck Front Wheel								
Stop Location	(mm)								
	-1800	-1300	-890	-440	F.W.	440	890	1300	1800
	Strain (με)								
Exterior Span									
TW1-W2	9	26	23	32	92	32	23	26	9
TW1-W1	NA	14	41	59	45	41	41	14	NA
TW1-M	NA	NA	34	26	76	69	21	NA	NA
TW1-E1	NA	22	12	50	126	40	12	22	NA
TW1-E2	16	5	30	75	75	75	30	5	16
Interior Span									
TW2-W2	2	6	15	48	51	48	15	6	2
TW2-W1	NA	4	11	32	76	24	11	4	NA
TW2-M	NA	NA	18	47	43	20	10	NA	NA
TW2-E1	NA	13	28	25	35	21	25	28	NA
TW2-E2	9	19	16	22	36	22	16	19	9

Note: The shaded areas represent values that were obtained based on symmetry of the strain gauges, rather than actual strain gauge readings.

Table 5.2 Transverse Deck Strain Results taken from Finite Element Simulations.

Span and	Location Relative to Truck Front Wheel								
Stop Location	(mm)								
	-1800	-1350	-900	-450	F.W.	450	900	1350	1800
	Strain (με)								
Exterior Span									
TW1-W2	14.28	18.03	25.07	38.39	56.22	37.14	22.56	14.27	9.23
TW1-W1	14.56	18.15	25.05	38.14	56.12	36.52	21.90	13.39	6.94
TW1-M	14.70	18.12	24.83	37.79	55.36	35.91	20.98	10.27	5.77
TW1-E1	14.65	17.89	24.47	37.21	54.81	34.93	16.46	9.07	4.69
TW1-E2	14.41	17.49	23.85	36.50	53.64	27.68	15.23	7.95	4.05
Interior Span									
TW2-W2	17.10	19.48	25.29	37.41	54.57	34.46	19.42	10.94	6.29
TW2-W1	15.93	18.26	23.97	36.12	53.03	33.13	18.21	10.13	7.08
TW2-M	14.69	16.96	22.66	34.69	51.89	31.92	17.39	11.83	7.34
TW2-E1	13.36	15.59	21.24	33.40	50.41	31.08	20.71	12.02	8.37
TW2-E2	11.96	14.17	19.87	32.08	49.76	37.86	20.87	13.07	9.29

Table 5.3 Transverse Deck Strain Comparison of Field Measured and FE Simulation Data.

Span and Stop Location	Location Relative to Truck Front Wheel (mm)								
	-1800	-1300	-890	-440	F.W.	440	890	1300	1800
	ANSYS/ACTUAL (%)								
Exterior Span									
TW1-W2	158.7	69.4	109.0	120.0	61.1	116.1	98.1	54.9	102.6
TW1-W1	NA	129.6	61.1	64.6	124.7	89.1	53.4	95.7	NA
TW1-M	NA	NA	73.0	145.4	72.8	52.0	99.9	NA	NA
TW1-E1	NA	81.3	203.9	74.4	43.5	87.3	137.2	41.2	NA
TW1-E2	90.1	349.8	79.5	48.7	71.5	36.9	50.8	159.0	25.3
Interior Span									
TW2-W2	855.1	324.7	168.6	77.9	107.0	71.8	129.5	182.3	314.6
TW2-W1	NA	456.5	217.9	112.9	69.8	138.0	165.5	253.2	NA
TW2-M	NA	NA	125.9	73.8	120.7	159.6	173.9	NA	NA
TW2-E1	NA	120.0	75.9	133.6	144.0	148.0	82.8	42.9	NA
TW2-E2	132.8	74.6	124.2	145.8	138.2	172.1	130.5	68.8	103.2

Table 5.4 Transverse Deck Strain Comparison of Field Measured and FE Simulation Data Banded by Strain Gauge.

Span and Stop Location	Location Relative to Truck Front Wheel (mm)								
	-1800	-1300	-890	-440	F.W.	440	890	1300	1800
	ANSYS/ACTUAL (%)								
Exterior Span									
TW1-W2	158.7	69.4	109.0	120.0	61.1	116.1	98.1	54.9	102.6
TW1-W1	NA	129.6	61.1	64.6	124.7	89.1	53.4	95.7	NA
TW1-M	NA	NA	73.0	145.4	72.8	52.0	99.9	NA	NA
TW1-E1	NA	81.3	203.9	74.4	43.5	87.3	137.2	41.2	NA
TW1-E2	90.1	349.8	79.5	48.7	71.5	36.9	50.8	159.0	25.3
Interior Span									
TW2-W2	855.1	324.7	168.6	77.9	107.0	71.8	129.5	182.3	314.6
TW2-W1	NA	456.5	217.9	112.9	69.8	138.0	165.5	253.2	NA
TW2-M	NA	NA	125.9	73.8	120.7	159.6	173.9	NA	NA
TW2-E1	NA	120.0	75.9	133.6	144.0	148.0	82.8	42.9	NA
TW2-E2	132.8	74.6	124.2	145.8	138.2	172.1	130.5	68.8	103.2

Table 5.5 Longitudinal Tensile Normal Stresses at the Top of Bridge Deck over Interior Pier.

	Coordinates (mm)			Normal Stress (MPa)
Point	x	z (-)	y	z
1	364	32850	1570	0.34173
2	1655	33600	1570	0.38893
3	3014	34350	1570	0.71678
4	4305	35100	1570	0.59190
5	5664	35850	1570	0.76337
6	6995	36600	1570	0.48917
7	8314	37350	1570	0.45692
8	9605	38100	1570	0.22407
9	10964	38850	1570	0.12541
Max	5376	36075	1570	0.79095

Table 5.6 Increase in Compressive Strength and Modulus of Elasticity with Time.

Time	Fraction fc'	f_c'=4,000 psi	E (psi)	E (MPa)
1	0.21	840	1652017	11390
2	0.4	1600	2280000	15720
3	0.54	2160	2649121	18265
4	0.63	2520	2861377	19729
5	0.687	2748	2988018	20602
6	0.74	2960	3101135	21382
7	0.77	3080	3163372	21811
8	0.8	3200	3224407	22232
9	0.8267	3306.8	3277773	22599
10	0.853	3412	3329503	22956
11	0.873	3492	3368309	23224
12	0.893	3572	3406674	23488
13	0.904	3616	3427592	23632
14	0.913	3652	3444611	23750

Table 5.7 Longitudinal Stress Results from Shrinkage Analysis.

Z-Stress (MPa)										
Node Location	Time, t (days)									
	1	2	3	4	5	6	7	8	9	10
1	0.338	0.443	0.488	0.504	0.504	0.501	0.492	0.482	0.473	0.462
2	0.279	0.360	0.394	0.406	0.404	0.402	0.394	0.386	0.378	0.369
3	0.307	0.393	0.429	0.441	0.440	0.437	0.428	0.419	0.411	0.401
4	0.278	0.355	0.388	0.398	0.397	0.394	0.386	0.378	0.370	0.362
5	0.306	0.390	0.426	0.438	0.436	0.433	0.425	0.416	0.407	0.398
6	0.278	0.355	0.388	0.398	0.397	0.394	0.386	0.378	0.370	0.362
7	0.306	0.394	0.432	0.444	0.443	0.440	0.432	0.423	0.414	0.405
8	0.279	0.360	0.394	0.405	0.404	0.402	0.394	0.386	0.378	0.369
9	0.337	0.443	0.491	0.508	0.507	0.505	0.497	0.487	0.477	0.467
Daily Avg	**0.301**	**0.388**	**0.426**	**0.438**	**0.437**	**0.434**	**0.426**	**0.417**	**0.409**	**0.399**
Girder Avg	0.319	0.413	0.453	0.467	0.466	0.463	0.455	0.445	0.436	0.427
Non-Girder Avg	0.278	0.357	0.391	0.402	0.401	0.398	0.390	0.382	0.374	0.366

Table 5.8 Longitudinal Stress and Possible Transverse Cracking Results from Shrinkage Analysis.

Z-Stress (MPa)										
Node Location	Time, t (days)									
	1	2	3	4	5	6	7	8	9	10
1	0.338	0.443	0.488	0.504	0.504	0.501	0.492	0.482	0.473	0.462
2	0.279	0.360	0.394	0.406	0.404	0.402	0.394	0.386	0.378	0.369
3	0.307	0.393	0.429	0.441	0.440	0.437	0.428	0.419	0.411	0.401
4	0.278	0.355	0.388	0.398	0.397	0.394	0.386	0.378	0.370	0.362
5	0.306	0.390	0.426	0.438	0.436	0.433	0.425	0.416	0.407	0.398
6	0.278	0.355	0.388	0.398	0.397	0.394	0.386	0.378	0.370	0.362
7	0.306	0.394	0.432	0.444	0.443	0.440	0.432	0.423	0.414	0.405
8	0.279	0.360	0.394	0.405	0.404	0.402	0.394	0.386	0.378	0.369
9	0.337	0.443	0.491	0.508	0.507	0.505	0.497	0.487	0.477	0.467
Daily Avg. Stress	0.301	0.388	0.426	0.438	0.437	0.434	0.426	0.417	0.409	0.399
Cumulative Stress	**0.301**	**0.689**	**1.114**	**1.552**	**1.989**	**2.423**	**2.849**	**3.266**	**3.675**	**4.074**
(at time, t)										
Modulus of rupture	1.819	2.510	2.916	3.150	3.289	3.414	3.482	3.550	3.608	3.665
No Cracking?	TRUE	TRUE	TRUE	TRUE	TRUE	TRUE	TRUE	TRUE	FALSE	FALSE
10% Comp. Strength	0.588	1.120	1.512	1.764	1.924	2.072	2.156	2.240	2.315	2.388
No Cracking?	TRUE	TRUE	TRUE	TRUE	FALSE	FALSE	FALSE	FALSE	FALSE	FALSE

Figure 5.1 Bridge B-20-133/134.

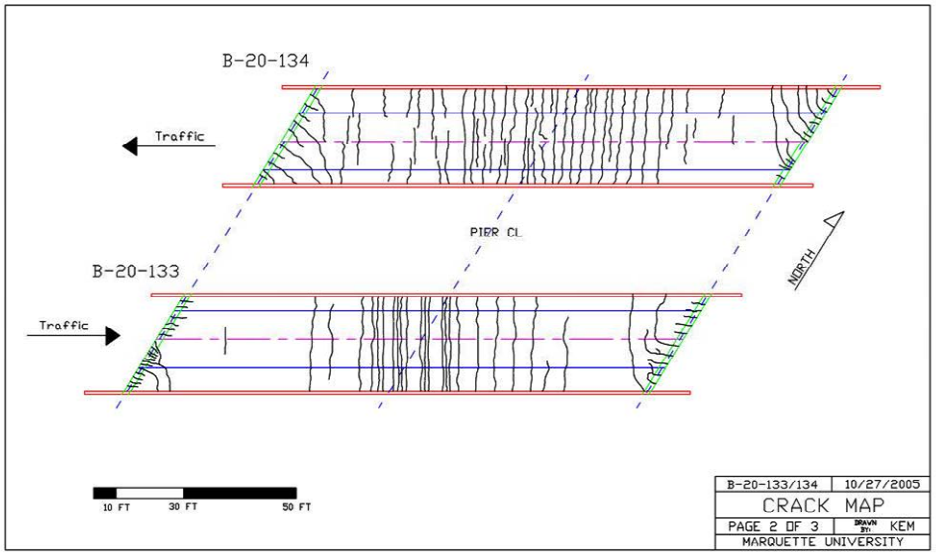

Figure 5.2 Crack Map of Bridge B-20-133/134.

Figure 5.3 Cracking with Efflorescence (South Side of B-20-133 above Central Pier).

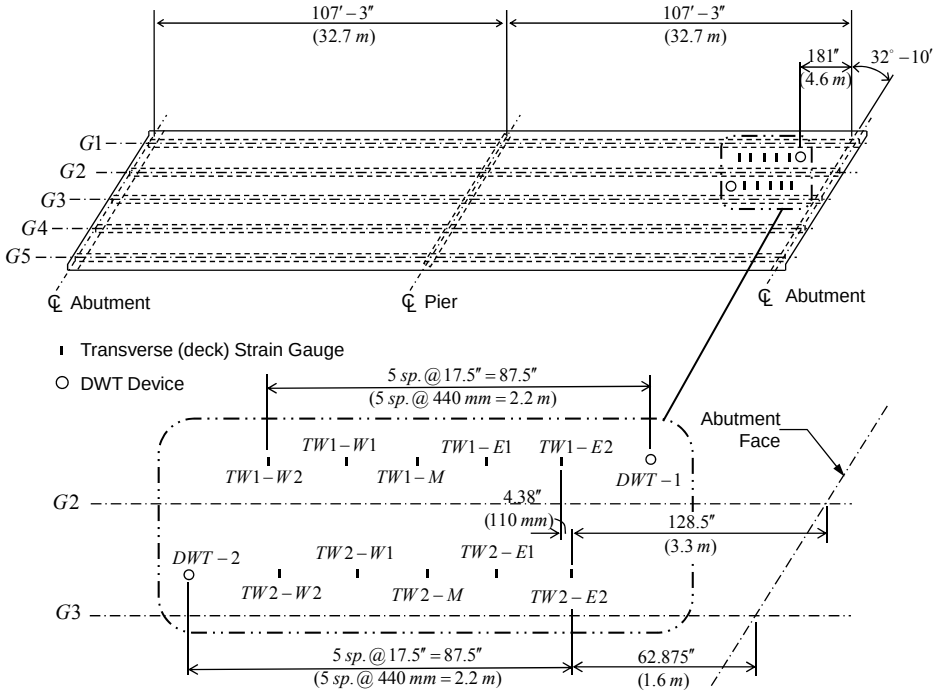

Figure 5.4 Bridge B-20-133 Plan and Instrumentation Layout.

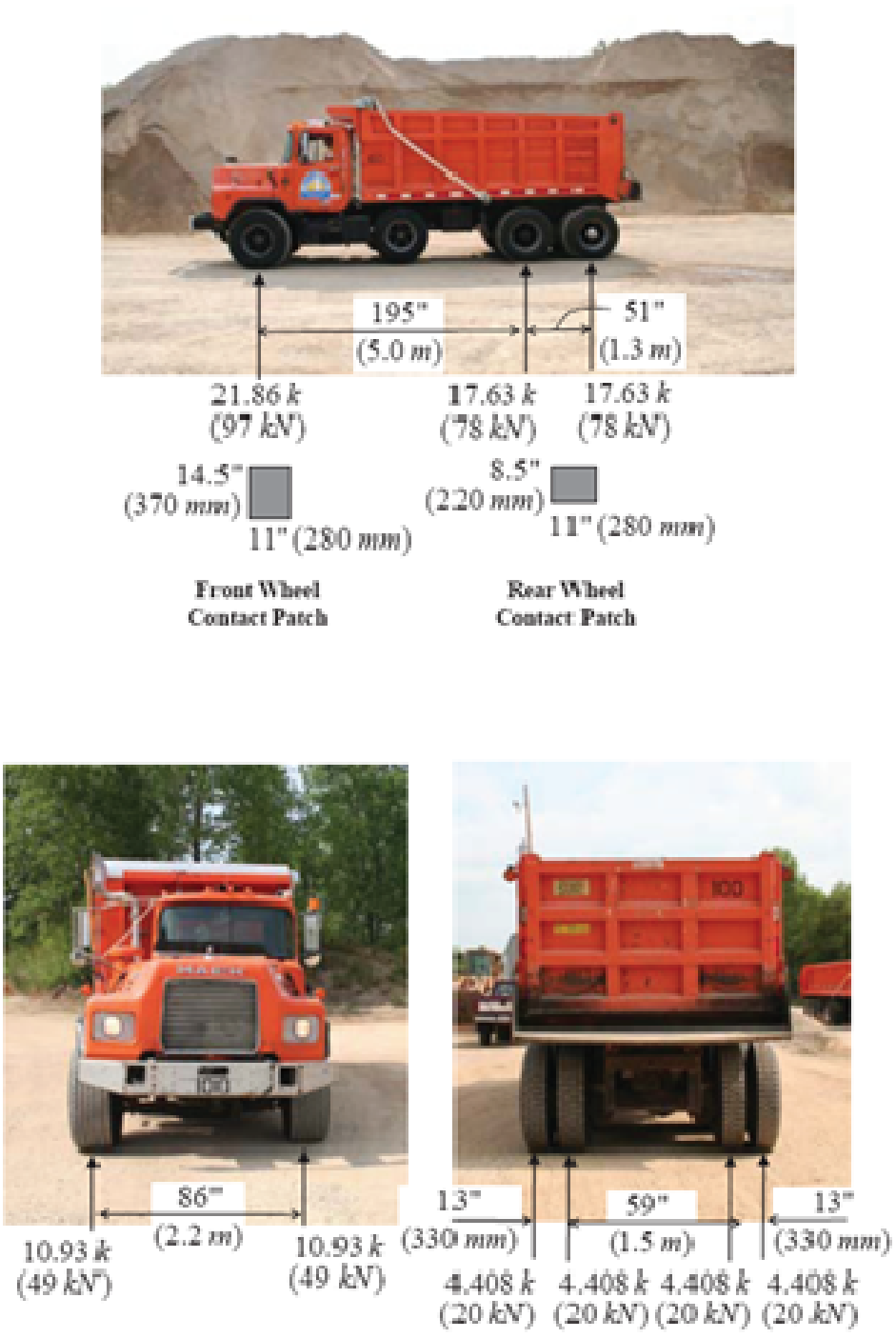

Figure 5.5 Calibrated Tri-Axle Dump Truck with Axle Configuration used in the Testing.

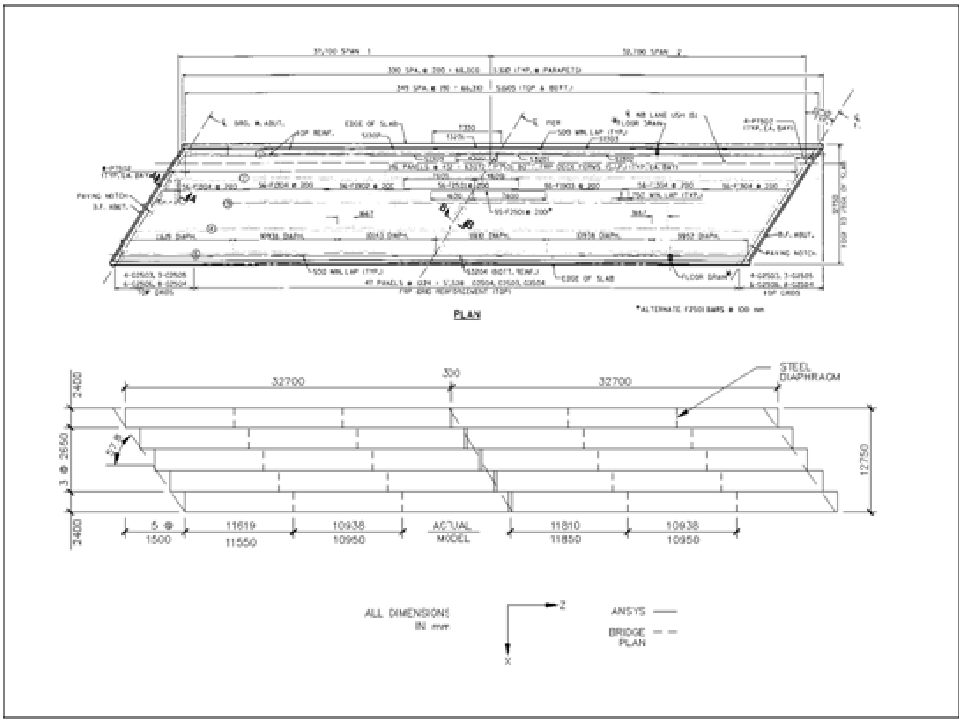

Figure 5.6 Actual Bridge vs. Finite Element Model.

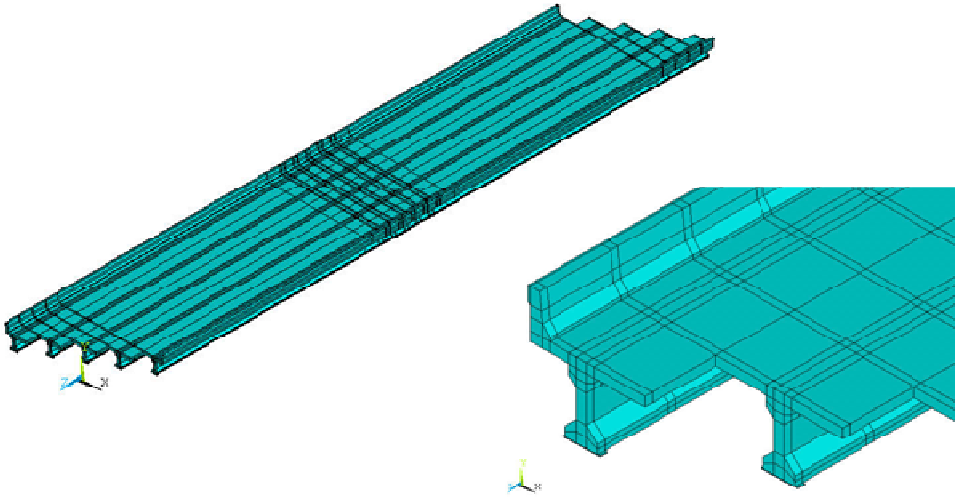

Figure 5.7 Finite Element Bridge Superstructure and Skew.

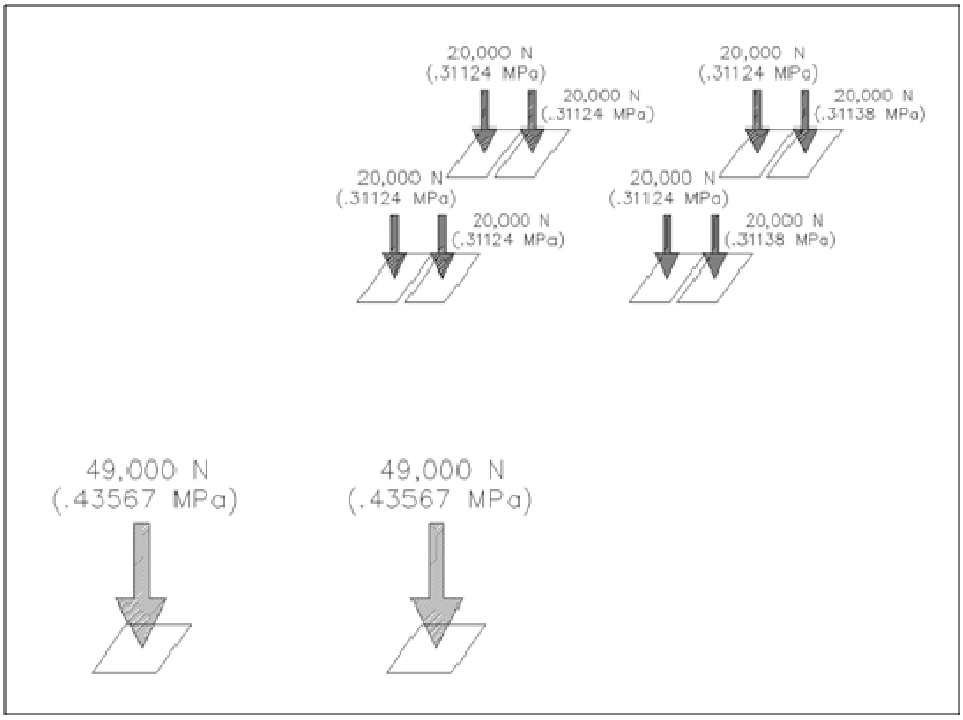

Figure 5.8 Tire Point Load Modeling.

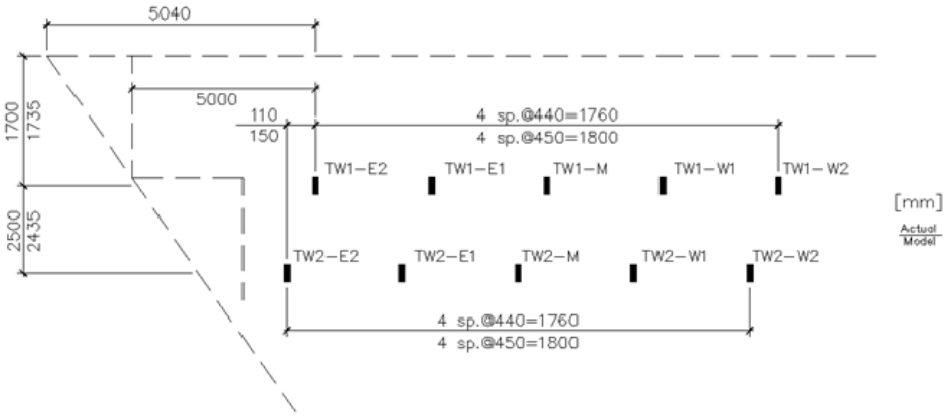

Figure 5.9 Actual vs. Finite Element Model Strain Gauge Locations.

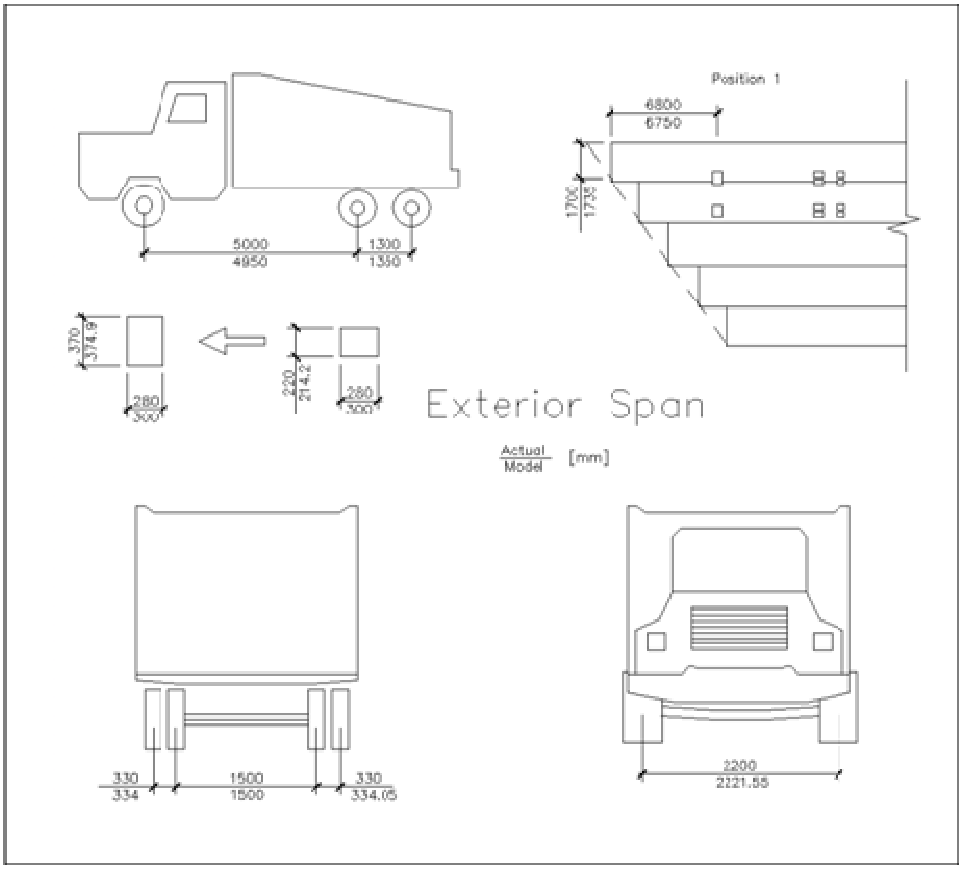

Figure 5.10 Actual vs. Finite Element Model Tri-Axle Dimensions (Exterior Loading).

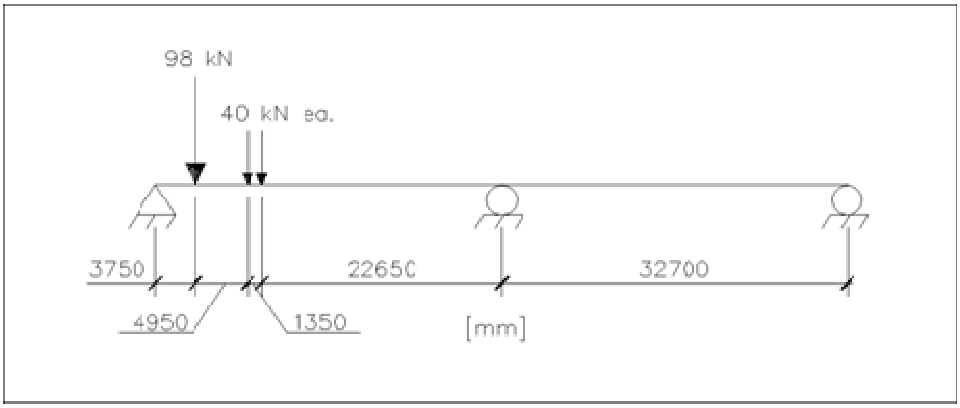

Figure 5.11 MASTAN2 Model of 2-Span Bridge.

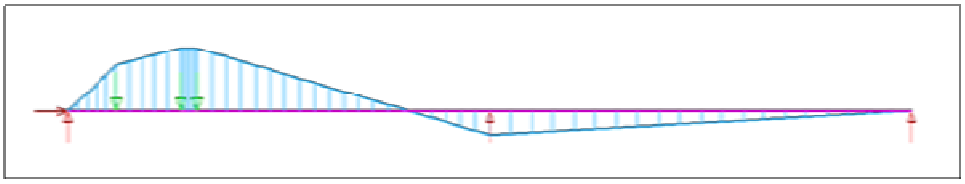

Figure 5.12 Moment Diagram Corresponding to the Loading Scenario in Figure 5.11.

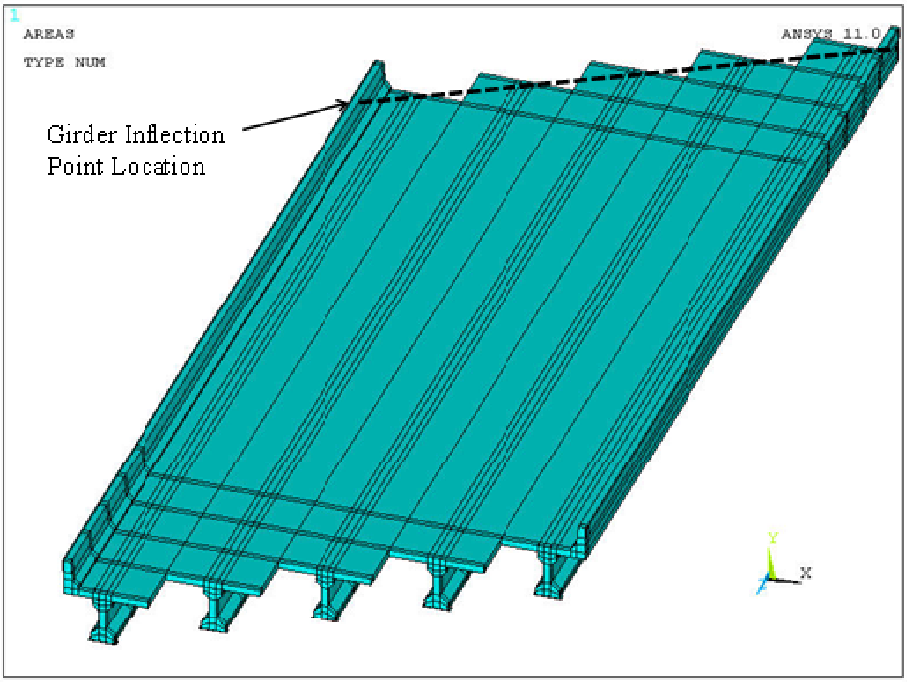

Figure 5.13 Partial Bridge Model.

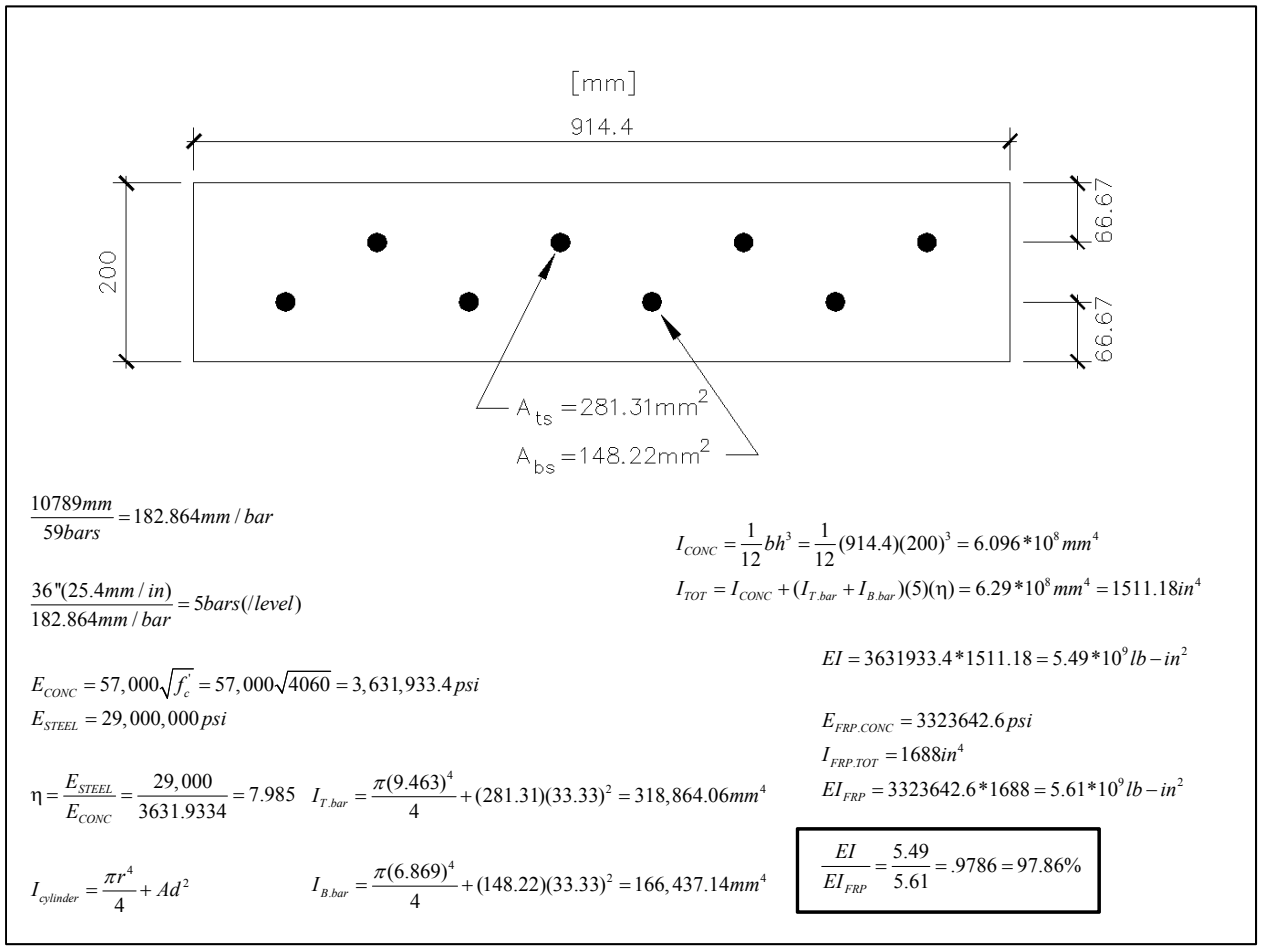

$$\frac{10789mm}{59bars} = 182.864mm/bar$$

$$\frac{36"(25.4mm/in)}{182.864mm/bar} = 5bars(/level)$$

$$I_{CONC} = \frac{1}{12}bh^3 = \frac{1}{12}(914.4)(200)^3 = 6.096*10^8\,mm^4$$

$$I_{TOT} = I_{CONC} + (I_{T.bar} + I_{B.bar})(5)(\eta) = 6.29*10^8\,mm^4 = 1511.18in^4$$

$$EI = 3631933.4*1511.18 = 5.49*10^9\,lb-in^2$$

$$E_{CONC} = 57,000\sqrt{f_c'} = 57,000\sqrt{4060} = 3,631,933.4\,psi$$

$$E_{STEEL} = 29,000,000\,psi$$

$$E_{FRP.CONC} = 3323642.6\,psi$$

$$I_{FRP.TOT} = 1688in^4$$

$$EI_{FRP} = 3323642.6*1688 = 5.61*10^9\,lb-in^2$$

$$\eta = \frac{E_{STEEL}}{E_{CONC}} = \frac{29,000}{3631.9334} = 7.985 \qquad I_{T.bar} = \frac{\pi(9.463)^4}{4} + (281.31)(33.33)^2 = 318,864.06mm^4$$

$$I_{cylinder} = \frac{\pi r^4}{4} + Ad^2 \qquad I_{B.bar} = \frac{\pi(6.869)^4}{4} + (148.22)(33.33)^2 = 166,437.14mm^4$$

$$\frac{EI}{EI_{FRP}} = \frac{5.49}{5.61} = .9786 = 97.86\%$$

Figure 5.14 Equivalent Stiffness Calculations.

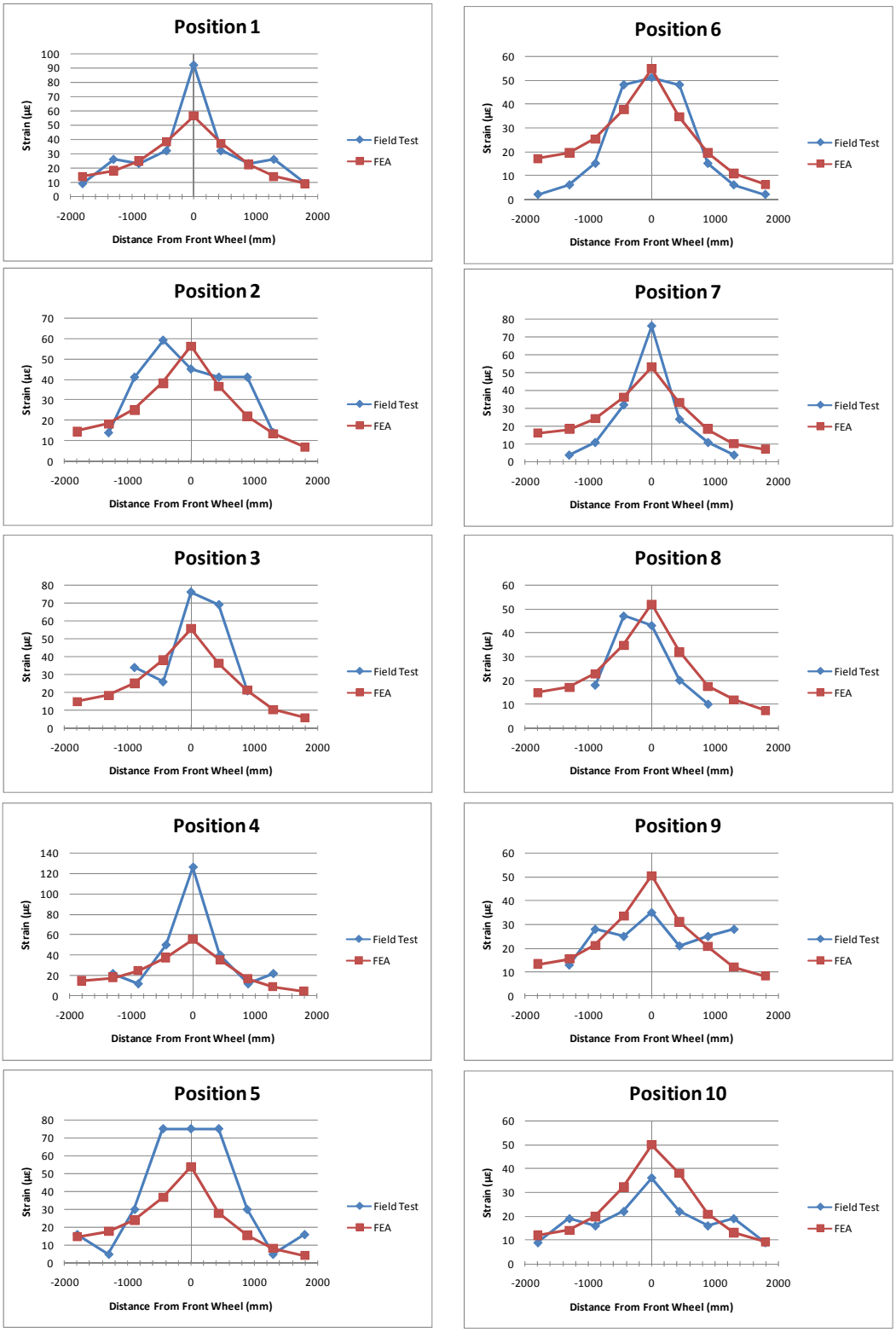

Figure 5.15 Transverse Deck Strains obtained from finite element analysis and field load test.

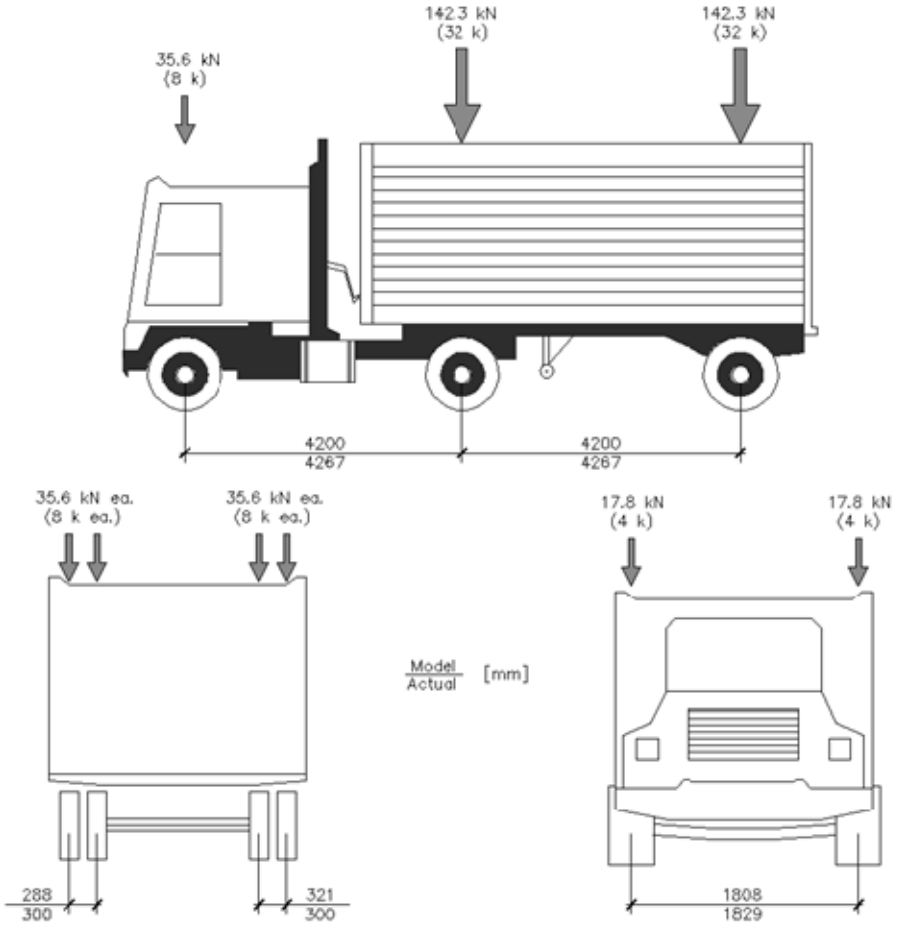

Figure 5.16 HL-93 Truck Loading and Wheel Spacing.

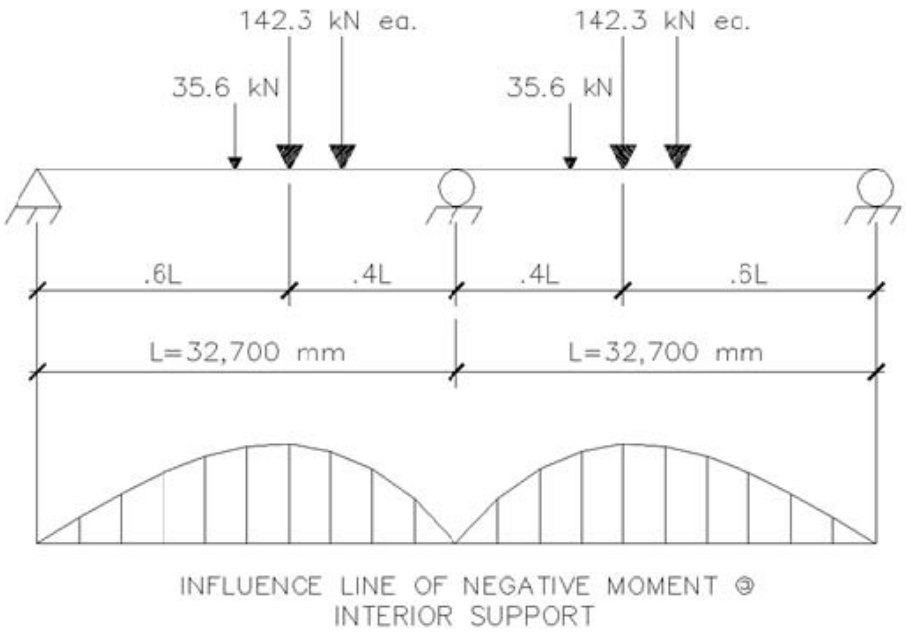

Figure 5.17 Theoretical Truck Loading for Maximum Moment at Interior Pier.

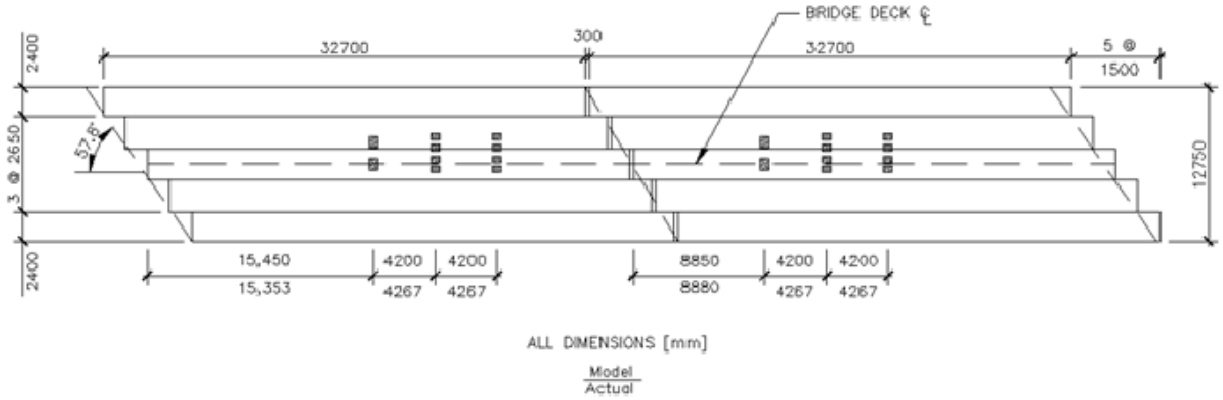

Figure 5.18 Plan View of HL-93 Loading Locations.

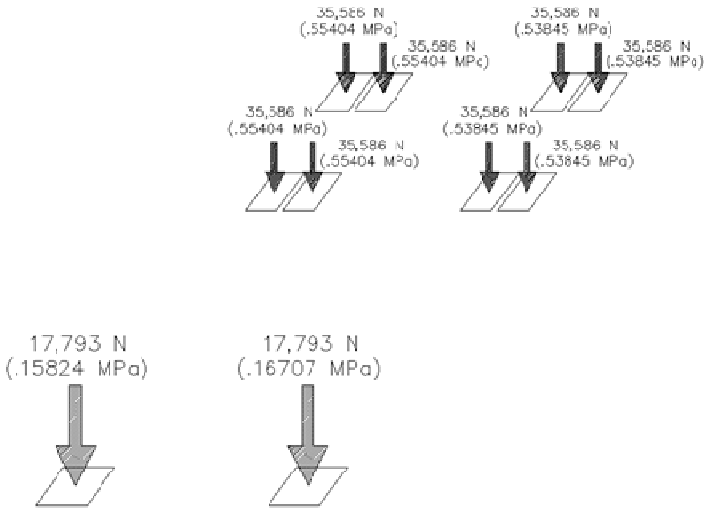

Figure 5.19 Tire Pressure Loading Based on Contact Areas.

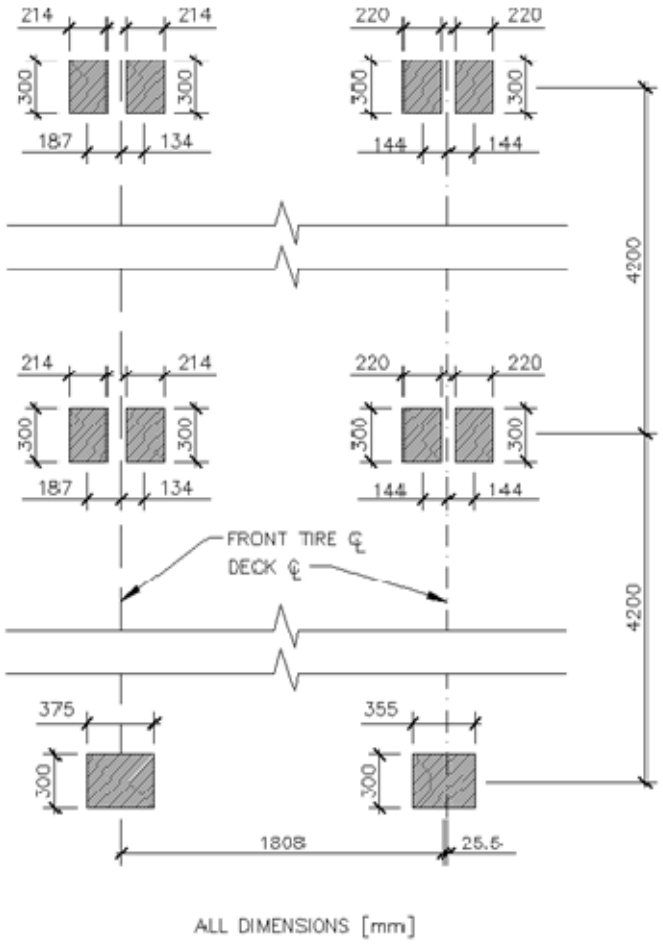

Figure 5.20 Tire Contact Areas and Relative Spacing.

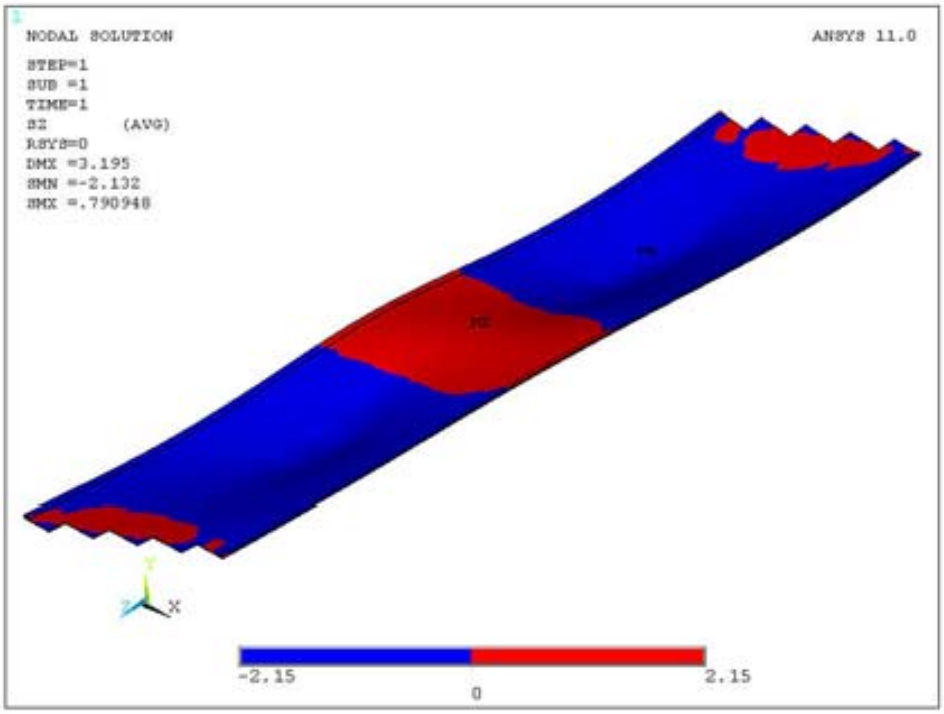

Figure 5.21 Stress Contour at the Deck Top Surface Caused by the HL-93 Trucks.

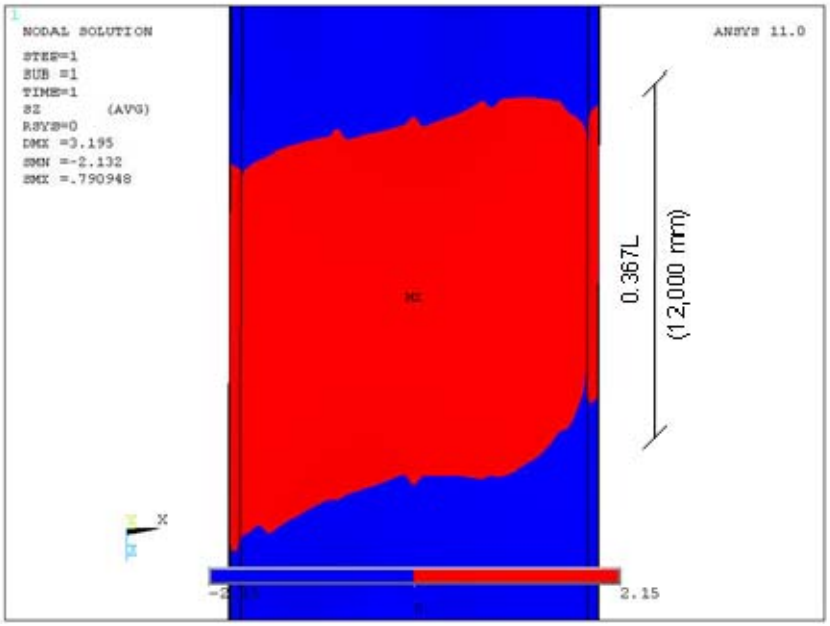

Figure 5.22 Tensile Stresses at Top of Deck over Interior Pier.

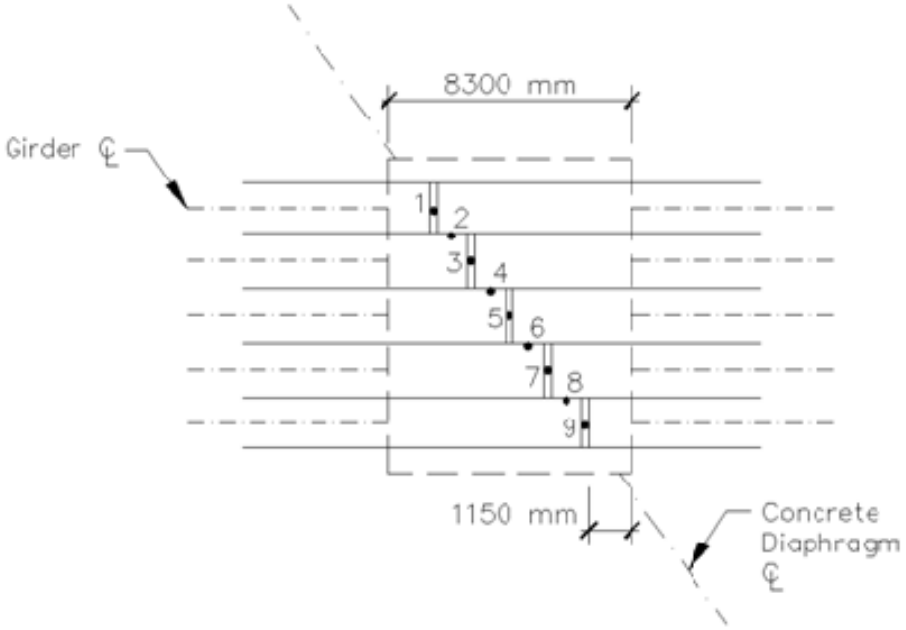

Figure 5.23 Nodal Locations over the Interior Pier.

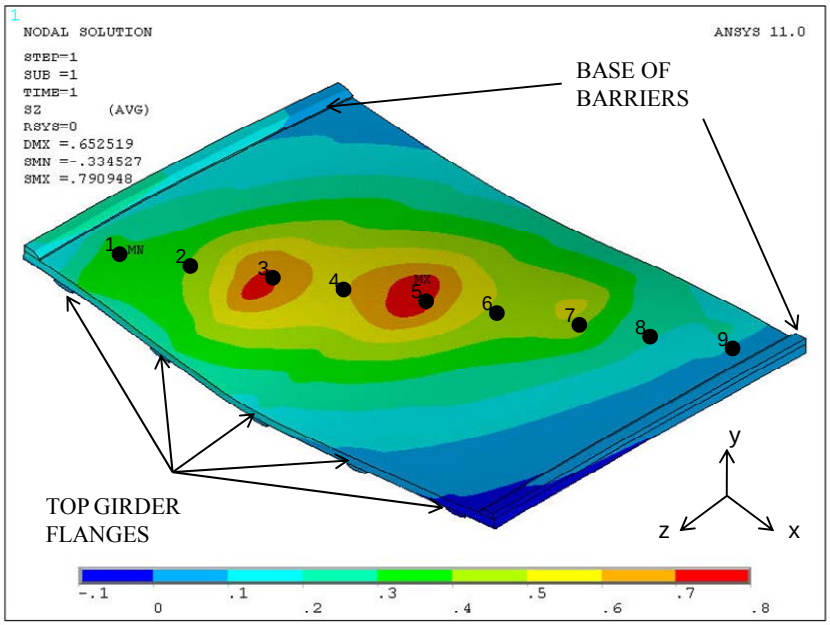

Figure 5.24 Nodal Locations over the Interior Pier.

Figure 5.25 Topographic Map of United States Humidity (Tadros and Al-Omaishi 2003).

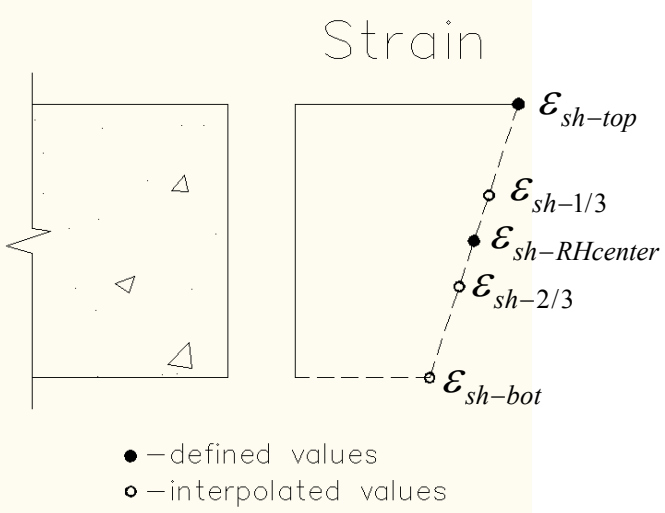

Figure 5.26 Shrinkage Strain Distribution throughout the Deck.

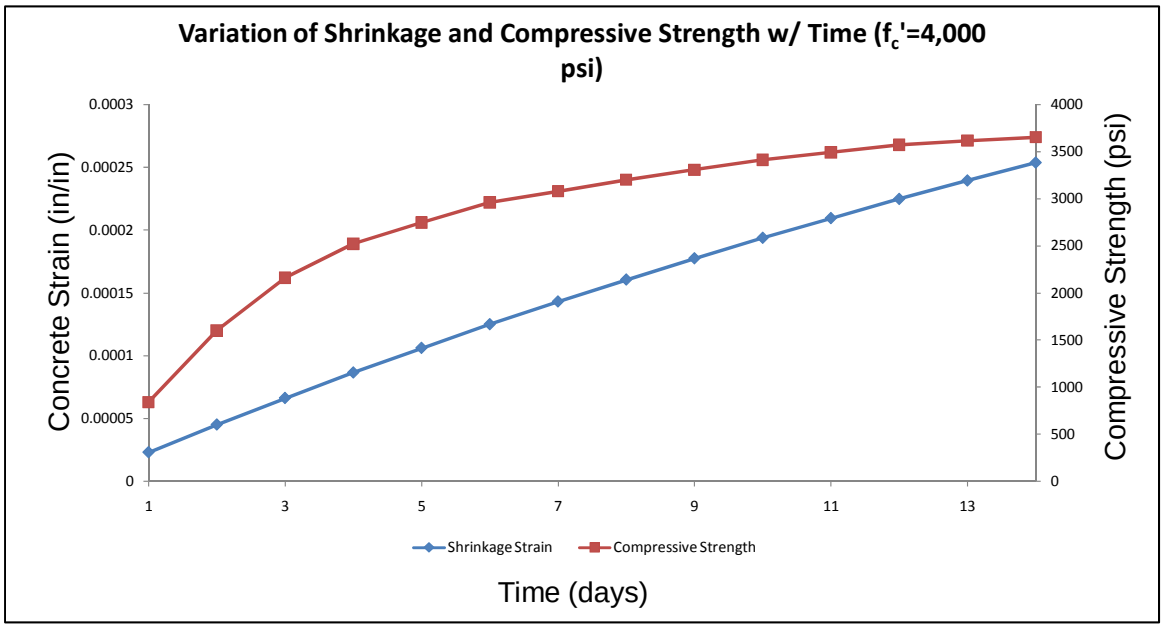

Figure 5.27 Variation of Shrinkage Strain and Compressive Strength.

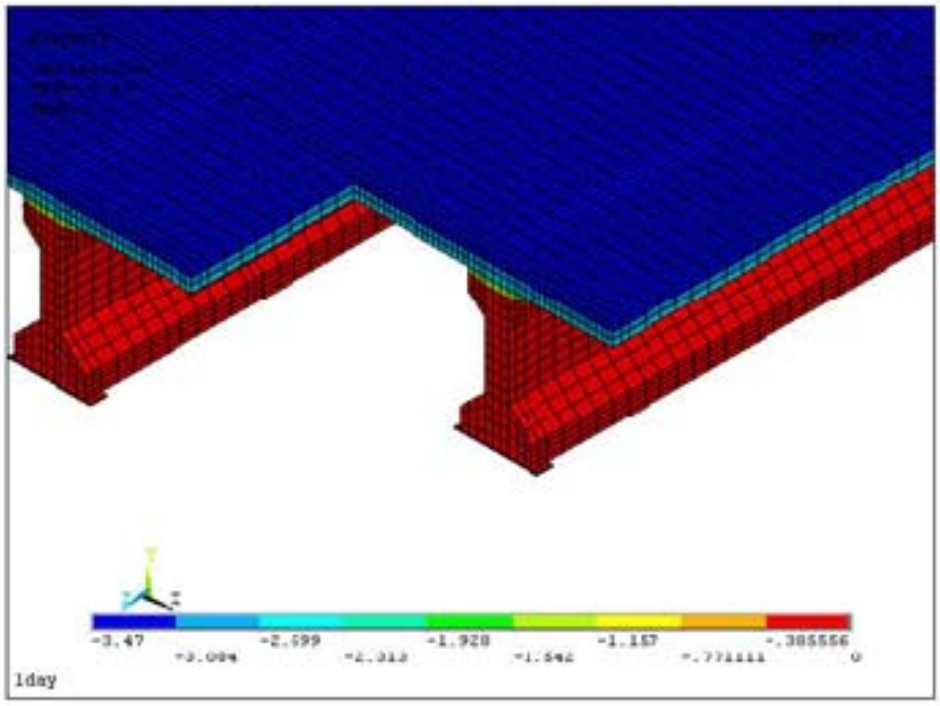

Figure 5.28 Temperature Distribution throughout the Finite Element Model.

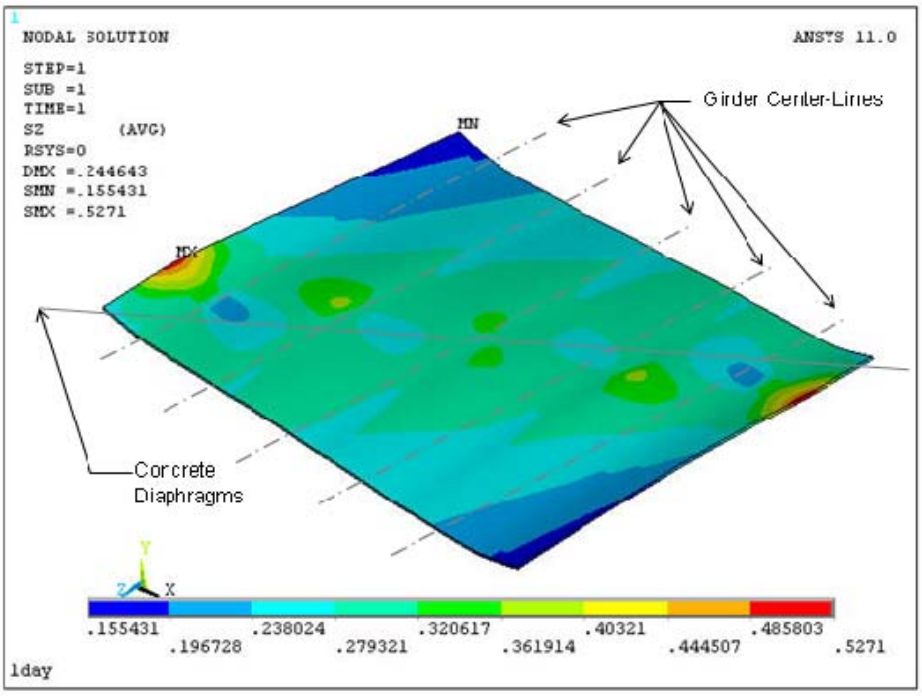

Figure 5.29 Longitudinal Stress Contour on Top of Deck from Shrinkage Analysis.

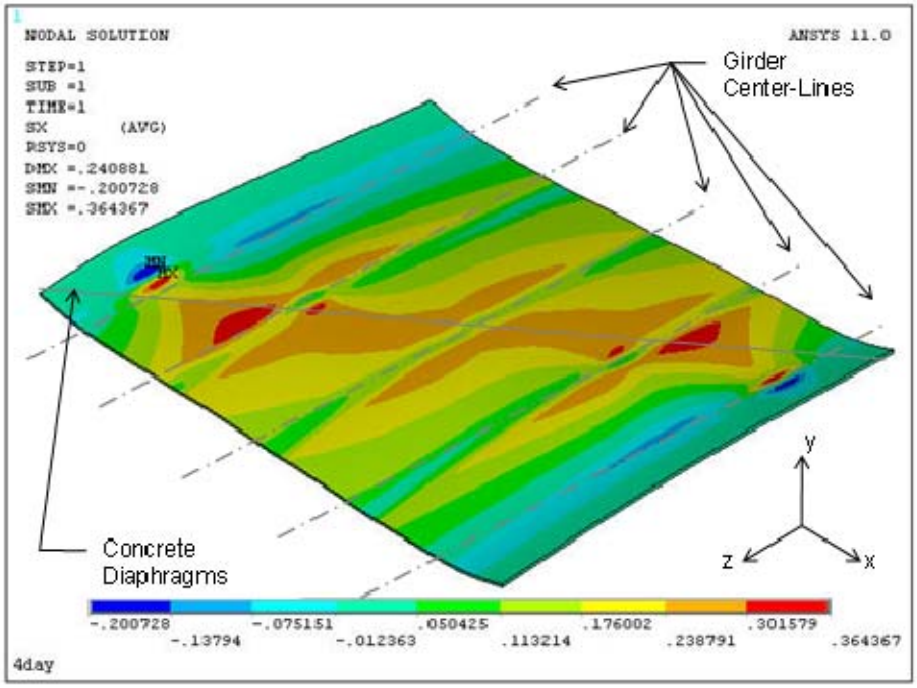

Figure 5.30 Transverse Stress Contour on Top of Deck from Shrinkage Analysis.

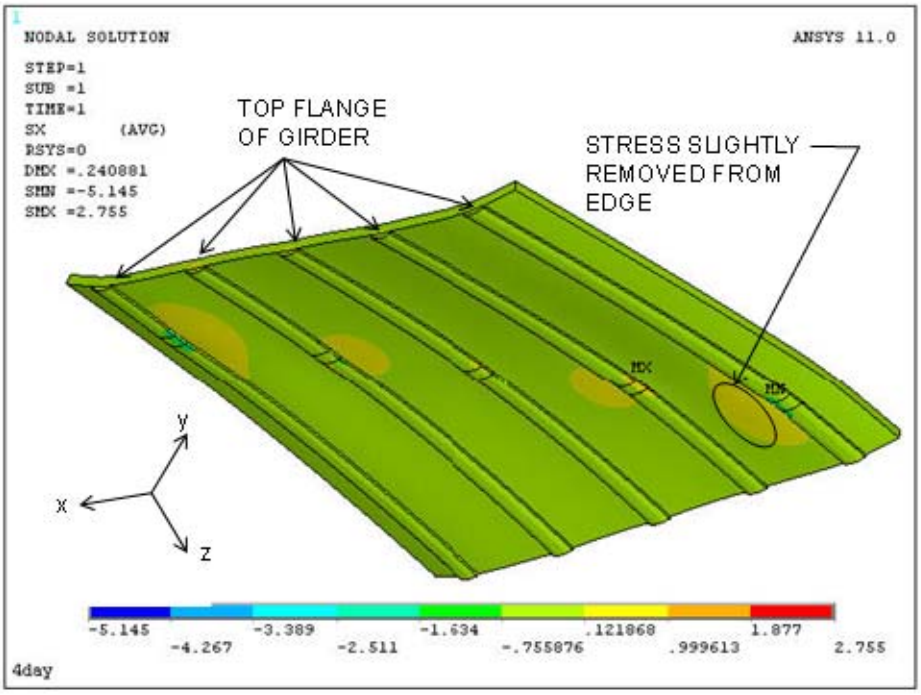

Figure 5.31 Transverse Stress Contour on Bottom of Deck from Shrinkage Analysis.

Chapter 6
Concrete Properties of Bridge Deck

INTRODUCTION

The literature review and finite element analysis conducted indicated that concrete shrinkage may be a major factor affecting the extent of early-age bridge deck cracking. Concrete shrinkage is affected by the components used in the concrete mix, curing conditions and ambient environment. As demonstrated in Equations 5.1 to 5.6, concrete shrinkage can be related to concrete compressive strength at specific ages. Finite element analysis conducted indicated that the tensile stress in concrete deck is affected by the material's modulus of elasticity. When the tensile stresses imparted to the concrete are larger than the tensile strength of concrete, cracking will occur. Therefore, concrete properties at early ages are very important when evaluating bridge deck cracking. Compressive testing cylinders were collected from two newly constructed bridges in the metro-Milwaukee area (Racine Ave. Bridge and Humboldt Ave. Bridge) to evaluate unconfined compression strength, tension strength and modulus of elasticity gain with time. The cylinders were tested in the structural testing lab at Marquette University and results of these tests are presented in this chapter.

RACINE AVENUE BRIDGE CONCRETE TESTING

The Racine Avenue Bridge (B-67-113) in Waukesha County, Wisconsin was the first bridge for which bridge deck material property changes with time were evaluated. This bridge constitutes an overpass for Racine Avenue over IH-43. The following sections describe the testing done to evaluate the variation of concrete properties with time.

Concrete Deck and Cylinder Casting

The Racine Avenue Bridge superstructure utilizes steel girders. The new bridge deck was poured on July 13th, 2009. The typical concrete mix design is listed in Table 6.1. Its target air content is 6% and target slump is 4 inches. The concrete placement began at 5:00 am to avoid the high temperature affects on fresh concrete. The research team cast thirty-eight 6x12 (in.) concrete cylinders during the period of 5:30 – 8:30 am. These cylinders were cast from concrete randomly taken from six different concrete trucks, with each set of cylinders labeled A-F, respectively.

Each cylinder was cast in two segments. One-half the concrete was added to the cylinder mold before the concrete was vibrated using a hand-held vibrator. Once thoroughly vibrated (approximately 10 seconds, or until the concrete obtained a "smooth" texture), the remaining half of the concrete was placed

in the cylinder mold, at which time the cylinder was once again vibrated. The cylinder was then leveled, and a plastic bag was placed over the cylinder mold as shown in Figure 6.1. The plastic bag would help simulate the curing conditions (cover) in the field, on the actual bridge deck. After 24 hours curing in the field, the cylinders were transported to Marquette University where they were placed outside in a shaded area for the remainder of their curing. The cylinders were placed outside of building and under a large vehicle to prevent overheating of the cylinders, while once again attempting to simulate the curing conditions at the bridge site.

Laboratory Testing

The cylinders were then tested for compressive strength, tensile strength, and modulus of elasticity at time intervals of 2.25, 3.25, 5.25, 7, 14, and 28 days after casting. Testing consisted of three cylinders for each test in the testing day. The modulus of elasticity and compressive strength tests were performed using the same set of cylinders and a total of 6 cylinders were tested each day.

The cylinders were brought to the Marquette materials laboratory where the plastic bags were removed and the cylinders were removed from the molds. In general, the cylinders maintained the proper 6 in. diameter and 12 in. height, and therefore dimensions of 6x12 in. used in all calculations. In the few cases where the cylinders did not maintain the proper dimensions, the results were not recorded, or a specific note was made next to the results denoting this inaccuracy. Some of the plastic cylinder molds had a tendency to bulge during curing and therefore, some of the diameters of the cylinders were slightly larger than 6 inches, or the cylinders took on an elliptical shape.

Compressive Strength Testing

The unconfined compressive strength of the cylinders was obtained through the use of a Forney compression-testing machine, which complies with the ASTM C 39 standard. Un-bonded steel caps were used for compressive and modulus testing. The caps consisted of 60 durometer neoprene bearing pads (suggested for strengths of 2,500-7,000 ksi) coated with a polysaccharide powder used as a lubricant), placed in steel retainers, as shown in Figure 6.2. Once capped, the specimens were centered within the compressive machine. According to ASTM C 39, the specimen is allowed to be loaded at an increased rate during the first half of the test, and therefore the cylinder was loading at a rate of 40,000-50,000 lb/min for the initial half of the test. However, because the exact compressive strength of the specimens was generally unknown, the increased rate was only applied up until 30,000-60,000 lb (depending on the age of the specimen). Once this stage was reached, the loading was applied at a much slower rate of approximately 20,000 lb/min. While ASTM C 39 suggests loading rates up to 42 psi/s (near 70,000 lb/min), the strength of the cylinders was unknown, and there was a large concern with “shocking” the cylinder. Therefore, the much lower loading rate was implemented.

ASTM C 39 suggests that compressive failures may exhibit 6 distinct forms, as shown in Figure 6.3. Failure types 5 and 6 are common for unbounded caps (as used in this research), and therefore, the standards suggest that if either of these failures occur, the specimen should be continually loaded to insure that the ultimate strength has been reached. This was done in all tests conducted.

Modulus of Elasticity Testing

The same cylinders tested for compressive strength were used for evaluating the modulus of elasticity of the concrete. A displacement gauge was installed on the cylinders to measure the displacement, and therefore, the Young's Modulus can be calculated. ASTM C469 was implemented for the modulus of elasticity testing. The slightly modified test setup is shown in Figure 6.4. There are two hose clamps and one displacement gauge in the setup. One clamp (which was connected to a small steel plate) was tightened near the base of the cylinder. The other clamp (connected to the gauge) was tightened near the top of the cylinder. For proper calculations, it was very important that the gauge and steel plate be properly aligned, and therefore significant time was spent on the alignment of the gauge. Once attached, the cylinder was capped (as previously defined in compressive testing), and centered in the Forney machine.

Loading was initially applied until there was a "tight" connection between the cylinder caps and the machine. The gauge was then "zeroed", and the load was applied at a rate of near 10,000 lb/min. The gauge readings (in inches) were then recorded at 0.0005 in. increments, as well as the corresponding load. The loading was continued until approximately 40% of the ultimate compressive strength was reached. However, because the ultimate loading was unknown, values were usually read until the displacement approached 0.0030 in. At this loading point, the load was held, and the clamps and displacement gauge were removed. The load was then continued until the cylinder failed therefore, leading to the unconfined compression strength.

Splitting Tensile Strength Testing

The tensile strength of the concrete was determined through the use of the splitting tensile strength test described in ASTM C 496. Initially, the concrete cylinder was placed longitudinally on a piece of wood. ASTM C 496 recommends a piece of plywood with dimensions of at least 1/8 in. thickness x 1 in. wide x 12 in. length. Plywood bearing strips having nominal dimensions of 1/4 x 1 3/8 x 12 in. were used in the testing. Once the concrete was centered on the lower plywood strip, an addition strip was centered on the top of the cylinder. The cylinder was then tested using the Forney machine, with an anvil shaped replaceable head. A brass bearing strip was added under the origin plywood bearing strip to obtain the proper height with the testing machine. The entire set-up can be seen in Figure 6.5.

In theory, the loading should induce tensile stresses on the plane containing the applied load, and relatively high compressive stresses in the area immediately around the applied load. However, because the member is in tri-axial compression it is capable of sustaining much higher compressive stresses, and therefore the member should fail in tension. This tensile stress can be expressed as follows:

$$T = \frac{2P}{\pi l d} \tag{6.1}$$

T is the splitting tensile strength (psi); P is the max applied load (lbf); l is the longitudinal length of the concrete member (12 in.); and d is the diameter of the concrete member (6 in.)

ASTM C 496 suggests that the loading should be applied continuously without shock at a rate of 100-200 psi/min, which in turn equates to a rate of 11,300 – 22,600 lb/min. The loading was continuously applied at a rate near 14,000 lb/min until failure was reached, at which point the maximum load (P) was recorded.

Compressive Strength

For each test interval, three cylinders were randomly picked for compressive and Young's Modulus tests. The typical failure mode was Type 5 as shown in Figure 6.3. The results of the compressive strength testing can be seen graphically in Figure 6.6. In this figure, the "raw compressive strength" represents the results of the 18 cylinder breaks (3 per day), while the "raw averaged compressive strength", represents the average of the three breaks over each day. Unfortunately, not all the cylinders maintained the proper dimensions during the curing process (not perfectly round/ non-level surface). Due to the time sensitive nature of the testing, and the equipment available, the cylinders could not be altered, and therefore a special note was made for each of three improperly shaped cylinders. The "edited" and "edited averaged compressive strength" graphs represent the same break data with the removal of the data corresponding to the improperly shaped cylinders.

The general trend of strength gain in the concrete cylinders appears reasonable. The data suggests that the concrete has an f_c' value of 6.5 ksi. Concrete's with compressive strengths larger than 6.0 ksi are usually deemed as "High Strength Concrete" (HSC). For high strength concretes, a majority of the strength is gained within the first 24 hours after casting. In the data obtained, the concrete gained over 50% of its strength before 48 hours, as one would suspect for a high strength concrete.

Modulus of Elasticity

With the knowledge of the original gauge distance, the surface area of the cylinder ($\pi r^2 = 28.27$ in^2), and the corresponding displacements and applied forces, discrete stress/strain points were plotted for each individual cylinder. A linear trend line was then fitted through each set of data points, with the slope of the line representing the Young's modulus of the material. It should be noted however, that the regression lines were not required to have a zero intercept ($x = y = 0$). Because of the relatively small amount of data points obtained for each cylinder, it was considered more important to gain a more accurate slope of the data points available rather than specify zero initial stress. However, one could impose the zero intercept, and still record the slope of the lines to obtain the Young's modulus of the cylinders. The data points and regression lines for different concrete ages can be seen in Figure 6.7.

Researchers have reached a general consensus that the nature and type of coarse aggregate used in high strength concretes plays a large role in the elastic properties of the concrete. This is generally attributed to the highly dense hydrated cement paste-aggregate bond that makes HSC behave like an ideal composite material (Baalbaki et al 1992). Therefore, the variations in constituent properties of the concrete results in no perfectly reliable equation relating the compressive strength of all high strength concrete to a single corresponding Young's Modulus. As with the unconfined compressive strength of the material, HSC shows a significant rise in (static) modulus of elasticity within the first 24 hours after casting (Mesbah et al 2002).

Despite variations in constituent material properties, several governing bodies have attempted to determine a relationship between the compressive strength of HSC, and the concrete modulus of elasticity. The most commonly accepted equations for normal strength concretes are found in ACI 318 (ACI Structural Concrete Building Code Committee) and commonly accepted equations for high-strength concrete can be found in ACI 363 (ACI High Strength Concrete Committee). CEB 90 (Euro-International Concrete Committee (CEB) Code 90) also contains equations for high-strength concrete. The predictive equations for elastic modulus are given below with units assumed to be MPa,

$$\text{ACI 318} \qquad E_c = 4.73(f_c)^{1/2} \tag{6.2}$$

$$\text{ACI 363} \qquad E_c = 3.32(f_c)^{1/2} + 6.9 \tag{6.3}$$

$$\text{CEB90} \qquad E_c = 9.5(f_c + 8)^{1/3} \tag{6.4}$$

It should be noted that these equations have been found to show the best relationships with concretes using limestone aggregate (as is the case with the concrete obtained for the Racine Ave. deck pour). However, previous research has shown that the HSC equations do a relatively poor job of estimating

Young's Modulus with concrete strengths less than 20 MPa (approximately 2,900 psi) (Mesbah et al 2002).

Figure 6.8 illustrates the compressive strength/modulus data obtained from the Racine Avenue bridge concrete, and its relationship to the previously discussed equations for Young's Modulus. As previously mentioned, three compressive cylinders did not conform to the 6-inch by 12-inch standard dimensions. Therefore, the data obtained from those cylinders should be considered unreliable and are not included in Figure 6.8. It appears that the Racine Ave. bridge deck concrete data has a strong correlation with both the previously discussed ACI equations, with the exception of two outliers.

Tensile Strength

As with the compressive strength tests, the results (peak stresses) of the splitting cylinder tests (as calculated in accordance with ASTM 496) were plotting as a function of time at which they were tested. Once again, raw data was plotted, as well as the averages of the three tests recorded over each day. Figure 6.9 illustrates the results. The general trend in strength gain appears logical for the sampling range analyzed. The majority of the concrete's compressive strength and modulus of elasticity are gained in the first 24 hours. Therefore, it appears logical that a majority of the tensile strength was also gained in that time.

In general, the splitting tensile strength of concrete is assumed to be equal to 10% of the compressive strength of the concrete. A power series trend line was added to the previously discussed average compressive strength data to get an estimate of the compressive strength of the concrete at a given time to evaluate this approximation. Ten percent of the unconfined compression strength was plotted with the averaged tensile strength, as shown in Figure 6.10. It can be seen in the figure that the data for the first seven days fit the 10% approximation quite well. However, the data appears to indicate that after 7 days the actual tensile strength is less than 10% of the compressive strength with an increasing discrepancy as the concrete hardens. According to ACI Committee 363, the splitting tensile strength of concrete can be estimated as 10% of the compressive strength of the concrete, however, as the concrete increases in strength, this number has been shown to decrease to only 5% of the compressive strength. In Figure 6.10, 5% of the experimental unconfined compressive strength is plotted as a minimum limit (the lower trend line). It can be seen that the experimental tensile strength data clearly falls within the previously suggested range of compressive strength (5-10%).

HUMBOLDT AVENUE BRIDGE CONCRETE TESTING

The Humboldt Avenue Bridge (B-40-726) is a bridge with prestressed concrete girders over Milwaukee River in Milwaukee, WI. The new bridge deck was poured on November 20th, 2009. Nine 6x12 in.

cylinders were obtained from three different batches of concrete. The experimental results for this bridge deck clearly show that the tensile strength and Young's Modulus have strong correlation to the corresponding compressive strength.

After the concrete cylinders were cast, they were left in field at the bridge construction site for three days. Three cylinders were tested in the lab immediately after they were shipped to Marquette University. The remaining six cylinders were left outside of building to preserve similar curing conditions as that of the bridge deck. Three cylinders were tested at the age of 7 days and the final three cylinders were tested at the age of 14 days. The 28-day strength was calculated based on the trend of compressive strength development as shown in Figure 6.11. It can be seen that the three-day compressive strength of Humboldt Ave. bridge deck concrete (3,230 psi) is similar with that of Racine Ave. Bridge (3,860 psi). However, its 14-day strength (4,240 psi) is much lower than that of Racine Ave. Bridge (5,660 psi). This difference likely comes from the constitutive materials used to meet the WisDOT standard mix design. However, it is also likely that the difference is also due to curing conditions. The Humboldt Ave Bridge deck was poured with relatively low environmental temperature compared to the Racine Ave Bridge deck (poured during the summer). Normally lower curing temperature will cause lower concrete strength. However, the compressive strength development trend of the Humboldt Ave Bridge has similar trend as that of Racine Ave Bridge, i.e., the majority strength was developed in first three days.

SUMMARY

The concrete strength of the two bridge decks was high (6,500 psi for Racine Ave. Bridge and 4,900 psi for Humboldt Ave. Bridge) although it might not be the original designed for such high strength. The concrete compressive strength and Young's modulus were developed quickly in the first one to three days of its life. As discussed in previous chapters, such quick development of strength and modulus may cause significant shrinkage and tensile stress in the deck. As a result, there may be a tendency for early-age cracking in the bridge decks.

REFERENCES

ASTM C39 (2009). *Standard Test Method for Compressive Strength of Cylindrical Concrete Specimens*, ASTM International, 100 Barr Harbor Drive, West Conshohocken, PA.

ASTM C469 (2002). *Standard Test Method for Static Modulus of Elasticity and Poisson's Ratio of Concrete in Compression*, ASTM International, 100 Barr Harbor Drive, West Conshohocken, PA.

ASTM C496 (2004). *Standard Test Method for Splitting Tensile Strength of Cylindrical Concrete Specimens*, ASTM International, 100 Barr Harbor Drive, West Conshohocken, PA.

Baalbaki, W., Aicin, P., and and Ballivy, G. (1992). "On Predicting Modulus of Elasticity in High-Strength Concrete", *ACI Materials Journal*, Vol. 89, No. 5, pp. 517-520.

Mesbah, H.A., Lachemi, M., and Aitcin, P. (2002). "Determination of Elastic Properties of High-Performance Concrete at Early Ages", *ACI Materials Journal*, Vol. 99, No. 1, pp. 37-41.

Table 6.1 Racine Avenue Bridge Deck Concrete Mix Design

Note: Stone weights include moisture, sand is given in SSD condition

Material	Type	Manufacturer	Notes
Cement	Type I Portland	St. Mary's Cement	ASTM C-150 (Cement)
Flyash	Class "C"	LaFarge North Am.	ASTM C-618 (Flyash)
Slag	N/A	N/A	N/A
Sand	Torpedo	Vulcan Dousman	ASTM C-33 (torpedo)
Stone #1	Limestone	Link Aggregates	ASTM C-33 67(#1stone)
Stone #2	Limestone	Vulcan Materials	ASTM C-33 -4 (#2 stone)
Admix 1	Air Entrainment	Axim	ASTM C-260 (AE 260)
Admix 2	Mid-Range WR	Axim	ASTM C-494 (800N)
Admix 3	Retarder	Axim	ASTM C-494 (1000R)

Mix #	Cement Lb.	Flyash Lb.	Slag Lb.	Sand Lb.	*Stone #1* Limestone	*Stone #2* Limestone	Water Gal.	Admix 1	Admix 2	Admix 3
P2 312	428	183	0	1,250	1,031	844	28.0	4.6 oz	37 oz	12 oz

Mix #	Mix Description	Air %	Slump	Mix Placement
P2 312	WI A/FA 30% QMP	6.0%	4	Handpour / Exterior

Figure 6.1 Cylinder in Mold with Plastic Cover.

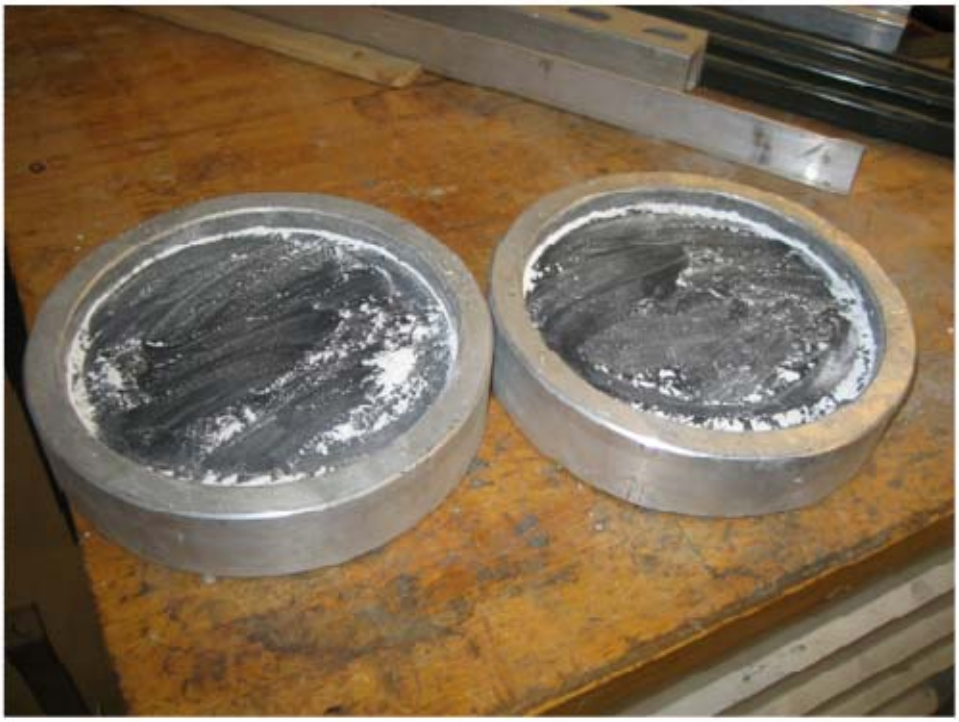

Figure 6.2 Unbonded Cylinder Caps.

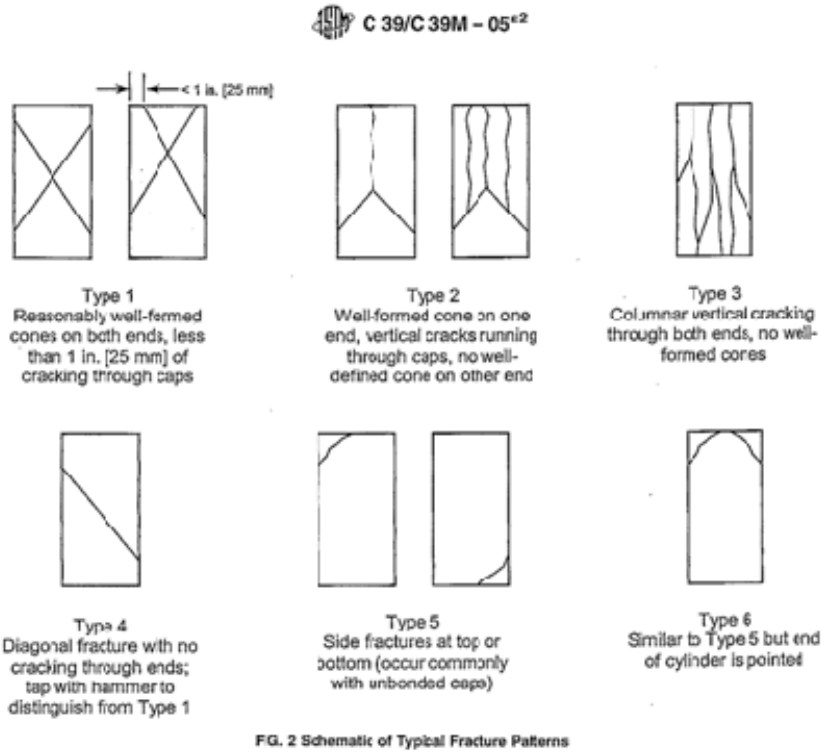

Figure 6.3 Typical Unconfined Compressive Failures (ASTM C39).

Figure 6.4 Modulus of Elasticity Test Setup.

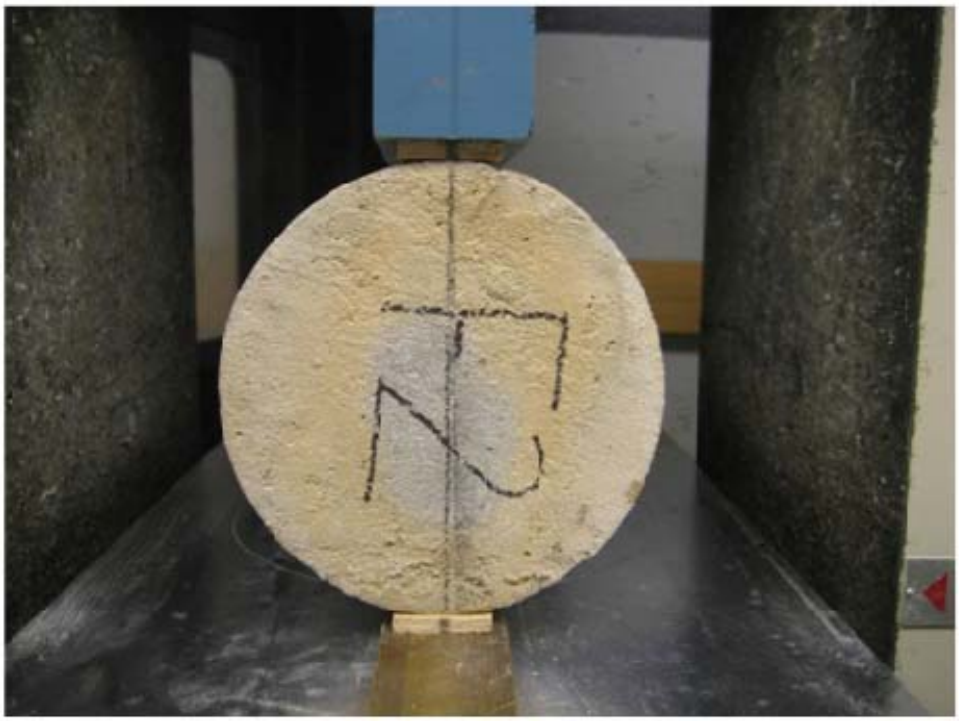

Figure 6.5 Splitting Cylinder Test Set-up.

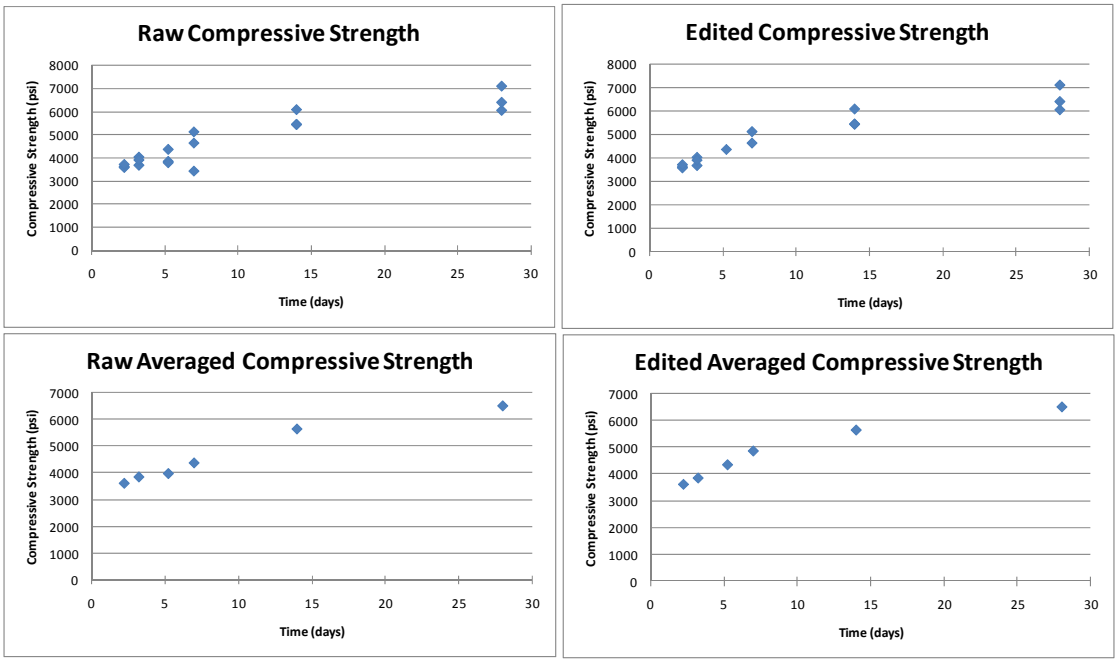

Figure 6.6 Compressive Strength Data of Racine Avenue Bridge Deck.

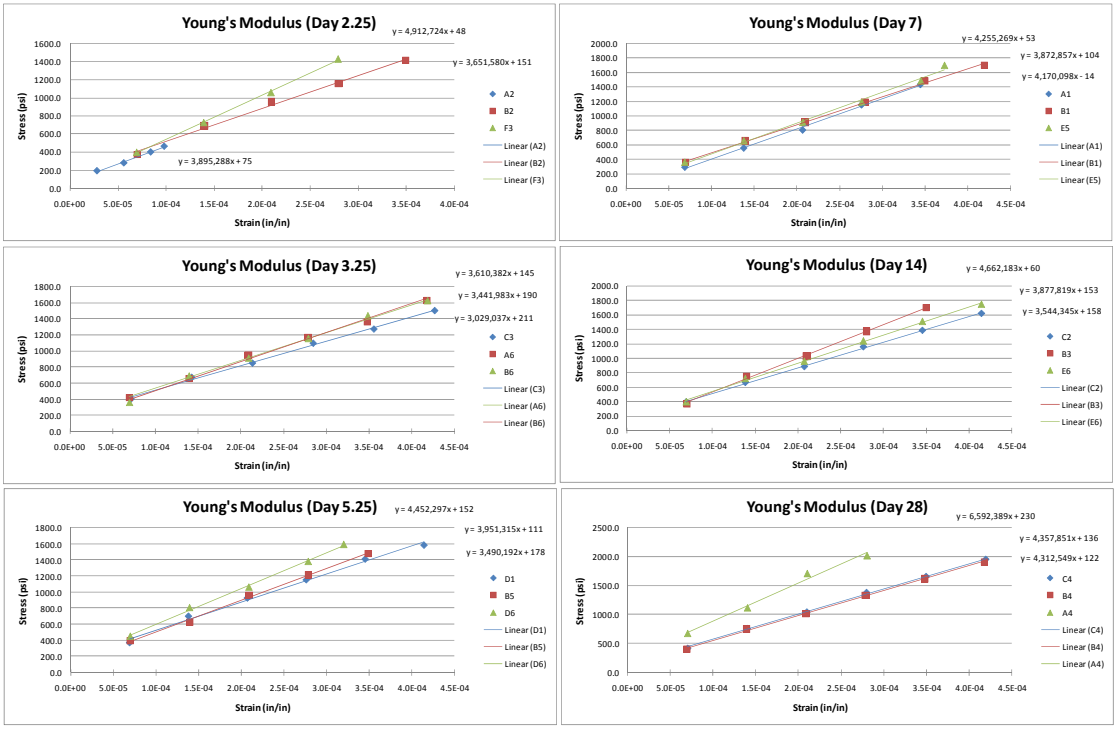

Figure 6.7 Young's Modulus Data of Racine Avenue Bridge Deck.

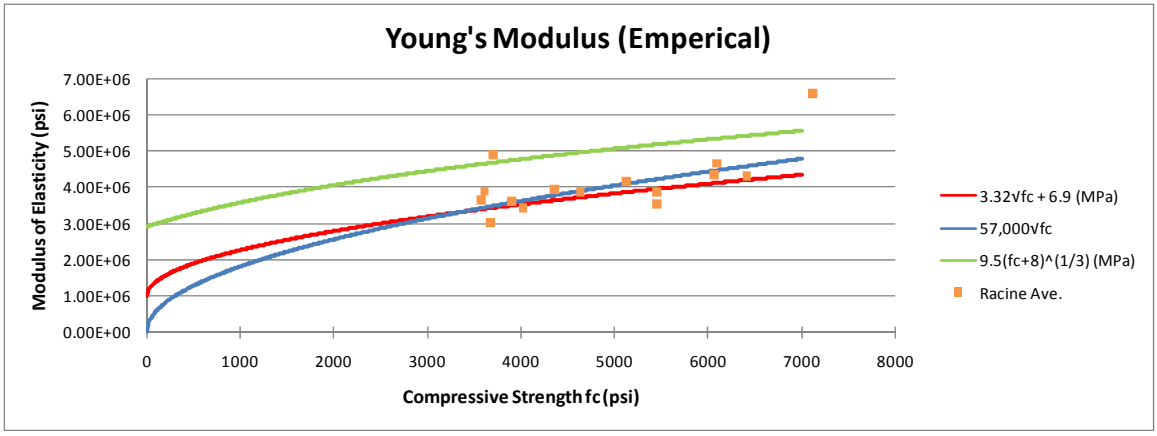

Figure 6.8 Test Results for Compressive/Modulus Relationship.

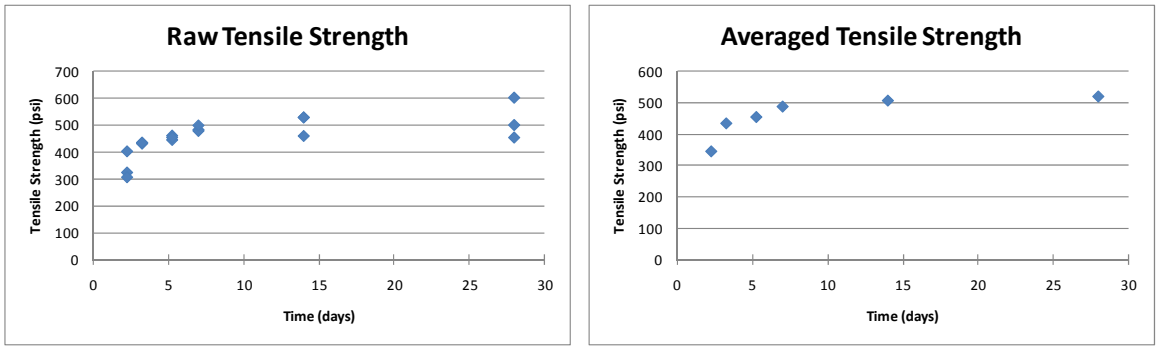

Figure 6.9 Splitting Tensile Strength Data of Racine Avenue Bridge Deck.

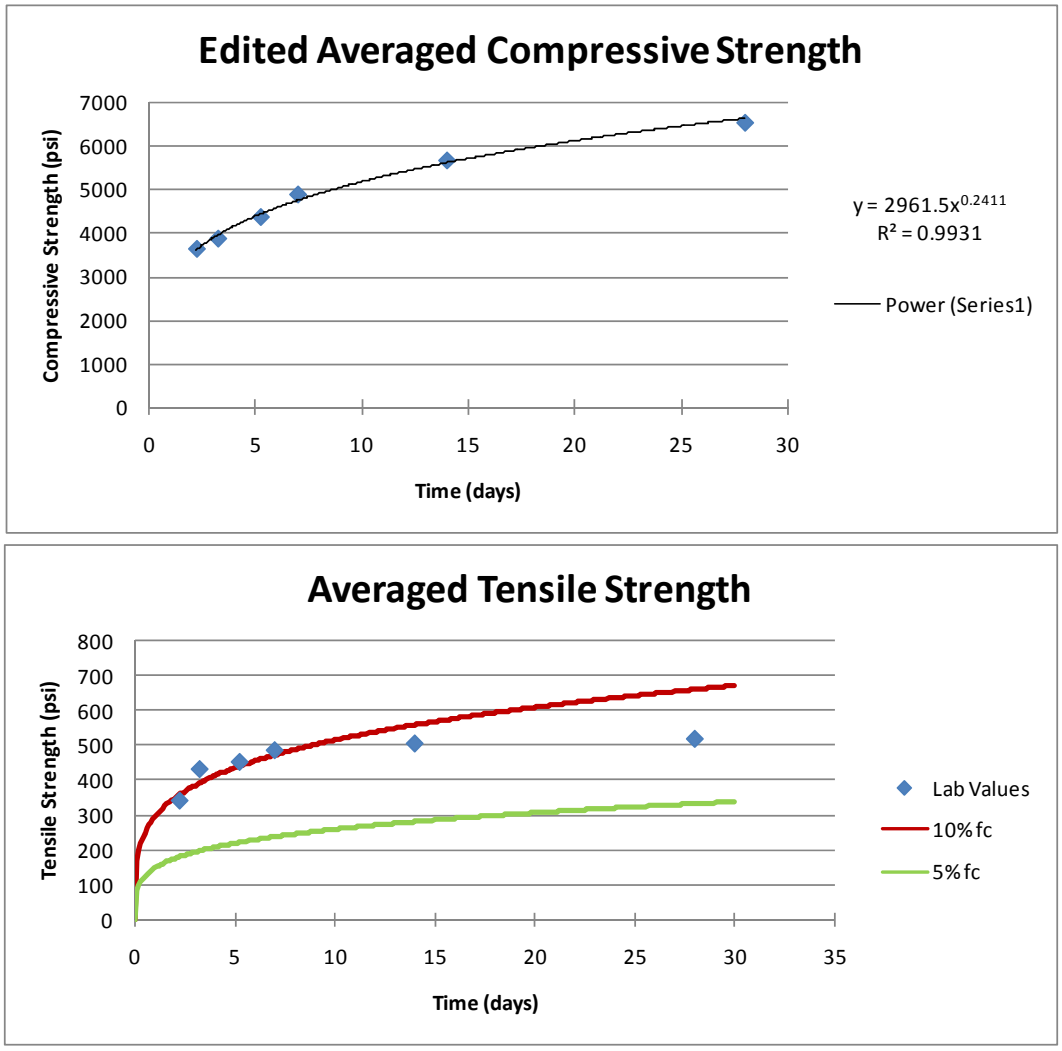

Figure 6.10 Tensile Strength vs. 10% and 5% of Compressive Strength.

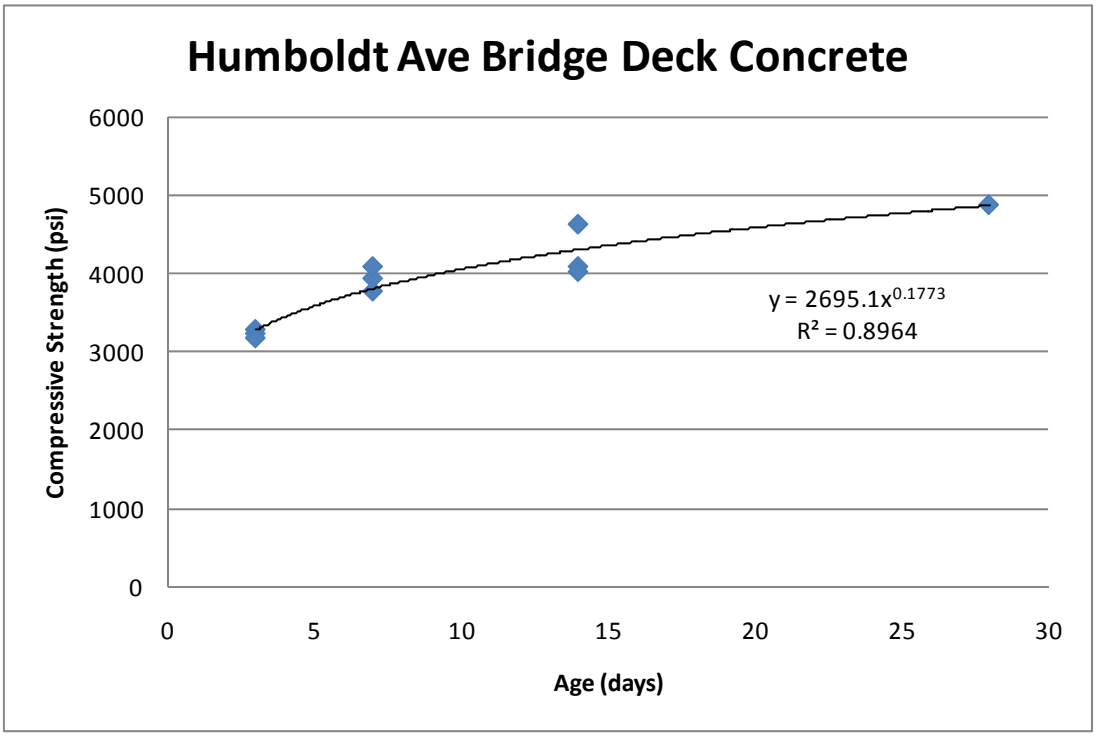

Figure 6.11 Compressive Strength Data of Humboldt Ave. Bridge Deck.

This page has intentionally been left blank.

Chapter 7
Summary, Conclusions, Recommendations and Future Research

SUMMARY

The research team conducted an extensive review of available U.S. and international research findings, performance data, and other information related to concrete bridge deck cracking. The major types of cracking in bridge decks were categorized into transverse, longitudinal, diagonal, map, and random. While the exact causes are unknown, the variables potentially affecting cracking were categorized as material properties, site conditions, construction procedures, design specifications, and traffic/age.

Fifteen bridge structures in the recently completed Marquette Interchange were analyzed using 21 of the previously determined variables thought to cause cracking. The data did not include the type, spacing, or location of any of the cracks. It appeared as though none of the 21 variables had a significant effect on bridge deck cracking. However, it should be noted that specific constituent proportions of components in the concrete mixes, hardened concrete properties, and traffic data were not obtained for any of the structures. In addition, significant cracking on the structures was noted only after the structures were open for traffic. It is therefore possible that traffic loading may also have a significant impact on bridge deck cracking (e.g. cracking resulting before traffic opening is accentuated by traffic loading) and this was subsequently evaluated for a two-span continuous precast concrete girder superstructure.

Sixteen bridges in Milwaukee area were investigated through visual inspection. These bridges included simple spans (B-67-296/297) and two slab bridges (B-67-293/294). These two kinds of bridges suffered from medium levels of cracking. All other bridges inspected were continuous superstructure bridges. All bridges classified as having serious cracks appeared to be to have continuous superstructure configurations and three of four seriously cracked bridges utilized prestressed concrete girders. Among the three bridges with minor or no cracks, two of them are using steel I-beams. It should be emphasized that several of the steel girder superstructures inspected were part of a re-decking effort associated with the Marquette Interchange reconstruction. The precast girder superstructures examined were not part of re-decking construction efforts.

Because most factors likely to affect deck cracking were not available for further investigation in these bridges only the superstructure configuration can be considered. Furthermore, several important parameters (e.g. concrete properties, traffic, etc.) were not available and the number of bridges investigated is relatively small. As a result, no definitive conclusion can be drawn with regard to bridge

superstructure type. However, this part of investigation indicates that the bridge structure type is definitely a factor that may affect early-age deck cracking.

In order to quantify the tendency for shrinkage and traffic-induced strains to cause cracking in bridge decks of continuous superstructures, a finite element simulation focusing on a typical precast girder two-span continuous superstructure bridge was conducted. The bridge prototype chosen as the basis of the numerical model is structure B-20-133/134located in Waupun, Wisconsin. The bridge was modeled using the ANSYS finite element analysis software system. The finite element model was calibrated using the in-situ field load testing data. Two HL-93 truck loading models were simultaneously applied to the model to study the traffic load-introduced strains. Temperature load was used to represent the strains induced by drying shrinkage in order to evaluate tendency for shrinkage introduced tensile strains in the concrete bridge deck to cause premature (early-age) cracking.

The literature review and finite element analysis conducted indicates that concrete shrinkage is a major factor affecting the likelihood and severity of deck cracking. Concrete shrinkage can be related to concrete compressive strength at specific ages. The finite element simulation conducted shows that the tensile stress in concrete deck is affected by the material's modulus of elasticity. When the tensile stress is larger than the tensile strength of concrete, the deck will crack. Therefore, the concrete properties in early age are very import for studying the deck cracking. Cylinders were collected from two newly constructed bridges in Milwaukee area, i.e., Racine Ave. Bridge and Humboldt Ave. Bridge. The cylinders were tested at different ages. The data from cylinder testing conducted at several time intervals up to 28 days indicates that the unconfined compression strength accrues very quickly. In fact, the target 28-day unconfined compression strength is reached in less than 4-5 days after placement. Elastic modulus and tensile strength is also increasing with the unconfined compression strength.

CONCLUSIONS

Based on the previous research in literature review, the following recommendations can be made to reduce deck cracking.

- Apply curing compounds as quickly as possible, cover the concrete to prevent excessive evaporation, and erect wind breakers and sunshades. These precautions will help inhibit plastic shrinkage cracking.
- Limit the amount of cement to 600 lb/yd^3 of concrete for bridge decks, as increased cement content increases the early modulus of elasticity of the concrete making it susceptible to high early-age stresses as shrinkage occurs.
- The water/cement ratio should not exceed 0.4. This will intern limit the early strength gain of the concrete as well as attempt to limit the moisture loss throughout the concrete.

- The total percent volume of cement and water not exceed 27.5%.
- The total air content is not less than 6%. This should decrease moisture loss (less water), as well as help with concrete freezing and thawing.
- The theoretical evaporation rate should not exceed 0.25 lb/ft2/hr, as an increased evaporation rate will cause increased moisture loss.
- Pour positive moment regions of the deck first, limiting the peak displacement of the concrete.
- Pour at a rate no slower than 0.6 span lengths/hr, minimizing the effect of newly poured concrete on the curvature of the previous cast concrete.
- A top reinforcement clear cover of 2.5 inches, attempting to strike a balance between limiting settlement cracking, and allowing the top reinforcement to control cracking.

To properly determine the cause of deck cracking, additional data will be required. The fifteen bridge superstructures in the Marquette Interchange evaluated are not enough to develop a complete understanding of deck cracking. In addition, the structures analyzed are all quite similar in construction, design, and superstructure configuration. It is crucial to know what types of cracks occur and at what locations they occur, to properly determine their causes. Additional variability in bridge superstructure configurations may also help in distinguishing cracking relationships, as the variables will have a larger range over which a pattern could develop.

Traffic data and structure age may also be beneficial in analyzing the crack data. In the case of the Marquette Interchange, the structures were built and opened over a four year window. As such, each structure was subject to varying traffic loads, and freezing/thawing periods. It is possible that either of these variables may increase the tendency for deck cracking.

While additional data are required, it may be more significant to obtain data related to the constituent components of materials and chemicals to develop mix designs meeting the MC330 WisDOT standard mix. Currently, concrete material properties are believed to be the most significant cause of deck cracking, as they relate to plastic and drying shrinkage (Schmitt and Darwin 1995). Without this batch-specific information, it is impossible to develop a complete understanding of deck cracking. It is recommended that this information be gathered as part of construction procedures.

Field investigation shows that the continuous supported bridges with prestressed concrete girders have more cracks than the simply supported bridges, and the bridges with steel I-beams. However, no definitive conclusion can be drawn because important parameters (e.g. concrete properties, traffic, etc.) were not available for the bridges considered and the number of bridges investigated was relatively small.

Finite element analysis for a typical precast-prestressed girder continuous superstructure shows that traffic loading by itself will likely not cause concrete deck cracking. However, the tensile stress introduced by concrete shrinkage may cause transverse cracks as early as 4 to 8 days after placing the concrete deck. At the age of 10 days, HL-93 loading caused tensile stress approximately equal to 21.6% of the modulus of rupture (used to represent the cracking strength) of the concrete, and 19.4% of the stress caused by concrete shrinkage. Therefore, even if the deck is not cracked due to concrete shrinkage, the combination of traffic load and concrete shrinkage appears capable of causing transverse cracking in the bridge deck over interior supports such as those seen in the bridge B-20-133/134.

The time-varying strength of concrete in the two bridge decks tested in this study was accumulated very quickly and the 28-day unconfined compression strength is likely much higher than the target unconfined compression strength. The concrete compressive strength and Young's modulus were developed in the first one to three days of its life. Such quick development of strength and modulus may cause significant shrinkage and tensile stress in the deck, and therefore may cause cracking in the deck.

RECOMMENDATIONS

The previous research and this study show that simply supported structures have less cracks than continuous structures. This is because simply supported structures have less constraint on the bridge deck. Therefore, when concrete shrinks, less tensile stress will be introduced. Therefore, when it is possible, it is recommended to use simply supported bridge superstructures to reduce the tendency for early-age deck cracking.

It is shown that concrete shrinkage can introduce significant tensile stresses in bridge decks within continuous superstructure configurations of sufficient magnitude to cause early-age cracking in the concrete the deck. Therefore, any method that can reduce concrete shrinkage will be helpful to reduce early-age deck cracking. During construction, the concrete should be covered to prevent evaporation, wind, and sunshine-induced heat gain to reduce shrinkage. Also, mix designs known to have lower tendency for shrinkage should be used. Typically, such concrete has low amount of cement and relatively low water/cement ratio. Thus, the research results seem to indicate that lower-strength concretes (e.g. 4,000 psi) should have lower tendency for early age deck cracking. It should be noted that the 28-day strength should be 4,000 psi. Typical modern bridge decks often have concretes that achieve this unconfined compression strength at 3-5 days.

Bridges built before the 1980's appear to have less cracking problems than those built after the 1990's. High strength concrete has seen much wider spread use after the 1990's. Modern bridge construction also includes pressure to open bridges to traffic very quickly after deck casting. As a result,

unconfined compression strength gain in modern concretes used for bridge decks is very rapid and the targeted 28-day strength at 3-4 days. Thus, modern bridge deck concrete is trending toward high-strength concrete behavior.

It is well known that high strength concrete has a higher tendency for increased shrinkage, rapid development of unconfined compression strength, and elastic modulus. This likely has a tendency for the formation of larger tensile stress in the bridge deck at early age and therefore, may cause early-age cracking. Therefore, lower strength concrete, especially lower strength development rate at early age should be used whenever the strength is enough for the traffic load requirement. It is also common that actually concrete strength is much larger than the design specified strength. Therefore, controlling the strength gain of the bridge deck concrete appears to be of benefit in reducing early-age deck cracking. It is recognized that opening bridges to traffic as early as possible is a necessity. However, a cost-benefit analysis of early opening and long-term degradation due to excessive cracking should be performed.

If it is possible, it is recommended that a longer curing period be provided and opening a bridge superstructure to traffic at later ages of the concrete appears to be beneficial. In such situations, concrete will have larger tensile strength when the deck is subjected to traffic load. Therefore, it will reduce the possibility of cracking.

FUTURE RESEARCH

Most bridge deck cracking happens at early ages of the concrete. However, there is lack of concrete properties at early ages for many recently completed bridges. Therefore, it appears that concrete properties (compressive strength, modulus of elasticity and tensile strength) should be monitored for all bridge decks. The crack development should also be monitored. The time of crack imitation, location of the cracks and crack pattern are critical to pinpoint the cause(s) of deck cracking. Furthermore, traffic loading and the residual tensile stresses caused by shrinkage exist in the deck may combined to cause early age deck cracking. Based on these discussions, it is proposed that phase II of this research effort would be beneficial to clarify the root causes of early-age bridge deck cracking in Wisconsin and to recommend methods to reduce the tendency for bridge deck cracking.

The research completed suggests that the deck cracking problem is very complex because there are many parameters affecting it. Therefore, in order to make phase II of this research more efficient, it is suggested to study only one parameter for each set of twin bridges. Following parameters were found to have significant effects on bridge deck early cracking and are relatively easy to control:

1. **Concrete strength**. All parameters except the bridge deck concrete strength are kept identical. One uses 3,500 psi (28-day) concrete and the other uses 6,000 psi. Because there is a tendency that actual concrete strength is higher than that which was specified, strict quality control should be applied to make sure that the concrete strength is close to the specified value at 28-days.
2. **Concrete cover**. All parameters except the concrete cover of the deck are kept identical. One uses 2 in. cover and the other uses 3 in. cover.
3. **Deck thickness**. All parameters except the thickness of the deck are kept identical. One uses standard thickness calculated through WisDOT bridge design manual and the other increases the thickness by 1 in. Ramey et al. (1997) found that a 1 in. increase in deck thickness can improve the deck performance significantly.
4. **Structure types**. For a set of twin bridges, all parameters except the structure type are kept identical. It is shown that simply supported bridges have much less decking cracking than continuously supported bridges. However, simply supported bridges require larger girder cross section and have a smaller span length possible. Therefore, this parameter is not as easy as the previous three to be implemented.

No matter which parameters are chosen to study, the following major tasks should be performed in any second phase of the current effort:

- Monitor concrete properties in early ages (e.g. with time) starting from the time of deck placement.
- Monitor crack development (crack initiation time, location and pattern) for all bridge decks.
- Monitor the construction load (correlated with the age of concrete) before opening to traffic.
- Record the opening date for the bridge and correlate it with the concrete properties found for the bridge deck concrete.
- Monitor the traffic loading and correlate it with crack development.

REFERENCES

Ramey,G.E., Wolff, A.R., and Wright, R.L. (1997). "Structural design actions to mitigate bridge deck cracking", *Practice Periodical on Structural Design & Construction*, Vol. 2, No.3, pp. 118-124.

Schmitt, T.R. and, Darwin, D. (1999). "Effect of Material Properties on Cracking in Bridge Decks", *Journal of Bridge Engineering*, Vol. 4, No. 1, pp. 8-13.

Wisconsin Highway Research Program
University of Wisconsin-Madison
1415 Engineering Drive
Madison, WI 53706
608/262-2013
www.whrp.org